

Reviews of Geophysics®



REVIEW ARTICLE

10.1029/2024RG000852

Key Points:

- A glacial forebulge is an ice load-driven bending-related and contemporaneously formed upheaval of the lithosphere outside a glaciated area
- Forebulge development leads to significant topographic changes of several tens of meters and is crucial to estimate sea-level changes
- Forebulge development alters lithospheric stresses, increasing seismic hazard potential due to possible fault reactivation in the area

Correspondence to:

C. Brandes,
brandes@geowi.uni-hannover.de

Citation:

Brandes, C., Steffen, H., Steffen, R., Li, T., & Wu, P. (2025). Effects of the last quaternary glacial forebulge on vertical land movement, sea-level change, and lithospheric stresses. *Reviews of Geophysics*, 63, e2024RG000852. <https://doi.org/10.1029/2024RG000852>

Received 20 AUG 2024

Accepted 28 MAY 2025

Author Contributions:

Conceptualization: Christian Brandes






Supervision: Patrick Wu

Visualization: Christian Brandes, Holger Steffen, Rebekka Steffen, Tanghua Li

Writing – original draft:

Christian Brandes, Holger Steffen, Rebekka Steffen, Tanghua Li, Patrick Wu

Effects of the Last Quaternary Glacial Forebulge on Vertical Land Movement, Sea-Level Change, and Lithospheric Stresses

Christian Brandes¹ , Holger Steffen² , Rebekka Steffen² , Tanghua Li³ , and Patrick Wu⁴ 

¹Institut für Erdsystemwissenschaften, Abteilung Geologie, Leibniz Universität Hannover, Hannover, Germany, ²Geodata Division, Lantmäteriet, Gävle, Sweden, ³Earth Observatory of Singapore, Nanyang Technological University, Singapore, Singapore, ⁴Department of Earth, Energy, and Environment, University of Calgary, Calgary, AB, Canada

Abstract A glacial forebulge is a bending-related upheaval of the lithosphere outside a glaciated area that co-occurs to the depression of the lithosphere below an ice sheet. The forebulge of the last glaciation attracted attention over more than one century, but quantitative descriptions on the geometry of the forebulge are rare. While many studies mention forebulge dynamics as a possible cause for a certain observation, very few studies provide a detailed and systematic exploration of the forebulge's precise dynamics. That way the forebulge became occasionally a rather mysterious structure with many unknowns. We aim to shed light into the forebulge discussion. After reviewing the history of forebulge research, we outline the theory behind the spatio-temporal forebulge development including controlling factors, and present forebulge observations in geological and geodetic records of North America and the northern parts of Central Europe. We use a state-of-the-art finite-element model that can fit multiple observations of the last glaciation simultaneously, to illustrate forebulge development in North America and northern Central Europe and address the issue of whether the zero-uplift hinge line is a good indication of the location of the forebulge front. Finally, we discuss effects of the forebulge on the sea-level change pattern and the evolution of lithospheric stresses, which can induce intraplate earthquakes. We also show that the existence of a glacial forebulge outside the ice margin is not consistent with the assumption of isostatic equilibrium at the Last Glacial Maximum, and there is no strain rate-stress paradox.

Plain Language Summary A glacial forebulge is a long hill that forms in front of a large glacier. The forebulge is caused by the ice mass that bends the lithosphere and by flow of Earth's mantle material away from the glacier. It is important to understand the formation, the geometry and motion of the glacial forebulge because this has, for example, an important effect on the sea level and earthquake activity in North America and Europe. We review the history of forebulge research, its observation, and the theory behind the forebulge development in space and time. We show that the type of material flow in the mantle controls how the forebulge moves while the thickness and rigidity of the lithosphere controls its height. A thick lithosphere makes the forebulge lower and further away from the glacier. If the lithosphere is thinner, the forebulge is higher and closer to the glacier. The highest part of the forebulge can migrate through time. We show forebulge effects on sea level in North America and Europe using a computer model and clarify how the melting of the huge ice sheets of the Last Ice Age could have triggered earthquakes in North America and Europe.

1. Introduction

The glacial *forebulge*, also named *peripheral bulge* or mistakenly as pleonasm *peripheral forebulge*, was recognized well over one century ago (Jamieson, 1882; Rudzki, 1899). Being a typical feature of the glacial isostatic adjustment (GIA) process, that is, Earth's response to the build-up and removal of large ice masses, it has repeatedly been investigated (Cathles, 1980; Daly, 1934; Fjeldskaar, 1994; Walcott, 1970). It is an ice load-driven bending-related upheaval of the lithosphere outside the glaciated area that co-occurs to the depression of the lithosphere below the ice sheet and just outside its margin (Figure 1). A glacial forebulge developed during the last glaciation along the west and east coasts of the United States and Canada, as well as in Central Europe and in the coastal regions of the North Sea in Northwestern Europe (Figure 2). The forebulge location has been estimated from geological information such as shoreline position changes (Barnhardt et al., 1995), from the architecture of fluvial networks (e.g., Panin et al., 2015; Van Balen et al., 2010), and with geodetic techniques such as Global Navigation Satellite System (GNSS) (Bogusz et al., 2019; N. Lau et al., 2020; Nocquet et al., 2005; Robin

© 2025. The Author(s).

This is an open access article under the terms of the [Creative Commons Attribution License](#), which permits use, distribution and reproduction in any medium, provided the original work is properly cited.

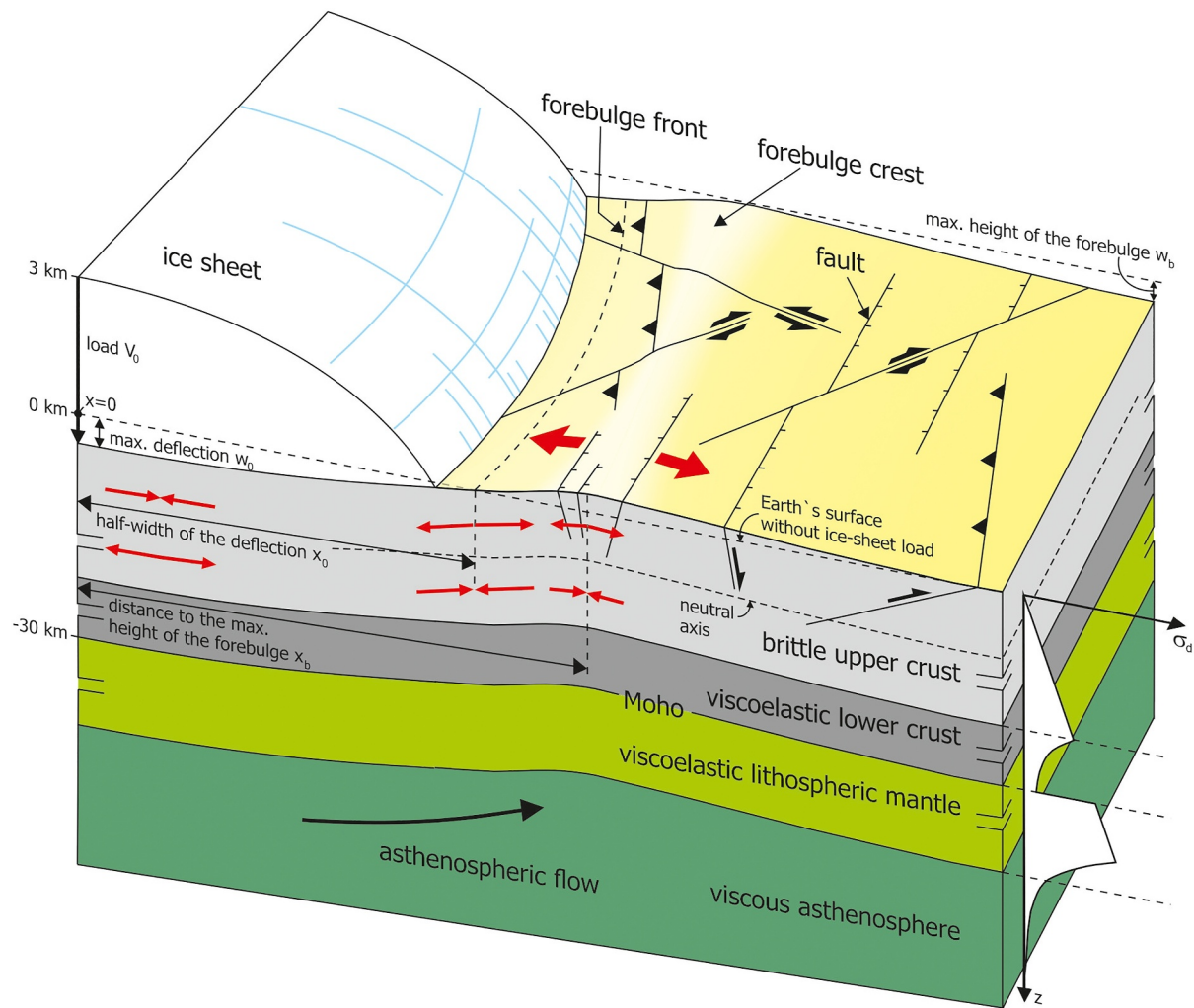


Figure 1. Conceptual model of the glacial forebulge. The load of the ice sheet bends the lithosphere and forms a depression below the ice sheet, where the Earth surface is pushed below the reference line. The reference line is the Earth's surface without the load of an ice sheet. Outside the ice-covered area, the glacial forebulge forms as an upheaval of the lithosphere above the reference line. The line where no deflection occurs is the forebulge front. The area of maximum forebulge height is the forebulge crest. Red arrows show directions of stresses induced by the ice load. Compressional stresses are indicated by arrows pointing at each other, while extensional stresses are shown by divergent arrows. The lithostatic strength envelope over depth is plotted in the right corner. Faults in the foreland of the glacier can be reactivated due to the lithospheric stress field changes. Please note that the y -axis uses a different scale for negative and positive values, respectively. Model based on Stewart et al. (2000), Grollimund and Zoback (2003), Keiding et al. (2015), and R. Steffen et al. (2021). Lithostatic strength distribution based on Bürgmann and Dresen (2008).

et al., 2020). A glacial forebulge is also present around the currently glaciated areas of Greenland (e.g., Sbarra et al., 2022) and Antarctica (e.g., Albrecht et al., 2024). However, the glacial forebulge of these areas is not much investigated and discussed, that is, with dedicated models and in observations, thus we will focus on North America and Fennoscandia.

Physically, the formation of the depression forces mantle material to flow from underneath the depressed area and accumulate outside the ice margin, forming a forebulge with a steeper slope on the load-facing side of the forebulge crest (i.e., down to the forebulge front and further to the load) but a gentler slope on the back side of the forebulge crest (Cathles, 1975) (Figures 1 and 3). The forebulge front is the line where no deflection occurs separating the depressed area from the forebulge. Hence, any point of the forebulge front has the same height as it had before the glaciation. The glacial forebulge area may grow and migrate during the growth of the ice sheet and may undergo migration and subsidence during the decay of the ice sheet (O'Keefe & Wu, 1998; Peltier, 1998). Forebulge migration, the lateral motion of the forebulge, is due to the flow of mantle material underneath the forebulge back to or from below the depressed land underneath the ice (Figure 1)—thus forebulge dynamics will persist for a few thousand years in the future. Due to the compressibility of the Earth, the value of the volume of

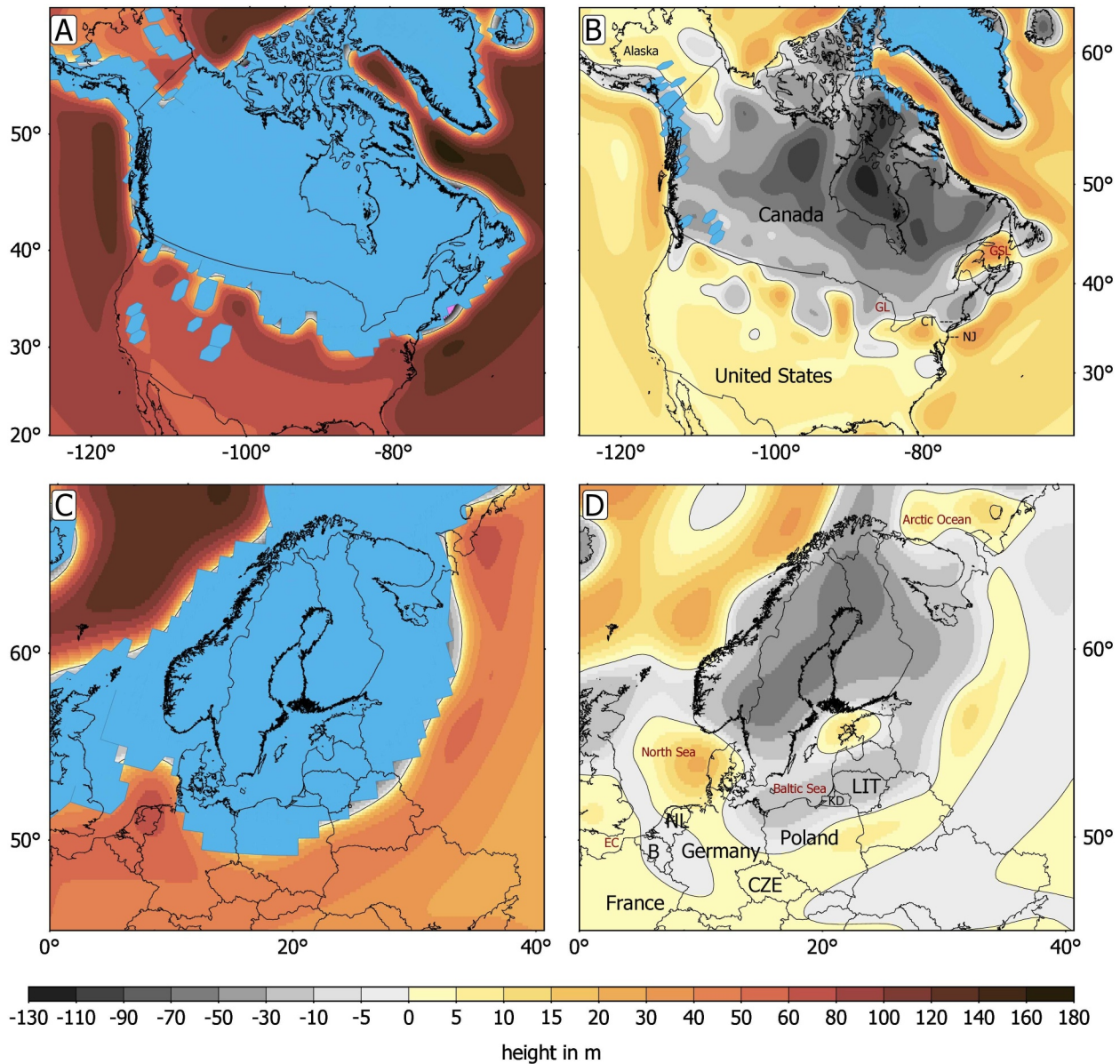


Figure 2. Model reconstructions of the glacial forebulge in North America and Europe. Time slices are 21 ka before present (last glacial maximum; (a, c) and today (b, d)). Blue color marks glaciated area. Warm colors indicate forebulge areas and grey colors represent subsidence compared to before the onset of glaciation. B = Belgium; CT = Connecticut; CZE = Czech Republic; EC = English Channel; GL = Great Lakes; GSL = Gulf of St. Lawrence; KD = Kaliningrad District of Russia; LIT = Lithuania; NJ = New Jersey; NL = The Netherlands. The model is based on a spherical, Maxwell viscoelastic and compressible glacial isostatic adjustment model applying ICE-6G_C ice model and VM5a earth structure from Peltier et al. (2015).

the forebulge (i.e., the volume from the reference line to the elevated surface, Figure 1) is not exactly compensated by the volume of the central depression (i.e., the volume from the reference line down to the depressed surface).

As the glacial forebulge migrates and decays after the onset of deglaciation, one expects the forebulge region to subside while the region within the forebulge front (mainly the formerly glaciated area) rises. Thus, there is a hinge line that separates the sinking and rising regions and where the uplift (vertical velocity) is zero. However, the hinge line (i.e., defined by a change in displacement) may not coincide with the forebulge front (i.e., defined by displacement), because the pattern and history of the forebulge decay, which may include forebulge migration, are affected by the spatio-temporal load change and Earth rheology. We will discuss this behavior with a state-of-the-art GIA model.

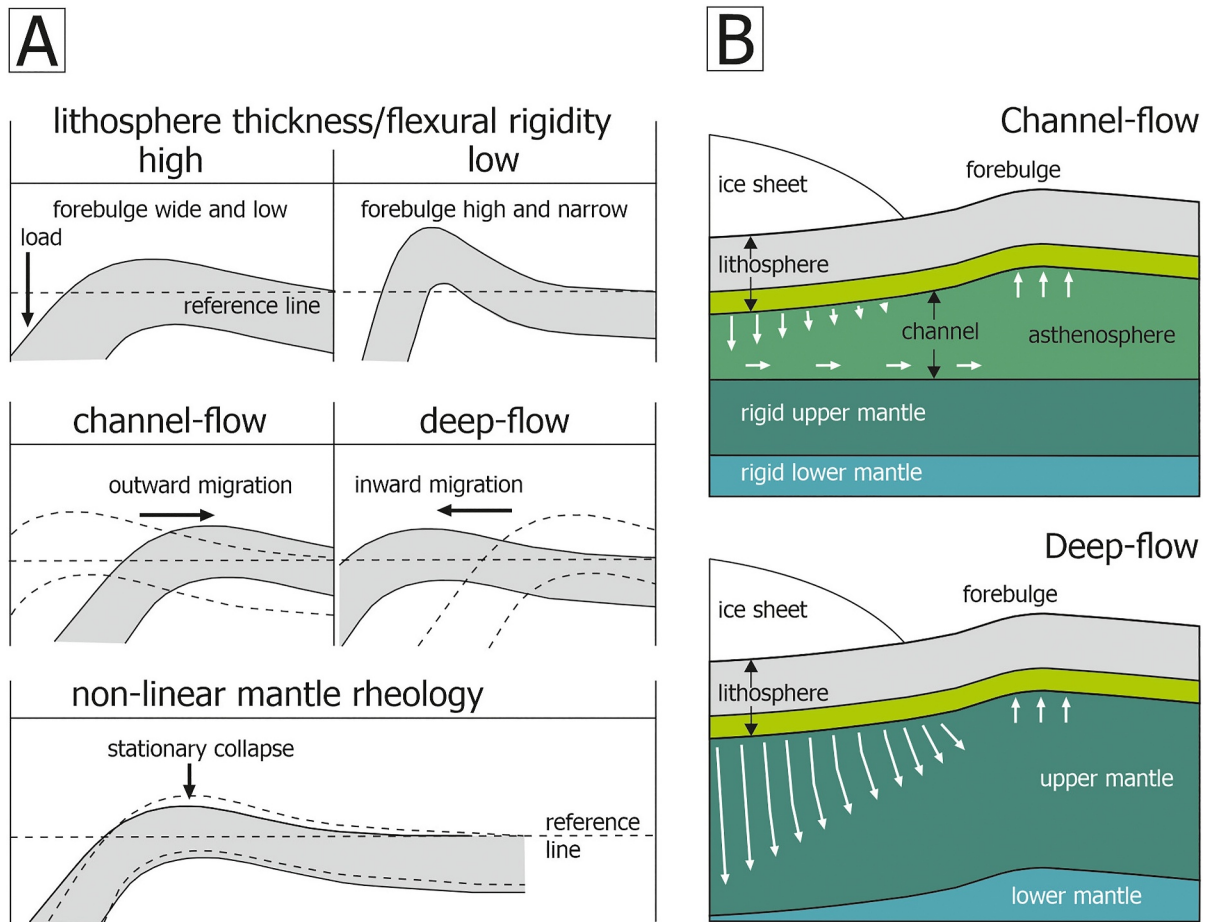


Figure 3. The controlling factors for forebulge evolution. (a) The geometry and location of the glacial forebulge is controlled by the flexural rigidity and thickness of the underlying lithosphere, as well as by the rheology and depth of the flowing asthenospheric material. Based on Wu and Peltier (1983), Wu (1993), Kaufmann et al. (1997), and Wu (1998). (b) Schematic model for channel-flow and deep-flow. In case of channel-flow large parts of the flow are horizontal, whereas in case of deep-flow mainly vertical flow occurs.

Theoretically, if the initial undeformed Earth surface was flat before the onset of glaciation, then the deformed surface that rises above the initial undeformed plane and located closest to the load is the forebulge. However, the initial Earth surface may not be flat (e.g., due to anomalous mass near the Earth's surface). This together with the presence of erosion and sedimentation adds uncertainties to the identification of a forebulge or the interpretation of its width and height from observational data. Furthermore, the geometry and thickness evolution of the ice sheet also influences the geometry of the forebulge and thus the deformation pattern during deglaciation.

As a typical feature of GIA, the forebulge affects land subsidence (Kiden et al., 2002), sea-level changes (Engelhart et al., 2009; Khan et al., 2015; Liverman, 1994; Newman & March 1968), spatial and temporal variations in the fluvial network (Anderson, 1988; Busschers et al., 2007; Pico et al., 2018; Reusser et al., 2004; von Drygalski, 1887; Wickert et al., 2019; Winsemann et al., 2015) including groundwater (de Wit et al., 2022), and the spatial and temporal distribution of seismicity, especially at the end and after the deglaciation phase (Craig et al., 2023; Grollmund & Zoback, 2003; Houtgast et al., 2005; Muir-Wood, 2000; Stewart et al., 2000; Van Balen et al., 2019). Such seismicity was long overlooked in the areas outside the former ice sheet, but recent studies point to significant tectonic activity and earthquakes in the glacial forebulge areas (e.g., Brandes et al., 2015; Houtgast et al., 2005; Müller et al., 2020; van Balen et al., 2021, 2024). Observations of the rate of vertical land motion and the change in topography or relative sea level (RSL) can consequently be used to understand and model the forebulge behavior.

Understanding the processes that control the formation and location of a forebulge is highly important as forebulge development and decay has led to significant topographic changes in the order of several tens of meters.

Consequently, quantifying the present-day forebulge location, height and decay rate has societal relevance. It may provide an estimate of future sea-level changes (e.g., along the east coast of North America and along the coasts of the North Sea and the Baltic Sea in Europe and Scandinavia) and may be used for distinguishing between natural and anthropogenic effects like subsidence due to groundwater extraction or hydrocarbon recovery. The estimated height of the forebulge during the last glaciation varies over a wide range from 60 m (Fjeldskaar, 1994) to 170 m (Mörner, 1979), depending on the region (North America, Europe) and the method and assumptions that were used. This underlines the still existing uncertainties in knowledge about the forebulge. Due to induced bending stresses in the lithosphere, seismic hazard potential in the forebulge can be increased even today and in the future.

The key aspects of this manuscript are to review the research on and the observations (for vertical land motion and topography/RSL) of the glacial forebulge of the last (Wisconsinan/Weichselian) glaciation over the last 140 years and to summarize the controlling factors for forebulge evolution, as well as the effect of the glacial forebulge on sea-level changes and the distribution of lithospheric stresses. While there are several reviews on the GIA process since the mid-1980s (e.g., Peltier et al., 2022; H. Steffen & Wu, 2011; Whitehouse, 2018; Wolf, 1986, 1993), none have focused explicitly on the forebulge. Although the glacial forebulge is an integral feature of GIA and its dynamics play important roles in RSL, land motion and glacially triggered earthquakes, most reviews focus on modeling aspects, global Earth and ice models and/or global GIA data but give only a cursory discussion about glacial forebulge dynamics and impact. The aim of the current review is to complement these reviews of GIA by focusing on the dynamics of the glacial forebulge.

Although this review will cover the historic development in forebulge dynamics where simple ice and Earth models were usually used, a special feature of this review is to include updated results of some of the more important historical papers with results from recent state-of-the-art Earth and ice models which gives the reader new perspectives in understanding forebulge dynamics. Another aim of this review is to check the accuracies of using these observations to infer forebulge location, width or height. As a consequence of the uncertainties of observational data, results from numerical GIA models (Cathles, 1980; Li & Wu, 2019; O'Keefe & Wu, 1998; Stea et al., 2001; Walcott, 1970) become very useful guides to our understanding of forebulge dynamics.

2. Timeline of Research on the Glacial Forebulge

2.1. The Early Years

Shaler (1874) was likely the first who mentioned an upheaval that developed outside the loaded area due to lithosphere loading. Shortly afterwards, Jamieson (1882) clearly described a glacial forebulge based on geological field observations. He assumed the depression below the ice sheet is controlled by the weight of the ice and the elasticity or yielding of the lithosphere, while the region beyond the ice shows an upheaval that can influence river flow. Based on an analytical approach, Hertz (1884) stated that a load-deflected elastic plate shows upheaval outside the load. Rudzki (1899) transferred this concept to geodynamics and reiterated that ice-sheet loading causes a depression below the ice and an uplifted area around.

Already in these early studies, the uplifted area (the forebulge) was interpreted to diminish during ice-sheet decay (Barrell, 1915). Nansen (1922) sequentially illustrated the response of the “lithosphere” to ice-sheet loading, including the flanking forebulges that he interpreted to move outward with the growing ice sheet like an upheaved wave. He included a bending related asthenospheric flow away from the deflection towards the forebulge outside the depressed area. Daly (1934) then distinguished two extreme models named the *bulge hypothesis* and the *punching hypothesis* to see which one can better explain peripheral uplift. The bulge hypothesis in the sense of Daly (1934) is a channel-flow model, where a very pronounced forebulge is caused by an outward flow of viscous material and supported by the dislocated material. The punching hypothesis in contrast is a deep-flow model and assumes that the “lithosphere” is “punched down” by the load, thus omitting any forebulges.

2.2. The Quantitative Approach

In the 1930s, a channel-flow model for the recent uplift of Scandinavia predicted a central uplifting area flanked by a region of subsidence, which corresponds to the decaying glacial forebulge (Van Bemmelen & Berglage, 1934). An analytical description of deep-flow in a uniform viscous half-space under a surface load also confirmed the formation of forebulges outside the load area but only during the unloading phase and not during

the loading phase (Haskell, 1935). Channel-flow can be promoted if mantle flow is “limited in depth by an effective rigid lower boundary” (Haskell, 1935).

The general analytical solution for the flexure of elastic beams (Hetényi, 1950) influenced the view on the forebulge in the following decades. The geometry of the glacial forebulge was calculated with an equation for elastic crustal deformation for North America and Greenland resulting in values of 80–185 m uplift for the forebulge crest (McGinnis, 1968). Subsequently, in an analytical solution for the steady-state flexural response of the crust to large-diameter surface loads, the crust is a thin elastic spherical shell that rests on an inviscid liquid mantle (Brothie & Silvester, 1969). From this flexure theory, the distance of the forebulge from the ice margin is found to be independent of the load size but depends on the flexural rigidity of the deflected plate (Walcott, 1970).

The flexural rigidity of a plate is determined by the elastic properties of the plate and is proportional to the cube of the plate thickness. Given the flexural parameter, the location of the forebulge can be estimated and the maximum forebulge height is found to be about 3.4% of the maximum depression underneath the load center (Brothie & Silvester, 1969). However, very simple ice and Earth models were considered in these early studies. Also, the steady-state flexure theory neglects viscoelastic relaxation in the sub-lithospheric mantle, thus the results are only applicable after long periods of loading when the viscoelastic sub-lithospheric mantle has completely relaxed.

Since the 1970s, Earth and ice models for GIA studies became more realistic. For example, radially stratified spherical, self-gravitating viscoelastic Maxwell Earth models were used, and the effects of the lithosphere, asthenosphere, mantle, and core structure can be included (Cathles, 1975; Peltier, 1974). While calculating the viscosity of the asthenosphere, Lliboutry (1971) stated that the forebulge is smaller than predicted by ideal plasticity models. Mörner (1979) calculated 170 m for the forebulge height of the Scandinavian Ice Sheet and derived that the mass transfer mainly took place by flow of low viscosity material in the asthenosphere. In this model, the subsidence related to the forebulge decay is uniform and parallel to the uplifting area. He argued that the mass transfer from the subsiding forebulge area took place between 16 and 8 ka before present (BP) (Mörner, 1979). Additional research showed that the mantle properties have a direct impact on the geometry of the glacial forebulge. A fluid upper mantle (UM) enhances the forebulge formation (Cathles, 1980).

A further improvement of the models was the implementation of the sea-level equation (Farrell & Clark, 1976) to include the effect of self-gravitation in the oceans. Global glaciation and deglaciation history models began to be used. However, the effect of the Earth's rotation on the sea was neglected and the coastlines were assumed to be that of the present-day. The latter approximation is inaccurate in places where the coastal bathymetry shows a gentle slope (e.g., Southeast Asia) and in the near field where water can accumulate in regions once covered by ice sheets (e.g., in places like eastern Canada and the Hudson Bay). Furthermore, due to inadequate knowledge of ice history before the last glacial maximum (LGM), many studies assumed that isostatic equilibrium was achieved at the LGM (ca. 20 ka BP). However, this assumption has led to the so-called “postglacial strain rate-stress paradox” (Craig et al., 2016; Grosset et al., 2023), which we will show is no longer a point of contention (details are explained in Section 7).

In the 90s, numerical modeling studies of GIA on a flat Earth with non-gravitating oceans were introduced that are based on a Fourier transformation approach (Fjeldskaar & Cathles, 1991) and these simulations were used to quantify the glacial forebulge related to the last glaciation of Scandinavia (Fjeldskaar, 1994). Brevik and Jensen (1992) used an elastic approach to model the glacial forebulge. The study of Fjeldskaar (1994) that describes the evolution of the forebulge in the vicinity of Scandinavia gives a detailed forebulge study in that region. It is shown that the forebulge reached its maximum height of 60 m at 15 ka BP, at a distance of 100 km from the maximum ice margin, followed by a decay to 40 m that was reached at 11 ka BP. During the decay, the forebulge was stationary (Fjeldskaar, 1994). By comparing the modeling results with the present-day uplift pattern and the tilting of shorelines, Fjeldskaar (1994) concluded that the Scandinavian lithosphere has an elastic thickness of less than 50 km above a 75 km thick asthenosphere. He derived a mantle viscosity of 1.0×10^{21} Pa s and an asthenosphere viscosity of 1.3×10^{19} Pa s. This Earth structure, partly with minor modifications, is still advocated by the author in recent works (e.g., Fjeldskaar & Bondevik, 2020), although all other GIA modeling studies prefer a model without low-viscosity asthenosphere and much more differentiated mantle structure, that is, at least a subdivision in upper and lower mantle (LM) (H. Steffen & Wu, 2011; Whitehouse, 2018).

Since the 1990s, the sea-level equation has been modified to include the effects of time-dependent coastlines (P. Johnston, 1993) and rotational feedback (Bills & James, 1996; Han & Wahr, 1989; Milne & Mitrovica, 1996).

In the meantime, many global ice models were developed and refined, such as ANU-ICE (Lambeck et al., 2014), the ICE-xG series (ICE-3G, Tushingham & Peltier, 1991; ICE-4G, Peltier, 2002; ICE-5G, Peltier, 2004; ICE-6G, Peltier et al., 2015; ICE-7G, Roy & Peltier, 2018), GLAC-1D (Abe-Ouchi et al., 2013; Briggs et al., 2014; Tarasov & Peltier, 2002; Tarasov et al., 2012, 2014) and PaleoMIST (Gowan et al., 2021). However, these ice models assume that mantle rheology is linear while microphysics of rocks show that mantle rheology can also be nonlinear or composite (i.e., both linear and nonlinear creep can co-exist). Recently, a global ice model that is based on composite rheology (Huang et al., 2019) has been developed. In addition, the effects of lateral heterogeneities in mantle rheologic structure have been considered (e.g., Bagge et al., 2021; Kaufmann et al., 1997, 2005; Li et al., 2018; H. Steffen et al., 2006; H. Wang & Wu, 2006; Whitehouse et al., 2006; Wu, 2005; Wu & van der Wal, 2003; Wu et al., 2013; Yousefi et al., 2021; Zhong et al., 2003, 2022). Furthermore, models for the investigation of glacially triggered fault reactivation and earthquakes have been introduced (e.g., Brandes et al., 2012, 2015, 2018; Hampel et al., 2009, 2010; Hetzel & Hampel, 2005, 2006; P. Johnston et al., 1998; Lund, 2015; Lund & Näslund, 2009; R. Steffen et al., 2014a, 2014b, 2014c, 2020; Turpeinen et al., 2008; Wu & Hasegawa, 1996a, 1996b; Wu & Mazzotti, 2007). The progress in GIA modeling since the 1970s led to numerous papers in GIA studies; however, only a few papers address the dynamics and impact of the forebulge. In the following sections, we will review the progress of our understanding of the forebulge.

3. The Controlling Factors of the Glacial Forebulge

The structure and material properties such as the effective thickness of the lithosphere and the viscosity of the mantle (which includes the asthenosphere) are controlling factors of the geometry, location and temporal evolution of the glacial forebulge (Cathles, 1975; Walcott, 1970). Especially the spatial and temporal behavior of the glacial forebulge (inward migration, outward migration or stationary decay) is related to the lithosphere and mantle properties. For example, Oakley and Boothroyd (2012) attribute the lack of a migrating forebulge in southern New England to the lithosphere rigidity or to lateral changes in the mantle temperature.

The outermost layer of the solid earth is the upper crust, which is underlain by a lower crust (Figure 1). Upper and lower crusts have a quartz/feldspar composition. The Moho separates the crust from the mantle (Figure 1). The mechanically strong uppermost mantle (mantle lithosphere) and the crust together form the lithosphere. The UM has a composition that is dominated by olivine. Below the base of the lithosphere, a low viscosity ductile layer, called the asthenosphere (Figure 1), may exist if the temperature is warm enough. As we will see below, both the effective thickness of the lithosphere and the viscosity of the lithosphere and mantle are determined by the composition and temperature inside the Earth.

The mechanical properties of the lithosphere control its deformation behavior (e.g., Burov, 2011) and also have an impact on GIA processes (e.g., Wolf, 1993). A key parameter in this context is the lithosphere strength that is influenced by the thermal structure, crust-mantle decoupling and bending stresses, where the curvature of the plate depends on the load distribution and the rheological structure (Burov & Diament, 1995). Characteristic for a continental lithosphere is a multi-layer rheology (Watts & Burov, 2003). However, this rheology is not yet fully understood (Burov, 2011) and not well determined in many regions (Kuchar & Milne, 2015). Early GIA models have used a uniform elastic shell resting on an enclosed fluid substratum (e.g., Brothie & Silvester, 1969), whereas later in the 1990s, more realistic lithosphere models have been developed, which can incorporate a ductile layer (Klemann & Wolf, 1999; Wu, 1997).

Forebulge formation involves elastic and viscous processes and is controlled by the bending of the lithosphere. The elastic properties of the lithosphere attempt to keep the bending related curvature low—often resulting in the extension of the area of depression from the load to the forebulge front. The viscous properties of the mantle also affect forebulge migration and decay. Furthermore, the geometry of the ice sheet and the pattern and rates of deglaciation are important because they represent the load for forebulge formation and with high fluctuations regarding mass and geometry directly affect forebulge growth and decay. In reality, the presence of other nearby ice and ocean loads result in the interaction among the forebulges of these loads. We will focus on the effects of the elastic and viscous properties of the lithosphere below.

3.1. The Elastic Component: Flexural Rigidity and Lithosphere Thickness

The fundamental concepts behind forebulge formation are isostasy and flexure. The lithosphere is pushed down into the mantle by the weight of the load until a new stable state will be reached. The lateral strength of the

lithosphere leads to a distribution of the load over a larger area and causes a regional isostatic compensation in the sense of Vening-Meinesz. The lithosphere below the load can be regarded as an elastic beam that rests on a fluid substratum and the lithosphere is bent down due to the load (Lambeck & Nakiboglu, 1980; Watts, 2001; Watts et al., 2013).

The bending behavior of the lithosphere depends on the flexural rigidity (which is determined by the Young's modulus E , the Poisson's ratio ν and the cube of the elastic thickness h of the lithosphere) and thus, the forebulge location depends on the flexural rigidity of the deflected plate (Walcott, 1970). A higher flexural rigidity leads to a lower amplitude of the forebulge and a greater distance to the load because it pushes the deformation further outward (Kaufmann et al., 1997; Wu, 1998). In addition, the amplitude of the depression below the ice is lower. A decrease in flexural rigidity (or lithosphere thickness) in contrast, produces a forebulge with a greater amplitude that is closer to the load (Figure 3a). Although these relationships between flexural rigidity and forebulge properties were derived under the assumption of a uniformly thin elastic plate overlying an inviscid fluid, the relationships can be extended to a viscoelastic Earth. A viscoelastic material exhibits both elastic and viscous behavior when subjected to a deformation. The viscous component will be discussed in more detail below.

3.2. The Viscous Component and the Maxwell Time

The mechanical behavior of Earth materials and its reaction to, for example, loading and unloading, is strongly controlled by the material properties and by the duration and magnitude of applied stresses (N. Lau et al., 2020; Watts et al., 2013). A key parameter is the Maxwell time, which represents the transition between elastic and viscous behavior of a viscoelastic material and is defined as viscosity of the material divided by its shear modulus (Cathles, 1975; Peltier, 1974; Peltier et al., 1980, 1986). In a viscoelastic Earth, rocks can deform like an elastic solid, if the period of loading is short compared to the Maxwell time, but rocks can also flow like a fluid, if the period of loading exceeds the Maxwell time (e.g., Ivins et al., 2020; Peltier et al., 2022; Turcotte & Schubert, 2014; Yuen et al., 1982). Due to the cold temperature near the Earth's surface, the outer shell of the Earth has an extremely high viscosity, and the Maxwell time can be of the order of many millions of years. However, as the Earth's temperature increases with increasing depth, the Maxwell time decreases rapidly. Assuming a nonlinear creep law in the mantle, Minster and Anderson (1980) showed that the effective thickness of the lithosphere depends on magnitude and duration of the load as well as, in case of oceanic lithosphere, on its age. If the mantle creep law is linear, then the effective thickness of the continental lithosphere depends on the duration of the load.

The relationship between the effective thickness of the lithosphere and the duration of the load can be seen as follows: Applied surface loads are associated with a certain loading period—for example, an ice sheet has a loading period of the order of 100 ka (e.g., Hays et al., 1976; Toucanne et al., 2009) while mountains have periods of the order of many millions of years (e.g., Dewey, 2005). For the part of the Earth's outer shell, where the resident time of the load is less than the Maxwell time, it is considered as “elastic” since it can keep the surface loads from sinking into the mantle. The actual strength of this elastic layer is determined by the composition, tectonic structures and other factors which affect how the Maxwell time changes with depth. For glacial loads, the mechanically strong outer shell that does not relax to become a fluid within the load duration is the “lithosphere” seen by the glacial process, and its thickness is the “effective thickness” of the lithosphere. The thickness of this layer is typically of the order of 100 km or more under old and cold cratons but can thin laterally over continental margins or under oceans. The increase in temperature with depth leads to a general decrease in both viscosity and shear modulus (Ranalli, 1995), though the reduction in the shear modulus is comparatively less than that observed in viscosity. As a result, Maxwell time generally decreases with depth, and the time required to transition from elastic to fluid behavior becomes shorter with increasing depth. In other words, the deeper part of the mantle will generally start to creep or relax earlier than the rocks above. When the deeper rock material starts to creep and loses its strength, the stress will move upwards resulting in a process called “stress migration.” This also happens at the base of the lithosphere as the duration of loading starts to exceed the Maxwell time—thus the effective thickness of the lithosphere also decreases in time. Accordingly, the lithosphere “seen” by glacial loads is thicker than the lithosphere “seen” by mountain loading because the latter has a much longer resident time (H. C. P. Lau et al., 2021). Since the effective flexural parameter depends on the “effective thickness” of the lithosphere, it also decreases with increasing loading time. Consequently, the location and height of the forebulge may change after hundreds of thousands of years of glacial loading or unloading. However, this viscoelastic relaxation of the lower part of the lithosphere is only one of the reasons why the location and height of the forebulge may change with time. A more important reason is due to the much faster flow of rocks in the sub-lithospheric regions. This faster flow of rocks can

occur in two end member models that are called *channel-flow* and *deep-flow* (Figure 3b). They will be described in detail in the following section. Today, GIA models generally lie somewhere in between these two end members.

3.3. Channel-Flow Versus Deep-Flow

In the 1930s, the “classical” channel model was proposed. It has a low-viscosity layer overlying a rigid lower boundary. However, later studies on the structures of the Earth show that a rigid lower boundary is not realistic, so the proposed model was later revised to have a low-viscosity asthenosphere that overlies a high-viscosity mantle or LM. Channel-flow, such as that occurring in the lower crust, has been described as Poiseuille or pipe flow (Bird, 1991; Castellanos et al., 2020). But in pipe flow, the flow velocity at both the upper and lower rigid boundaries must be zero, so that the flow speed in between has a parabolic shape. On the other hand, channel-flow in the Earth is different from pipe flow because, even if the lower boundary is rigid, the upper boundary is not and the flow velocity at the top boundary does not need to be zero there—otherwise tectonic plates cannot move. As a result, only the flow in the lower part of the channel can be described by the lower part of the parabolic flow in a pipe. In any case, channel-flow is thought to be mainly horizontal (at least in the lower part of the channel) whereas deep-flow is mainly vertical (Figure 3b). It has to be kept in mind that, even if the viscosity of the layer beneath the low viscosity channel is very high or rigid, the flow in the low viscosity channel can still behave as channel-flow or deep-flow—all depending on the characteristic horizontal dimension of the load relative to the thickness of the channel (Cathles, 1975). If the horizontal dimension of the load is large compared to the thickness of the “channel,” then the flow behaves as channel-flow. On the other hand, if the horizontal extent of the load is small compared to the thickness of the channel, then the flow behaves as deep-flow. In addition, if the characteristic horizontal dimension of the load relative to the thickness of the channel induces channel-flow, the speed would be much slower than that if deep-flow is induced. For a load size comparable to that of the Fennoscandian ice sheet, Cathles (1975) estimated that the flow in a 100 km thick channel is 153 times slower than deep-flow, but if the channel is 50 km thick, then the flow is 1,290 times slower than deep-flow (see Table IV-8 in Cathles, 1975). Thus, to give the same magnitude of predicted vertical deformation in Fennoscandia, the viscosity in the channel has to be at least a hundred times smaller than that predicted using deep-flow.

In the GIA modeling literature, there seems to be some disagreement on the dynamics of the forebulge in a channel-flow scenario. For example, it is not clear whether the forebulge decays in place (Fjeldskaar, 1994) or moves outwards while decaying (Kaufmann et al., 1997; Peltier, 1974). The reason lies in the difference in the assumptions made by the various models. e.g., some models treat the channel as a fluid (e.g., Fjeldskaar, 1994) but neglect the viscoelastic effect while others neglect the effects of the lithosphere (e.g., O’Keefe & Wu, 1998; Van Bemmelen & Berlage, 1934). Further complication arose because some models assumed that isostatic equilibrium was attained before glacial unloading while others assumed that isostatic equilibrium was attained before glacial loading.

In view of this, we show systematically in Figures 4 and 5 the dynamics of the forebulge during the loading and unloading phases of a simple boxcar load of 1,000 km width and height of 1,500 m. For these figures, the load is applied instantaneously at $t = 0$ ka, left there for 16 ka (Figures 4a–4c and 5a–5c) and then removed instantaneously (Figures 4d–4f and 5d–5f). All the Earth models have a uniform 84 km thick elastic lithosphere, and below it is either a viscoelastic channel (with a thickness of 366 km, 10^{19} Pa s viscosity and a rigid lower boundary, Figures 4a, 4d, 5a, and 5d), or a viscoelastic half-space with linear creep law (viscosity of 10^{21} Pa s, Figures 4b, 4e, 5b, and 5e) or a mixed model between the two models above (Figures 4c, 4f, 5c, and 5f). The mixed model also has an 84 km thick elastic lithosphere overlying a 10^{19} Pa s low viscosity UM with a thickness of 366 km just like the channel model, but the boundary at 450 km is not rigid, but overlies a viscoelastic half-space with viscosity of 5×10^{20} Pa s. In Figures 6–8, models are also introduced to study the effects of (a) non-linear creep law in a viscoelastic half-space below the lithosphere, (b) lateral thinning of the lithosphere outside the cratonic regions of Fennoscandia and Laurentide and (c) a quasi-parabolic ice sheet instead of a box-car ice load.

Note that the vertical and horizontal displacements are computed for incompressible Earth models to avoid the effects of Rayleigh-Taylor instabilities and fluid over-turning (Cambiotti et al., 2013; Klemann et al., 2003; Wong & Wu, 2019), which might happen to the simple Earth models used here. As a consequence, the magnitudes of the horizontal displacements (Reusen et al., 2023) and to a small degree also the magnitudes of the vertical displacement are imprecise, but the dynamics of the forebulge is not significantly affected.

To understand the results of the simple ice and Earth models (Figures 4–6), it is important to note that when a load is applied instantaneously and left on the surface of a viscoelastic Earth, there is first an instantaneous elastic

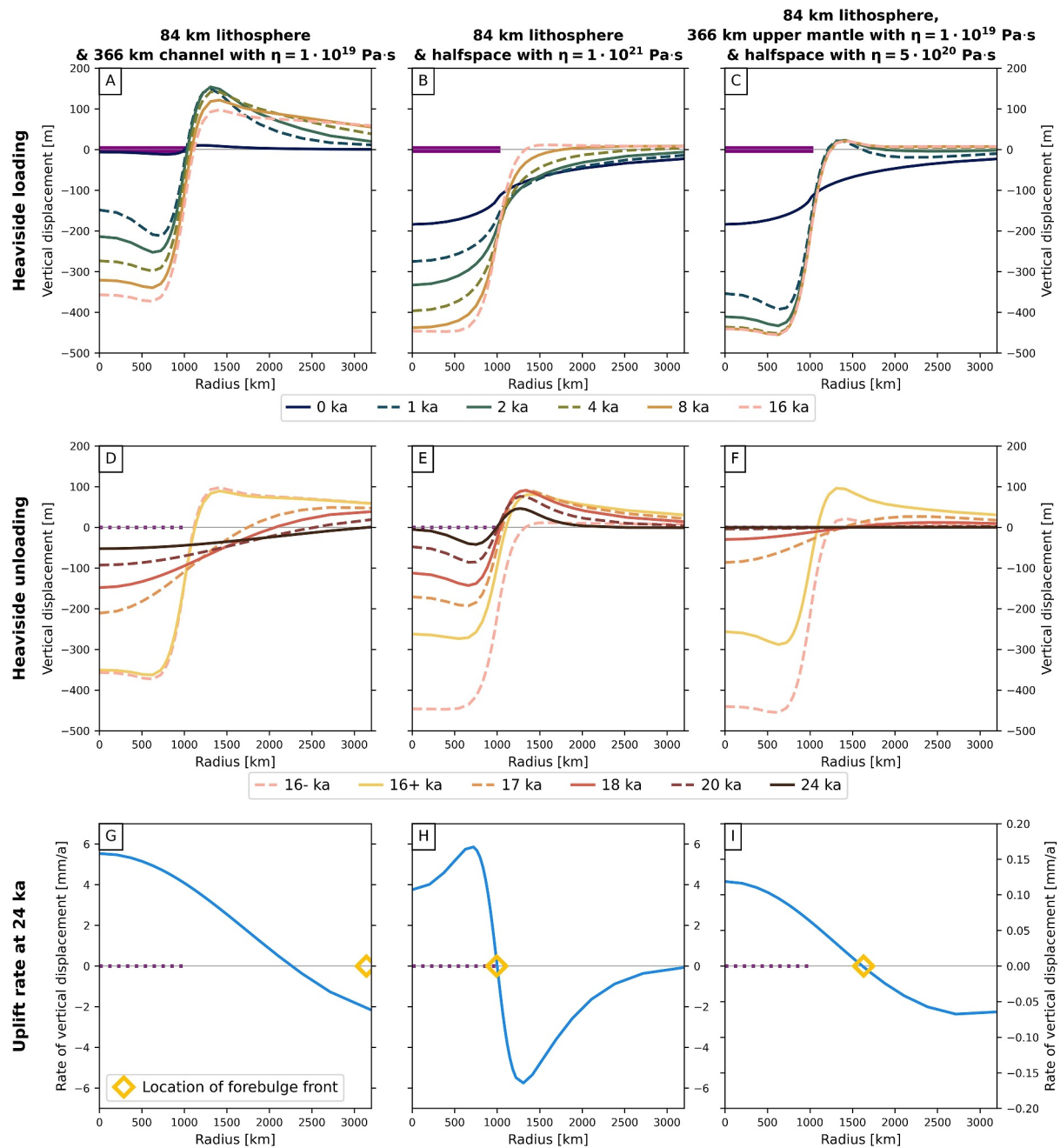


Figure 4. Vertical displacements due to 16 ka of Heaviside loading (a–c) followed by instantaneous unloading (d–f) of a boxcar load on top of a 366 km thick viscoelastic channel with viscosity of 1×10^{20} Pa s below a 84-km-thick elastic lithosphere (channel-flow model, left panel), a uniform viscoelastic half-space with viscosity of 10^{21} Pa s below a 84-km-thick elastic lithosphere (deep-flow model, middle panel), and a mixed model with a low viscosity layer under the 84-km-thick elastic lithosphere just as in the channel-flow model, except the boundary at 450 km is not rigid, but overlies a viscoelastic half-space with viscosity of 5×10^{20} Pa s. Horizontal purple thick line in (a)–(c) indicates the location of the load. Horizontal thin dotted line in (d)–(f) indicates the extent of the removed load. The bottom row in this figure shows the uplift rate as a function of distance from the load center during the deglacial phase (at 24 ka) for the three Earth models. Each yellow diamond represents the location of the forebulge front (where the downward vertical deformation changed to upward motion) as shown in the plots of the middle row. Please note the different y-axes in (g) and (h) compared to (i).

deformation (curves labeled as $t = 0$ ka in the figures) followed by viscoelastic creep which increases with time as the viscoelastic material relaxes to become more fluid-like (see pp. 26–29 in Cathles (1975) and pp. 7–13 in Wu (1978)). The time for the transition from elastic to fluid behavior is determined by the Maxwell time. When the surface load is removed instantaneously at 16 ka, the initial elastic deformation is recovered instantaneously

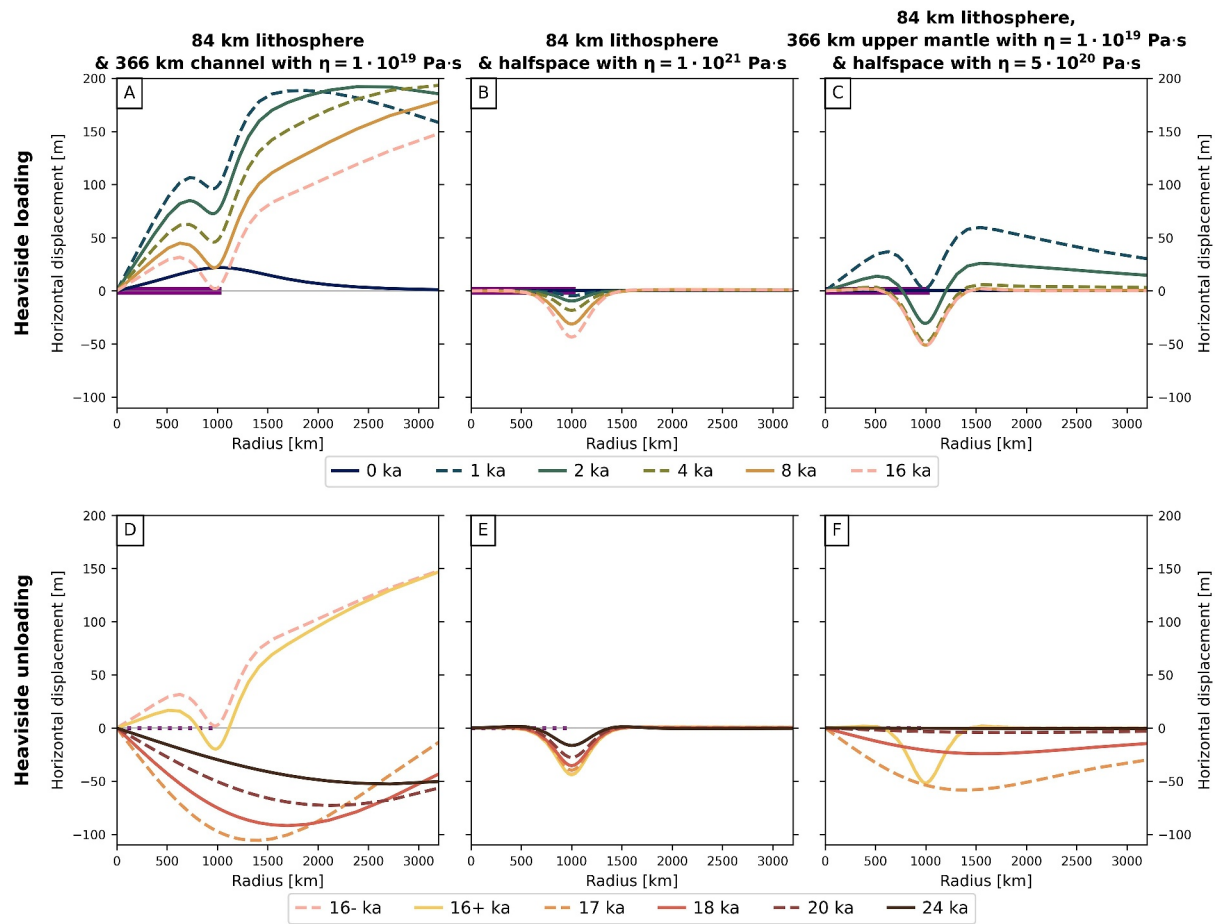


Figure 5. Same as Figures 4a–4f, except for horizontal displacements.

(shown by the difference between the curves labeled as $t = 16-$ to $16+$ ka) followed by viscoelastic creep. The removal of the load can be thought of as applying the same load as that at $t = 0$ but with a negative magnitude on the surface at $t = 16-$ ka. It is this recovery of the elastic deformation at $16+$ ka that significantly increases the height of the forebulge in all the models with a half-space (Figures 4 and 6).

When a channel-flow model with rigid lower boundary is used (Figure 4a), the vertical displacement shows a forebulge outside the ice load during the loading phase, which is almost stationary (i.e., neither move inwards or outwards) around 1,400 km. Its height grows from about 10 to 150 m during the first 2 ka, then decreases to about 97 m at 16 ka. A high forebulge is predicted because of the rigid lower boundary of the channel model. Once loading is removed, the peak of the forebulge migrates outwards with decreasing height (see Figure 4d).

The deep-flow model can be represented using a lithospheric half-space model where material transfer reaches the deeper portion of the mantle. In contrast to the channel-flow model, the height of the forebulge is very low (below 7.5 m in Figure 4b) during the loading phase and moves in time towards the load with increasing loading time. However, immediately after the load removal (Figure 4e), the elastic response to ice removal increases the height of the forebulge to 81 m at a distance of 1,400 km, which is followed by the forebulge decay (O’Keefe & Wu, 1998). After that, the peak of the forebulge migrates slightly inwards (Wu, 1998; Wu & Peltier, 1982, 1983) and becomes stationary after 20 ka.

For the mixed model (with a low viscosity layer over a viscoelastic half-space, Figure 4c), the height of the forebulge is around 22 m from 1 to 16 ka. The height of the forebulge is lower than the height in the channel-flow model because the boundary at 450 km depth is deformable here. At the same time, the height is higher than the height in the half-space model as the viscosity increase across 450 km depth is 50 times higher, which induces a channel-like flow. Comparing the rate of deformation between the mixed model and the lithospheric half-space, it

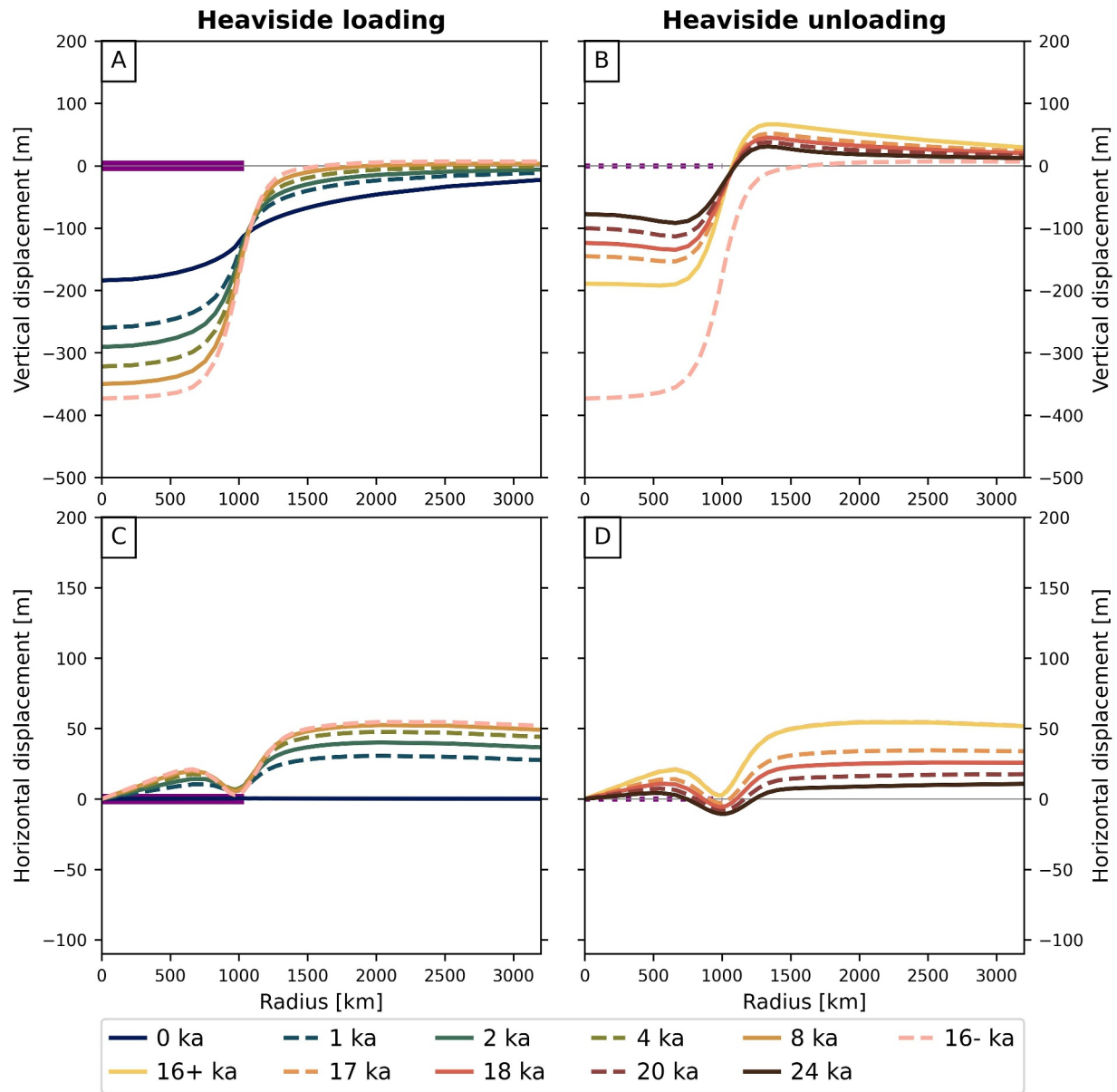


Figure 6. Vertical (a, b) and horizontal (c, d) displacements due to 16 ka of Heaviside loading (a, c) followed by instantaneous unloading (b) and (d) of a boxcar load on top of an 84-km-thick elastic lithosphere overlying a mantle with nonlinear creep that has $A = 3.33 \times 10^{-35} \text{ Pa}^{-3} \text{ s}^{-1}$ and stress exponent $n = 3$.

is evident that the deformation beneath the load reaches its limit at 8 ka (Figure 4c) already, which is earlier than for the lithospheric half-space. This behavior is because of the viscosity below 450 km being a factor of 2 lower than the viscosity in the lithospheric half-space.

Figures 4g–4i show the uplift rate as a function of distance from the load center during the deglacial phase (at 24 ka) for the three different Earth models. Each yellow diamond represents the location of the forebulge front (where the downward vertical deformation changed to upward motion) as shown in the plots of the middle row. The location of zero uplift rate (or hinge line) coincides with the location of the forebulge front for the lithospheric half-space and mixed model. However, the location of the forebulge front is several hundred kilometers away from the hinge line in case of the pure channel-flow model. Thus, the location of zero uplift rate deduced from geodetic measurements may be used to find the location of the forebulge front as a channel-flow model with a rigid boundary is not realistic. More discussion about this can be found in Sections 4 and 5.

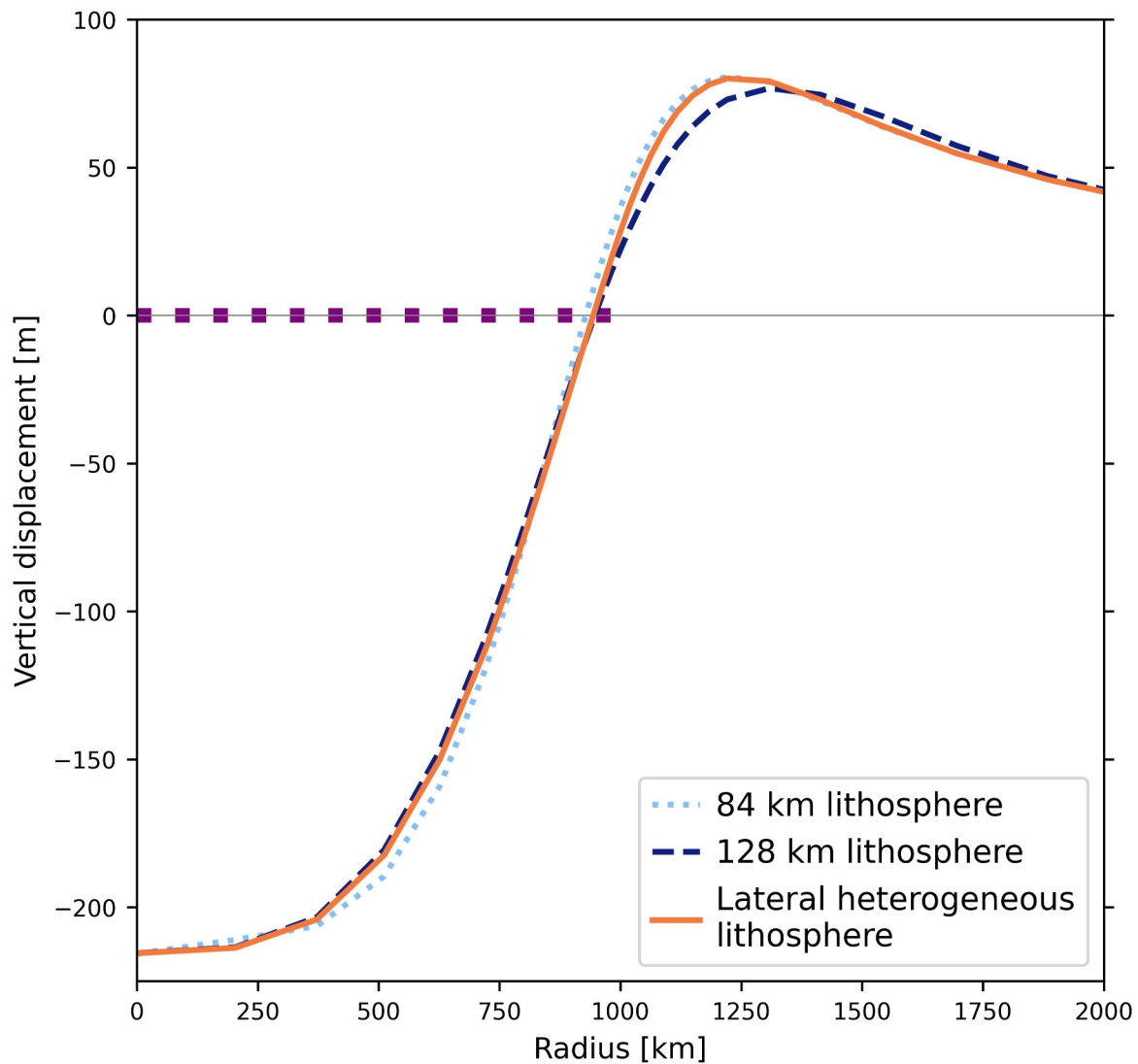


Figure 7. Effects of lateral variation of the lithospheric thickness on vertical displacements at 17 ka (1 ka after Heavyside unloading) for three lithospheric half-space models which have the same material properties below the lithosphere. The dotted and dashed curves are for uniformly thick lithospheres, while the orange curve is for a lithospheric model i.e. 128 km thick beneath the load but abruptly changed to 84 km thick outside. The loading history is the same as that used in Figure 4e except that a quasi-parabolic ice load is used.

The horizontal motions of channel-flow and deep-flow models are very different. The elastic horizontal displacement ($t = 0$ ka, black solid curve) of the channel-flow model (Figure 5a) reaches its maximum value near the edge of the load immediately after the load is applied—so, rock material accumulates just outside the load forming the forebulge. At 1 ka after loading, the horizontal motion has its maximum farther away at 1,883 km, but a local minimum is found near the edge of the load. Rocks within the load region continue to accumulate near the edge of the load, but outside the edge, rock material flows and accumulates farther away at the back of the forebulge. As time progresses during the loading phase, the magnitude of the horizontal motion beneath the ice load decreases in time, and less material accumulates near the edge. However, outside the load, the peak moves farther away—resulting in the growth of the back of the forebulge shown in Figure 4a. In contrast, in a deep-flow model with linear creep law (Figure 5b), the horizontal motion during the loading phase is mostly negative (towards the ice center) and focused near the edge of the load with increasing magnitudes as loading progresses. Though, these magnitudes are much smaller than that for the channel-flow model. Near the center of the load in Figure 5b, the horizontal motion is close to zero, implying motion is near vertical (inducing deep-flow).

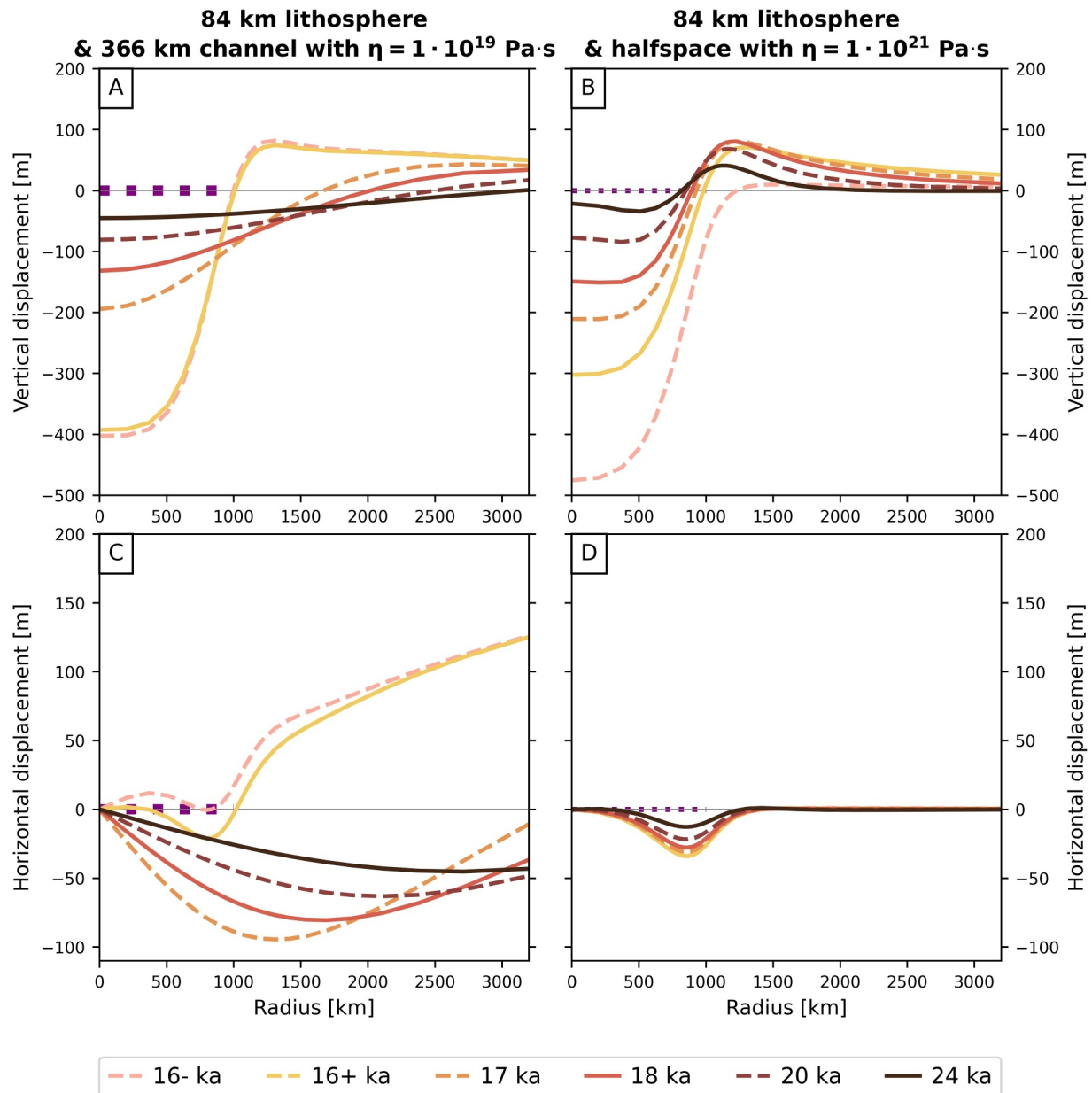


Figure 8. Similar to Figures 4 and 5 except a quasi-parabolic load is used instead of the boxcar load and only the vertical (a, b) and horizontal (c, d) displacements during the unloading phase for the channel (a, c) and half-space (b, d) models are shown.

During the unloading phase, the negative flow in the half-space model shows a decrease in magnitude over time and a constant location of the minimum of the horizontal displacement (Figure 5e). However, the horizontal motion for the channel-flow is more complicated. Immediately after the removal of the load (16+ ka), an area with negative motion (i.e., towards the ice center) is found near the edge of the former ice load in the channel-flow model (Figure 5d). At 17 ka, or 1 ka after load removal, the horizontal motion becomes negative except at the load center and at distance exceeding 4,200 km. After 17 ka, the minimum of the trough decreases in magnitude, but the location of the trough moves farther away. These results are different with the finding of O’Keefe and Wu (2002), because the thickness of the lithosphere also has a strong influence on horizontal displacement.

The horizontal motion in the mixed model is a mixture between channel-flow and deep-flow during the loading phase: In Figure 5c, the horizontal displacement curve for 0 ka is similar to the “0 ka” curve in Figure 5a, except the magnitudes are so small that the curve appears flat. At other times during the loading phase, the curves reached

a minimum near the edge of the ice load, which is somewhat like the curves in Figure 5a, except that the values of the minimum become negative after 1 ka and the magnitudes of the curves in Figure 5c are much smaller than those in the channel-flow model (Figure 5a). After 4 ka, the horizontal displacement from the mixed model becomes more like the horizontal displacement for deep-flow (Figure 5b). During the unloading phase, the curve at 16+ ka in Figure 5f is similar to that for deep-flow (Figure 5e), but afterwards, the curves become more like those for the channel-flow model in Figure 5d.

To summarize, Figures 4 and 5 show that channel-flow and deep-flow can have contrasting effects on the uplift and subsidence history in the peripheral region and the mixed model is somewhere between them. Since a channel-flow model with a rigid lower boundary is not realistic, recent GIA modeling studies prefer a model without low-viscosity asthenosphere but with viscosity contrast between UM and LM (H. Steffen & Wu, 2011; Whitehouse, 2018). With increasing lower-mantle viscosity, the location of highest subsidence within the forebulge region migrates away from the former glaciated area (Mitrovica et al., 1994). But if mantle viscosity does not strongly increase with depth, inward migration of the forebulge is promoted (Wu & Peltier, 1983). This is an important aspect as forebulge dynamics are sensitive to the viscosity of the LM.

The key issue is what viscosity contrast between the upper and lower layer is required to induce channel-flow-like behavior. Models between channel-flow and deep-flow have been developed to address this question, where they found that a viscosity contrast of a factor of 10 or more can induce channel-flow-like behavior and increase the height of the forebulge (O'Keefe & Wu, 1998; Stea et al., 2001). However, even a factor of 10^5 increase in the viscosity contrast cannot make the response exactly like that of a channel-flow with rigid lower boundary (O'Keefe & Wu, 1998). On the other hand, if a high viscosity garnet zone (e.g., Meade & Jeanloz, 1990) with limited thickness is sandwiched between layers of uniform viscosity in the mantle, and the top of the high viscosity layer is at 670 km, then for a load with characteristic length of 1,400 km, channel-like flow would be induced if the high viscosity garnet layer is much thicker than about 800 km. In addition, the high viscosity layer must be more than 100 km thick before its presence can be detected by RSL data (O'Keefe & Wu, 1998).

In the discussion of Figures 4 and 5, mantle rheology is assumed to be linear. However, it was shown by Karato and Wu (1993) that nonlinear rheology can be important for the analysis of GIA signals. Here, we will briefly show how non-linear mantle rheology affects the dynamics of the forebulge. Nonlinear rheology means that the strain-rate is proportional to the stress raised to the n th power (where n is the stress exponent and is greater than 1). This means the "effective viscosity" of the mantle is inversely proportional to the stress raised to the $(n-1)$ th power. Therefore, a large stress level will result in lower effective viscosity, but a low stress level gives a larger effective viscosity. For example, larger stresses are normally induced beneath an ice sheet, which results in a lower effective viscosity and faster mantle flow in this region. But when the load is removed, the stress level decreases, and mantle flow slows down.

The deep-flow model with a nonlinear half-space (Figure 6) has an 84-km-thick elastic lithosphere overlying a mantle with creep parameter $A = 3.33 \times 10^{-35} \text{ Pa}^{-3} \text{ s}^{-1}$ and a stress exponent of $n = 3$. The forebulge heights of this nonlinear half-space model (Figures 6a and 6c) are similar to the linear half-space model (Figures 4b and 4e), but the forebulge is not migrating towards or away from the ice margin during loading and unloading. Wu (1995) (Figure 5) showed that stresses are concentrating near the ice margin, which reduces the effective viscosity when the rheology is nonlinear. Thus, the flow inside the ice margin is effectively separated from the flow outside and so the forebulge does not migrate. This is supported by the horizontal motion for the deep-flow model with nonlinear creep law (Figure 6b), which shows that the horizontal motion becomes similar to the channel-flow model with displacements being positive or directed away from the load center. However, the horizontal peak outside the load does not migrate, and the magnitude of the horizontal motion increases with time.

The stationary decay of the forebulge presents a problem in explaining the observed RSL curves near the ice margin (e.g., in the northeastern United States, Figure 2), where an inward migration of a decaying forebulge is required (Wu, 1999). However, if a realistic ice model (e.g., ICE-3G) that includes a retreating ice margin during the deglacial phase is used together with ocean loading for a nonlinear mantle, then the forebulge does migrate (Wu, 1999).

Now, mantle rheology can be composite, meaning that both linear and nonlinear creep mechanisms can operate simultaneously in the mantle, and the mechanism with higher creep rate will become the dominant creep (Karato & Wu, 1993). For an Earth with uniform composite rheology, van der Wal et al. (2010) showed that nonlinear

creep was the dominant mechanism near the edge of the ice margin and below the load in the LM during glaciation, but after the end of deglaciation, linear creep can become the dominant mechanism away from the ice margin. Thus, the dynamics of the forebulge depend on the creep structure. The dynamics of the forebulge in North America predicted by a realistic ice model with composite rheology are described in Section 5.

In the simple ice and Earth models considered so far, the Earth is assumed to be laterally homogeneous. However, geophysical and geological evidence shows that the lithosphere beneath the old and cold cratons under Fennoscandia (e.g., Kaufmann et al., 2000) and Laurentia is thicker than the warmer and younger oceanic lithosphere nearby. To illustrate the effect of lateral variations in lithospheric thickness, three lithospheric half-space models are tested. The first one (light blue dotted curve in Figure 7) is the model used in Figures 4b, 4e, 5b, and 5e where a lithosphere with uniform thickness of 84 km overlying a uniform half-space is used. The second model is the same as the first one, except that the lithosphere has a uniform thickness of 128 km (dark blue dashed curve in Figure 7). The third model (orange curve in Figure 7) uses a laterally varying lithosphere. The thickness of the lithosphere is 128 km underneath the load but abruptly changes to 84 km outside. Comparison of the three curves shows that all models give similar results at 17 ka (1 ka after the start of Heaviside unloading). However, the location of the forebulge is farthest away when a 128-km-thick lithosphere is used. In addition, the forebulge height is also smaller for this model compared to the 84-km-lithospheric half-space model and the laterally varying lithospheric half-space model. These results agree with those shown in Figure 4 of Kaufmann et al. (1997), where more lithospheric models with lateral variation have been considered—including one where the lithospheric thickness changes gradually from under the craton to the surrounding ocean.

Beside lateral variation in lithospheric thickness, evidence from surface geology and seismic tomography shows that mantle properties (e.g., viscosity) vary not only radially, but also laterally (e.g., Kennett and Tkalcic 2008). A review on the GIA literature on lateral heterogeneities in the asthenosphere and mantle can be found in Peltier et al. (2022) and will not be repeated here. In Section 5 of this paper, the dynamics of the forebulge for the HetML140 Earth model (Li & Wu, 2019) that includes an elastic lithosphere with lateral thickness variation and both radial and lateral viscosity variations in the mantle will be shown (see Section 5).

In Figures 4–7, the ice load is assumed to be a boxcar load. But the sharp ice edge in a boxcar load is not realistic because ice profiles are better approximated by a quasi-parabolic profile. So, in Figure 8, we compute the vertical and horizontal motions (as in Figures 4 and 5) of the lithospheric channel (upper row in Figure 8) and the lithospheric half-space (lower row in Figure 8) models due to the Heaviside unloading of a quasi-parabolic ice model. Note that the quasi-parabolic ice load experiences no change in horizontal extent (i.e., no migration of ice margin). Comparison of the vertical displacements in Figure 8a with Figure 4d and also Figure 8c with Figure 4e shows that the changes mostly affect the amplitude and shape of the curves underneath the load and just outside the ice edge, but the dynamics of the forebulge, that is, whether it moves outwards or inwards is not affected. The same can be said for the comparison of the horizontal displacement between Figure 8b with Figures 5d and 8d to Figure 5e. Thus, using a quasi-parabolic ice profile has little or no effect on forebulge dynamics. Actually, the effect of a migrating ice margin as the ice sheet decays has a much larger effect on forebulge dynamics than the shape of the ice profile. The effect of ice margin migration will be shown in Section 5 for realistic ice and 3D Earth models with linear and composite rheologies, respectively.

This leads to the next factor that can affect forebulge dynamics—the ice history model. Modeling studies show that forebulge behavior is sensitive to the ice-sheet dynamics. The forebulge of the LGM in North America and Europe is shown in Figure 2 based on a GIA model applying the ICE-6G_C ice model and VM5a earth structure from Peltier et al. (2015). For the east coast of Canada, 2–3 ka later arrival of the glacial forebulge is calculated if a maximum ice model was used instead of a minimum ice model (Stea et al., 2001). This work indicates that forebulge decay is complex, with a time-dependent inward migration between 18–8 ka (80 m/a at 12 ka) and a stationary decay after 8 ka.

Mapping the development of the forebulge can provide useful information regarding the viscosity structure and rheology in the mantle, and the behavior of the forebulge is crucial for understanding future RSL positions along the coast of North America and Europe, as well as the potentially seismogenic reactivation of faults. These features will be illuminated in Sections 6 and 7, respectively. Next, we will summarize how the prominent forebulges in North America and Europe have been observed.

4. Observations of Forebulge Dynamics in North America and Europe

Geological observations of RSL and geodetic measurements can be used to estimate the forebulge location at some point in time. RSL can be derived from geological sea-level indicators. For GIA modeling, RSL is the most important quantity because a good data set of sea-level indicators can describe the GIA-related sea-level change over many thousand years (Whitehouse, 2018). This may allow the detection of the forebulge development and the migration of the forebulge front, for example, over the last glacial period. The migration can be determined from the sign change of sea-level rise versus sea-level fall. This tendency is an attribute in modern sea-level indicator compilations such as HOLSEA (Khan et al., 2019) and has, for example, been used to analyze the complexity of the Baltic Sea sea-level history (Rosentau et al., 2021).

In contrast to RSL data, geodetic observations such as tide gauges and GNSS provide the vertical velocity and thus help to identify the hinge line. Thus, they can approximate present-day's forebulge location but can (currently) not trace its migration. The limitation of tide gauges is that their distribution should cover and intersect the forebulge area. In addition, there are many other non-GIA processes (e.g., climate-related long-term changes in tides and loadings, local subsidence) overlapping the measurements which may hinder a sufficient separation of the GIA-related signal. The limitation of the latter is that GNSS station velocities or derived velocity fields in published studies generally show different patterns due to partly different station selections, reference frames (e.g., International Terrestrial Reference Frame) and processing parameters, different corrections, and, most importantly, different observation time spans of the stations.

4.1. North America

It is well known that the GIA process has an effect on the sea level (e.g., Walcott, 1972) and in this context, different studies in North America (e.g., Liverman, 1994; Newman & March 1968) have attributed parts of the rising RSL to the decay of the glacial forebulge. From the geological record (e.g., from stream longitudinal profiles and shoreline development) it became evident that the glacial forebulge migrated inwards during deglaciation. This has been clearly demonstrated for the east coast of North America (e.g., Davis & Mitrovica, 1996; Gornitz & Seeber, 1990; Peltier & Tushingham, 1991; Scott et al., 1987; Stea et al., 2001) and the direction of migration is from the south-west to north-east traceable to northeastern Canada (Bell et al., 2005; Gornitz & Seeber, 1990; Scott et al., 1987; Vacchi et al., 2018). The forebulge decay after the last glaciation is evident in meanwhile sophisticated RSL data sets for the east coast (Horton et al., 2009; Vacchi et al., 2018). Forebulge decay is the dominant process in the last 22 ka at the east coast (Barnhardt et al., 1995; Engelhart et al., 2009; Gornitz & Seeber, 1990; Li et al., 2020; Peltier, 2004; Walker et al., 2023) with implications on future sea-level changes (Love et al., 2016). Despite of all uncertainties, forebulge decay was interpreted to have contributed to a RSL rise at the US east coast (Delaware area) of approximately 20 m during the last 8 ka (Engelhart & Horton, 2012). Comparable values were estimated for the region of Nova Scotia to southern New Brunswick, where forebulge-decay-related subsidence in a range of 18–20 m has occurred since 8 ka BP (Dyke & Peltier, 2000). Pico et al. (2018) note that the deformation pattern in the Hudson River area differs from the general pattern of the Laurentide Ice Sheet forebulge and is influenced by a superimposed smaller forebulge of the Lake Erie ice lobe. Stanford (2010) derives a 40-m-high forebulge that was present at the end of the last glaciation in the area of the Hudson valley shelf, which had an influence on the sea level, but now has decayed.

A forebulge-related signal that causes a difference of about 0.5 mm/a in sea-level rise in an area from Connecticut to New Jersey was clearly identified in US east coast RSL data of the last 2 ka (Walker et al., 2021). This supports a tide-gauge analysis by Miller and Douglas (2006), who also found a forebulge subsidence mirrored in sea-level rise. In the long-term, such apparently small differences can have significant implications for coastal adaptation to future sea-level rise.

Analyzing tide gauge observations from 1900 to 2017, Piecuch et al. (2018) found that the forebulge decay along the US east coast is strongest in its central part (Mid-Atlantic Bight) where the peak is likely to occur in North Carolina, Maryland or Virginia. The average rate is calculated to be -1.4 ± 1.2 mm/a. South and north of the Mid-Atlantic Bight subsidence is less, whereas in the north even uplift can be possible. At a level of 69%, GIA is the first-order contribution to sea-level changes in this area. These findings were confirmed by Harvey et al. (2021).

In contrast, the forebulge situation at the west coast of North America is a bit less discussed, where sea-level change is further subject to a complex geodynamic situation with subduction zone tectonics, lower viscosity in

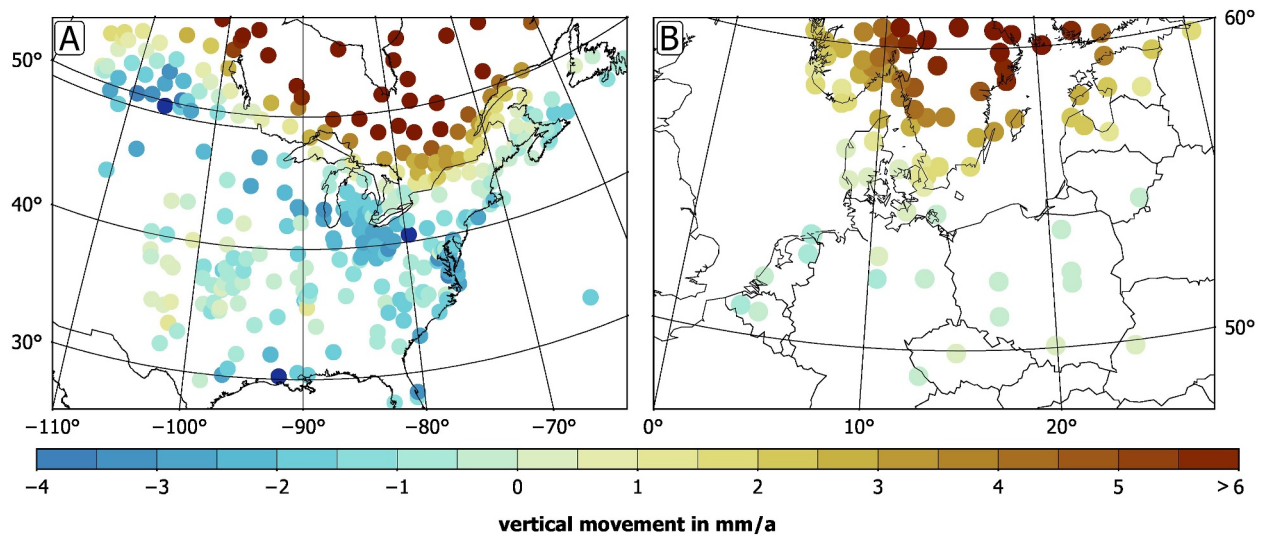


Figure 9. Vertical velocity field in (a) central North America and (b) southern Fennoscandia and northern Central Europe from Global Navigation Satellite System data. The forebulge area is implied by more bluish colors of vertical velocities at station coordinates. Data are taken from Peltier et al. (2015) (a) and Kierulf et al. (2021) (b).

the UM (compared to the east coast) and ongoing ice melt in mountains, among others (e.g., Yousefi et al., 2021). Sea-level curves along the west coast show a very different behavior since deglaciation (Clague et al., 1982; Letham et al., 2024; McLaren et al., 2014; Shugar et al., 2014). Most notably, there is a region of almost constant sea level on the central Pacific coast of Canada representing part of the hinge line between the forebulge area in the outer coastal islands and the formerly depressed area in mainland Canada (Letham et al., 2024; McLaren et al., 2011, 2014). Similarly, a forebulge likely developed in parts of southeast Alaska (Baichtal et al., 2021), while evidence for south-central Alaska is missing (Shugar et al., 2014). The forebulge development together with global sea-level fall during glaciation led to local sea-level fall of much more than 100 m. The forebulge was not static (as in other areas of the world), but its migration cannot be clearly traced everywhere (Shugar et al., 2014).

In GNSS-derived results, negative velocities that can be related to the forebulge decay are found for stations following an approximately 100-km-wide band along the US-Canadian border that includes the Great Lakes (GL) area (Figure 9a). Subsidence can reach a few millimeters per year in this area. The example of Peltier et al. (2015) uses the IGS08 realization of the ITRF2008 for a few 100 GNSS stations, whereas observation time span of most stations exceeds 6 years. The forebulge location and decay rates agree with those in Sella et al. (2007) using more than 300 GNSS stations with at least 3-years' time span in the IGB08 realization of the ITRF2000. This subsidence and the location of the hinge line were confirmed in a regional (Eastern North America) study (Goudarzi et al., 2016) with more than 100 GNSS stations of on average 9-year time span in ITRF2008. More than 3,200 stations with up to 21 years of observation time span in IGS08 on the North American Plate identified a hinge line crossing the south-central parts of central Canadian provinces, then lying on top of the northern GL making a turn to northeast, then following the northeastern US east coast states towards Canada (Kreemer et al., 2018). Maximum subsidence of up to -6 mm/a occurs in the north-central US. These hinge line and subsidence areas are supported with the vertical component of the Canadian NAD83v70VG crustal velocity model (Robin et al., 2020). The forebulge can also be identified in GNSS stations along the US east coast (Karegar et al., 2016, 2017), which show the maximum subsidence between 38°N and 40°N .

4.2. Europe

In Europe, the forebulge at the Polish coasts migrated between 9 to ca. 7 ka BP, followed by subsidence until ca. 4 ka BP (Uścińowicz, 2003). After 4 ka BP, a state of crustal equilibrium is suggested as no prominent forebulge-related signal could be extracted from the observations and their corresponding uncertainties (Uścińowicz, 2003). A strong influence of forebulge decay during and after deglaciation of the Scandinavian Ice Sheet is proposed for shoreline migration in Estonia (Rosentau et al., 2008; Saarse et al., 2007). Rosentau et al. (2007) discussed increased eastern European river incision and sedimentation rates due to the forebulge migration. The varying

tendencies in RSL changes in the Baltic Sea that can point to forebulge migration and decay were thoroughly discussed in Rosentau et al. (2021).

The forebulge influence is most prominent in the English Channel and the southern North Sea along the coasts of the Netherlands, Germany, and Denmark (Garcia-Artola et al., 2018; Hijma et al., 2025; Vink et al., 2007), the southern and south-eastern parts of the Baltic Sea (Meyer & Harff, 2005) and parts of the Russian Arctic Ocean coast (Baranskaya et al., 2018). Smaller effects are discussed for the Atlantic coast of France which are related to the gradually fading forebulge (Lambeck, 1997).

Based on analysis of RSL data along the Atlantic coasts from Portugal, Spain, and France, the maximum forebulge decay area moved from a location in the northeast (i.e., the southern North Sea) before 4 ka BP to a location in the northwest (i.e., south-west of the British Isles) in the late Holocene (Garcia-Artola et al., 2018). A north-south gradient in sea-level rise exists with the smallest values in the south, but different locations of the southernmost limit were found (Goslin et al., 2015; Lambeck, 1997; Leorri et al., 2012). An analysis of the forebulge history of western Europe with reprocessed observations and different GIA models found partly remarkable differences between model predictions and observations (Goslin et al., 2015). These differences might be related to inaccuracies in the global ice history, omission of lateral heterogeneity in Earth structure on a regional scale, or local subsidence/uplift caused by non-GIA processes (e.g., Chester et al., 2024; Li et al., 2024). Hence, the exact location of the forebulge maximum as well as its decay history are not defined yet.

The existence of the forebulge is also discussed for Norway (Chester et al., 2024), but it was deemed likely that every coastal Norwegian site is located inland of the hinge line and has been since the LGM (Creel et al., 2022). The westernmost islands of the Lofoten-Vesterålen archipelago are currently the closest to the hinge line (Creel et al., 2022). Hence, the effect of forebulge decay and migration cannot be extracted from corresponding Norwegian RSL data (yet).

GIA-related subsidence south of the Baltic Sea, which likely coincides with the forebulge decay, was first shown with ca. 10 GNSS stations in northern Central Europe (Lidberg et al., 2007). This result is based on ca. 7.5-year long GNSS measurements in the ITRF2000. An update with more than 20 GNSS stations in the proposed forebulge area, 10-years' time span and ITRF2005 lacks a forebulge pattern (Lidberg et al., 2010). Subsidence occurs only locally in the Netherlands and northeastern Poland. It is suspected that the ITRF2005 hampers a clear forebulge determination, because there are large differences between ITRF2000 and ITRF2005 (Argus, 2007). Instead, an ITRF2008 solution with 90 GNSS stations on the European Plate having maximum observation time span of 14 years (but most stations have much less than that) traced the forebulge area (ca. 20 stations) well with some local minima in each country (Argus & Peltier, 2010).

A subsidence pattern with minimum in the (northern) Netherlands was also indicated in another ITRF2008 solution with a further expanded time series compared to all solutions above (Kierulf et al., 2014). It has less than 10 stations in central Europe though. Again, an ITRF2008 solution but with almost 140 GNSS stations on the European Plate (more than 30 in the forebulge area) whose time span is up to 17 years generally confirmed earlier ITRF2008-based results (Peltier et al., 2015). An analysis of about 470 stations in ITRF2014 in northern Europe excluded more than 170 stations due to statistically insignificant signals within the uncertainties and found no clear forebulge pattern although subsidence is indicated in isolated areas of the Netherlands, Germany, Poland, and Lithuania (Bogusz et al., 2019). A much larger subsidence area is found instead in an ITRF2014 analysis with less than 20 stations south of the Baltic Sea (Lahtinen et al., 2019). There are some outliers in northeastern Germany (small uplift) and southern Lithuania (local subsidence), thus supporting earlier ITRF2008-based findings. A similar pattern but with less anomalies has recently been calculated in ITRF2008 with up to 15 years observation time span and with ca. 20 stations south of the Baltic Sea (Figure 9b; Kierulf et al., 2021). Maximum values can be found in Belgium and the southern Netherlands. Subsidence then becomes smaller to the east until central Poland, then becoming larger again towards the northeast.

Summarizing the studies above, the European forebulge covers the Netherlands, Belgium, northern Germany, Poland, and the southeastern parts of Lithuania. Maximum subsidence is found in the Netherlands, whereas it is likely that extensive gas extraction (Ketelaar, 2009) and sediment loading (Hijma et al., 2025; Vink et al., 2007) lead to additional subsidence. The hinge line of zero uplift is close to the Danish-German border and follows then the Baltic Sea coasts of Germany and Poland, then crossing the Kaliningrad District of Russia and southern Lithuania. Generally, the more stations become available, patterns become smoother and agree more and more

with each other. Nonetheless, a couple of question cannot be answered to date. Where is the hinge line exactly and is it still moving? What is its maximum subsidence and where? Where does it fade in the south? How does it extend in the east?

A possible help can be the analysis of repeated leveling. In Germany, the difference between the current official height system DHHN2016 and the previous DHHN92 indicates small uplift in northernmost and northeastern Germany (Dostal, 2018). The northern third of Germany is characterized with subsidence that fades from west to east near Poland. In the majority of Poland though, vertical motion is mainly between 1.5 and 3 mm/a of subsidence with local areas of much larger subsidence (Kowalczyk, 2006). More than 1 mm/a subsidence is found in southeastern Lithuania based on repeated leveling (Puziene et al., 2014).

5. Forebulge Dynamics Predicted by a State-of-the-Art Model of Glacial Isostatic Adjustment—An Example

Next, we will use a state-of-the-art GIA model to visualize the different observational findings, but also as guidance to understand the forebulge dynamics better. This recent state-of-the-art GIA model includes the effects of a spherical self-gravitating material-compressible Maxwell Earth. Lateral thickness variation of the elastic lithosphere and both lateral and radial variations in Earth rheology are included in the used Earth model HetML140 (Li & Wu, 2019), which assumes that mantle creep law is linear (however, in other state-of-the-art models, mantle rheology can be linear, nonlinear or composite rheology). The ice model considered is the ICE-6G_C global ice model (Argus et al., 2014; Peltier et al., 2015) and the ice growth phase before the LGM is also included. The sea-level equation solved includes the effects of rotational feedback, time-dependent coastlines, and grounding line migration (e.g., in Hudson Bay and places along the Labrador coast).

Using the 3D Earth model HetML140 with ICE-6G_C, we show modeled maps of migration of the forebulge front in North America in Figure 10a. An inward-migrating forebulge can be seen in Figure 10b, which plots the vertical displacement of the surface across a section along profile T1 in Figure 10a, indicating that the forebulge decays from 22 to 9 ka. But after about 9 ka, forebulge migration stops and the continual decay of the crest results in an apparent outward motion of the forebulge front. Figure 10b shows that the decay of the migrating forebulge in North America can result, due to the complex load history, in splitting of the forebulge region in more than one single displacement maximum. The complex ice melting and ocean loading in the Gulf of St. Lawrence can result in the brief development of a mini forebulge in front of the migrating forebulge (Figure 10a). These complex dynamics of the glacial forebulge will affect the sea level there.

Similarly, the forebulge front in Northern Europe moves inwards continuously and starts to decay at about 18 ka (Figures 10e and 10f). Comparing Figures 10b and 10f shows that the peak of the forebulge in Northern Europe at any time is generally lower than that in North America, especially when ice is present.

One may wonder if the location of the hinge line can be used to infer the present-day location of the forebulge front. Modeled maps of migration of the hinge line in North America (Figure 10c) show that the location and movement of the hinge line in North America is clearly related to the dynamics of the forebulge (Figures 10b and 10d). Some parts of the hinge line move inwards, while others move outwards between 22 and 15 ka, then it continues inwards until around 6 ka before moving slightly outwards again. The hinge line is located outside the forebulge front during the LGM. Then it moves close to the forebulge front around 9 ka, and since that time to the present, some parts of it move inside of the forebulge front. In Europe, the hinge line migrates continuously inward, starting at 18 ka (Figure 10g) and the hinge line is outside the forebulge front until about 3 ka, but is inside the forebulge front today (comp. Figures 10e and 10g). The forebulge decay rates were the largest at 9 ka (Figure 10h).

Comparing Figures 10a, 10c and 10e, 10g shows that the location of the present-day hinge line is generally close to, but not exactly the same as the location of the forebulge front. Thus, one may use the location of today's hinge line to estimate the location of the forebulge front but that is just an estimate only.

The results above are for a state-of-the-art GIA model with ICE-6G_C (Peltier et al., 2015) and Earth model HetML140 (Li & Wu, 2019) where the mantle creep law is linear. The results of another state-of-the-art GIA model (Huang et al., 2019) with a realistic ICE-C model and a layered Earth model with composite rheology and creep exponent $n = 3$ is shown in Figure 11. As described in Huang et al. (2019), the ice and Earth models are adjusted iteratively one-at-a-time until the predictions of the GIA model can fit the GIA observations in North America reasonably well. The final composite rheological model has different creep parameters in the UM and

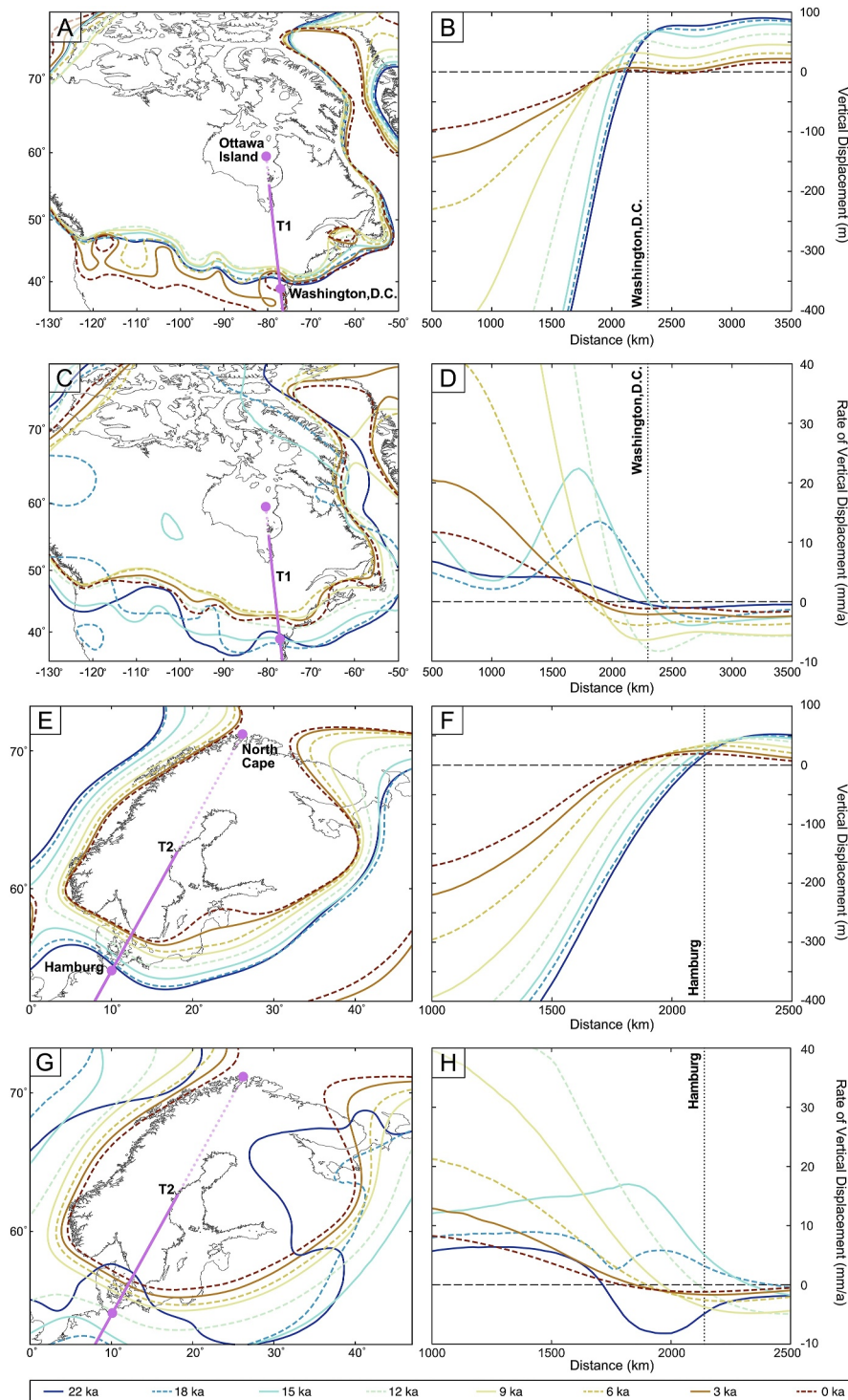


Figure 10. Glacial forebulge dynamics in North America and Northern Europe. The maps on the left column show the migration of the forebulge front (colored-coded lines in a and e) and the hinge lines for uplift rate (color-coded lines in c and g). The profiles in the right column show the time evolution of the radial displacement (b and f) and uplift rate (d and h) along the profiles T1 and T2 shown in the left column using the same color-coding. The results are predicted by the best material-compressible 3D glacial isostatic adjustment model HetML140 with ICE-6G_C (Peltier et al., 2015) in Li et al. (2020) and Li and Wu (2019).

LM, that is, $A_{UM} = 1.67 \times 10^{-35} \text{ Pa}^{-3} \text{ s}^{-1}$ and linear viscosity $\eta_{UM} = 3.00 \times 10^{21} \text{ Pa s}$ in the UM, and $A_{LM} = 8.87 \times 10^{-36} \text{ Pa}^{-3} \text{ s}^{-1}$ with $\eta_{LM} = 1.60 \times 10^{22} \text{ Pa s}$ in the LM. The ICE-C model is a modified version of the ICE-6G_C model with the growth phase of the ice sheet included and the sea-level equation solved. The ice

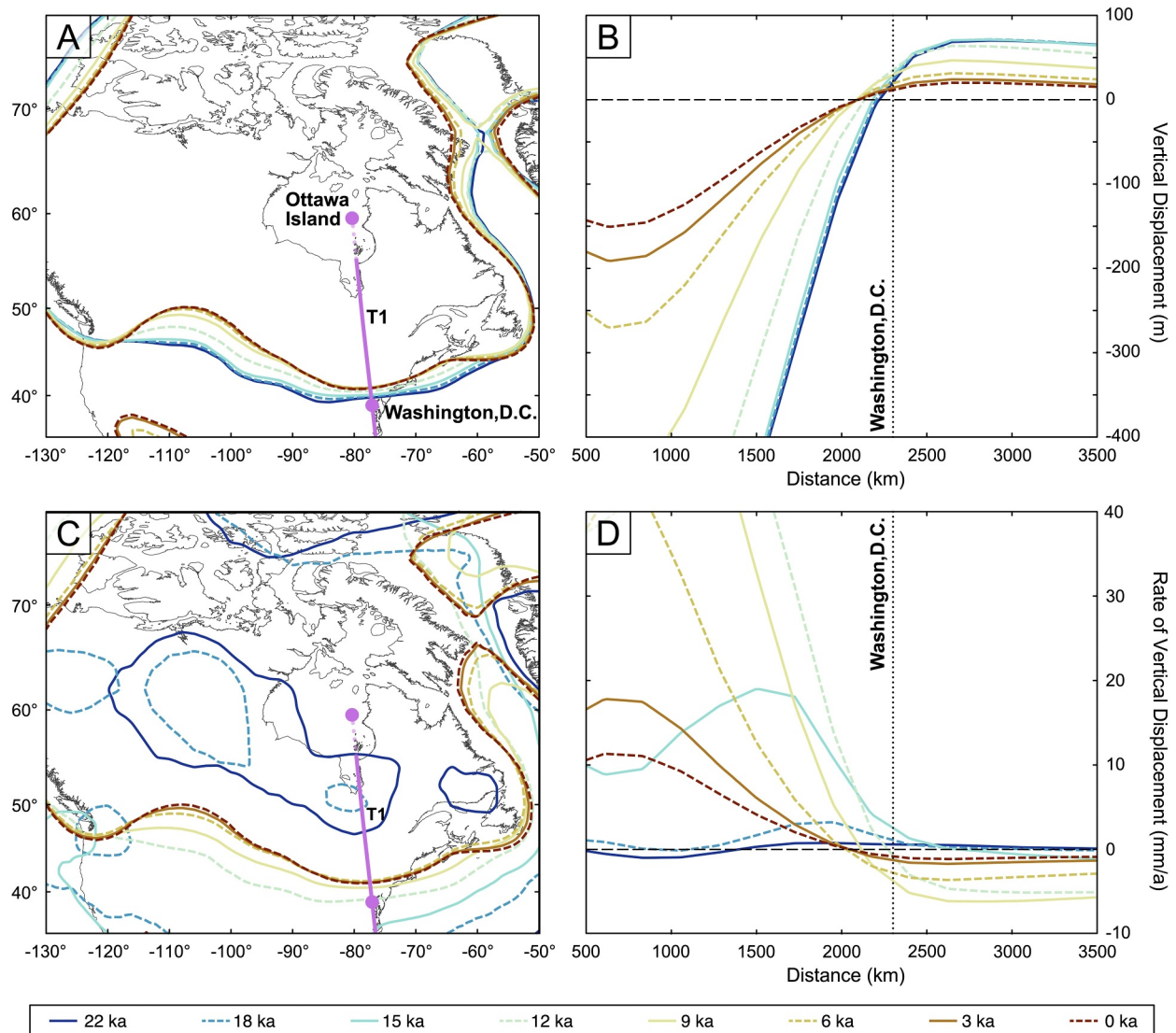


Figure 11. Same as Figures 10a–10d but based on results of Huang et al. (2019) using a glacial isostatic adjustment model with composite rheology and the ICE-C model (a modification of ICE-6G_C).

thickness history in ICE-C differs slightly from that in ICE-6G_C but the geological constraints (e.g., isochrone data on the migration of ice margin) were not altered.

The height evolution of the forebulge in Figure 11b beyond distance of around 2,500 km is similar to that of linear creep (Figure 10b) because linear creep was the dominant mechanism there. But below the ice load, the rebound motion is faster than that in Figure 10b, because non-linear creep being dominant, and the stress-induced lower effective viscosity results in faster uplift motion. Near the ice margin, the forebulge front migrates inwards from 18 to 12 ka BP because the ice margin in the ICE-C model migrates during that period. But soon after about 12 ka BP, the migration of the forebulge front stops and the height of the forebulge just decays in place—this is characteristic for non-linear creep (see Figure 6b).

In summary, two state-of-the-art GIA models with linear and composite rheologies, each with realistic ice models that include the migration of the ice margins during deglaciation, have been presented. These can serve as guidance to improve our understanding of forebulge dynamics during and after ice deglaciation.

6. Forebulge Effect on Sea-Level Change Pattern

As the GIA model solves the sea-level equation, it is possible to have a closer look at the forebulge effect on the global sea-level change, especially, how the forebulge decay affects estimates of future sea-level positions. During the early development of the sea-level equation, Clark et al. (1978) and Peltier et al. (1978) found that the pattern of global sea-level change can be divided into six major regions, each characterized by a unique RSL signature. Figure 12 exemplarily shows the RSL curves for these six zones which we calculated with our GIA model HetML140 with ICE-6G_C. RSL curves in **zone I** were glaciated areas, and their RSL curves are characterized by continuous emergence following deglaciation mainly due to postglacial rebound but for ocean sites close to the ice margin, the reduced gravitational attraction of the ice mass and the ocean water also causes a drop in sea level due to the migration of water from the near field of the ice sheets to the far field. RSL curves in **zone II** show continuous submergence due to the addition of melted water in the oceans and the decay of the forebulge, while the **transition** between zones I and II is also affected by the inward migration of the forebulge and thus show non-monotonic initial emergence followed by submergence (see Figure 12). In **zone III**, which is found in areas farther away from the ice centers, the RSL curves show submergence followed by small emergence a few thousand years ago. **Zone IV** and **zone V** are found in the far field at the back of the forebulge where the submergence before the end of deglaciation is due to the accumulation of meltwater. While zone IV is characterized by oceanic submergence followed by slight emergence and finally submergence again about 1–2 ka ago. On the other hand, the RSL curves in zone V show continuous emergence that begins immediately after the cessation of melting some 6 ka ago. The behavior in zone V is explained by the decay of the migrating forebulge which induces a flow of water, from both the far field and the deglaciation centers, to fill the regions vacated by the decaying forebulge. This ocean mass flow towards the back of the forebulge is called “equatorial ocean syphoning” (Mitrovica & Milne, 2002; Mitrovica & Peltier, 1991) and it dominates RSL variations in oceans of the far field at the end of deglaciation, when the volume of the ice sheets has not changed appreciably. This is manifested by the observed fall in sea level at oceanic islands in the far field after the end of deglaciation. Since these sites are located far from the continental margins, the fall in sea level after the end of deglaciation should not be confused with the effect of continental levering (e.g., Walcott, 1972) which is considered in zone VI. **Zone VI** is found along continental shorelines far from the centers of deglaciation and is due to the water loading of the adjacent ocean on the lithosphere—thus causing emergence due to “continental levering” or “crustal tilting.” The timing of emergence in zone VI is determined mainly by the local water loading and needs not be near the end of deglaciation as in zone V (see Figure 12). In summary, RSL curves in zones II, III, IV, and V are influenced by the dynamics at different parts of the glacial forebulge.

Note that the sea-level computation by Clark et al. (1978) and Peltier et al. (1978) is for a one-dimensional, non-rotating Earth where the coastlines do not change with time and only a few simple mantle viscosity models are considered. Also, the ice model used in these studies, ICE-1, had many assumptions: melting in the Antarctic ice sheet was ignored and the state of isostatic equilibrium was reached at the time of glacial maximum before deglaciation started. On the other hand, Mitrovica and Peltier (1991) used ICE-3G which includes melting in Antarctica, and the pseudo-spectral approach is used to solve the sea-level equation for a one-dimensional, non-rotating Earth with fixed coastlines to find the pattern of global sea-level change.

The pattern of the respective zones for our GIA model HetML140 with ICE-6G_C is shown in Figure 13. The RSL histories are computed on a regular $0.5 \times 0.5^\circ$ grid that spans the Earth's whole surface. Then, the RSL history at each grid location is inspected and a zone number is assigned according to its characteristic signature (see Figure 12). By giving each RSL location on the map a zone number, the map of the different zones can be contoured as shown in Figure 13. Note that **zone I** appears over the deglaciated areas in Antarctica, Patagonia, Laurentia, Greenland, Iceland, Fennoscandia and its extension into Svalbard, Barents Sea and Kara Sea. **Zone II** exists just outside zone I in both the northern and southern hemisphere—although in the northern hemisphere the extent is much farther away than in the southern hemisphere probably due to the greater volume of melted ice water there. Below 30° north and above 60° south, **zone V** occupies most of the ocean. Between zones II and V lie **zones III and IV**. This narrow band is dominated by zone III while zone IV only occurs in sporadic areas. These findings are different from that in Clark et al. (1978) and Peltier et al. (1978) where zones III and IV are much wider and zone V extends all the way south reaching Antarctica since their ICE-1 model did not include ice melting in the southern hemisphere. With the inclusion of melting in Antarctica and Patagonia, zones I to IV also appear in the southern oceans—although zones III and IV become very narrow, and zone V is pushed further north. Finally, zone VI, which is due to crustal tilting by local water loading, appears along the continental shoreline far from the centers of deglaciation.

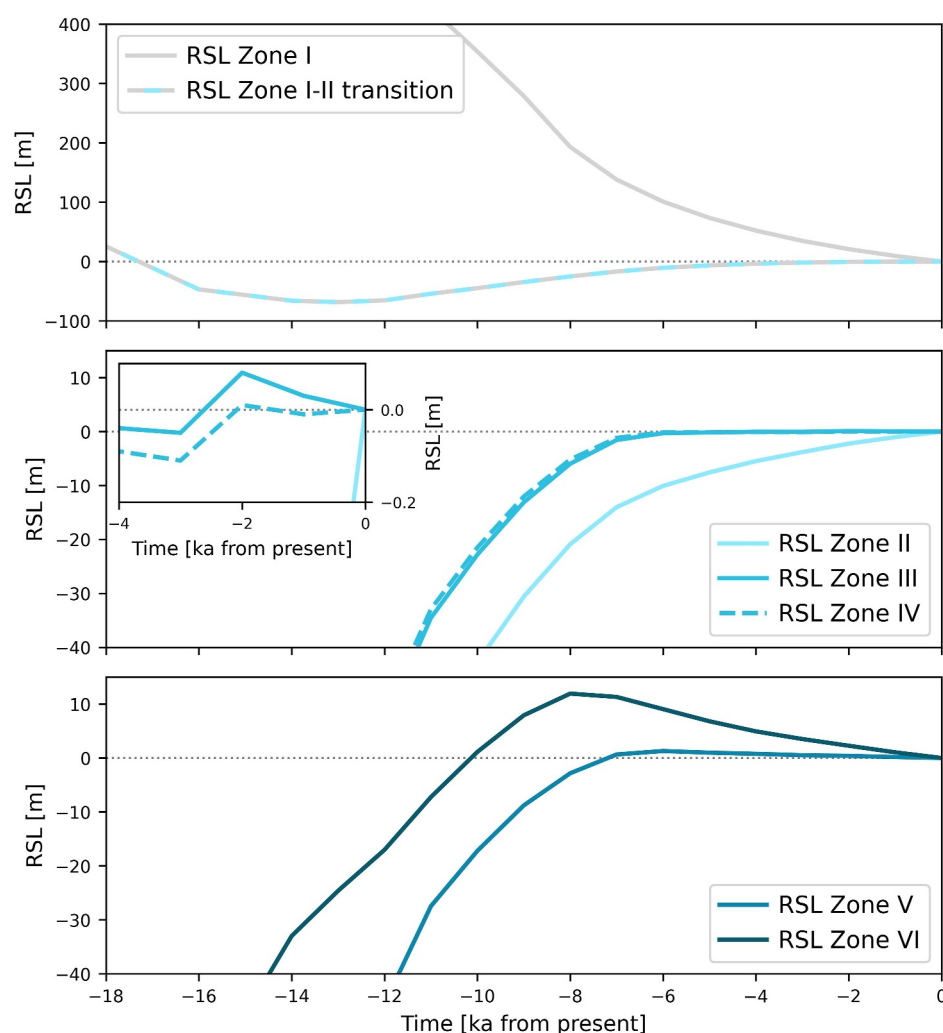


Figure 12. Typical pattern of relative sea level (RSL) signature associated with the various RSL zones as defined in Clark et al. (1978) and Peltier et al. (1978).

Overall, the geological RSL records are consistent with the sea-level change patterns derived from the GIA model (e.g., Engelhart & Horton, 2012; Khan et al., 2015, 2019; Tan et al., 2023), although some proxy records are affected by non-GIA processes (e.g., tectonics, compaction, post-depositional lowering), causing, e.g., that the mid-Holocene RSL highstands are not recorded in some areas in far-field continental shelves due to local to regional subsidence (e.g., Li et al., 2023; F. Wang et al., 2020; Zong, 2004).

This idea of a unique RSL signature associated with the various zones has been extended to the idea of a “sea-level fingerprint” for the rapid melting of a certain ice reservoir. Since rapid melting within a short time period (hundreds of years) is mostly sensitive to the elastic properties and not the viscous structure of the Earth, mostly the elastic response of the forebulge to the specific melting event is responsible for the sea-level fingerprint. Clark and Lingle (1977) were the first to model the sea-level changes associated with a uniform thinning of the West Antarctic Ice Sheet due to global warming. This and other similar studies of sea-level change, following a particular rapid melting pattern of ice reservoirs (Conrad & Hager, 1997; Mitrovica et al., 2001, 2011; Plag, 2006; Plag & Jüttner, 2001; Tamisiea et al., 2001), confirm that a distinctive sea-level fingerprint of the ice sheet can be obtained in principle. However, sea-level fingerprints are not easy to observe because of the large dynamic sea-level signals associated with ocean and atmosphere circulation (i.e., changing tides, currents and wind) and steric effects (i.e., changes in ocean volume due to density changes including both halosteric and thermosteric

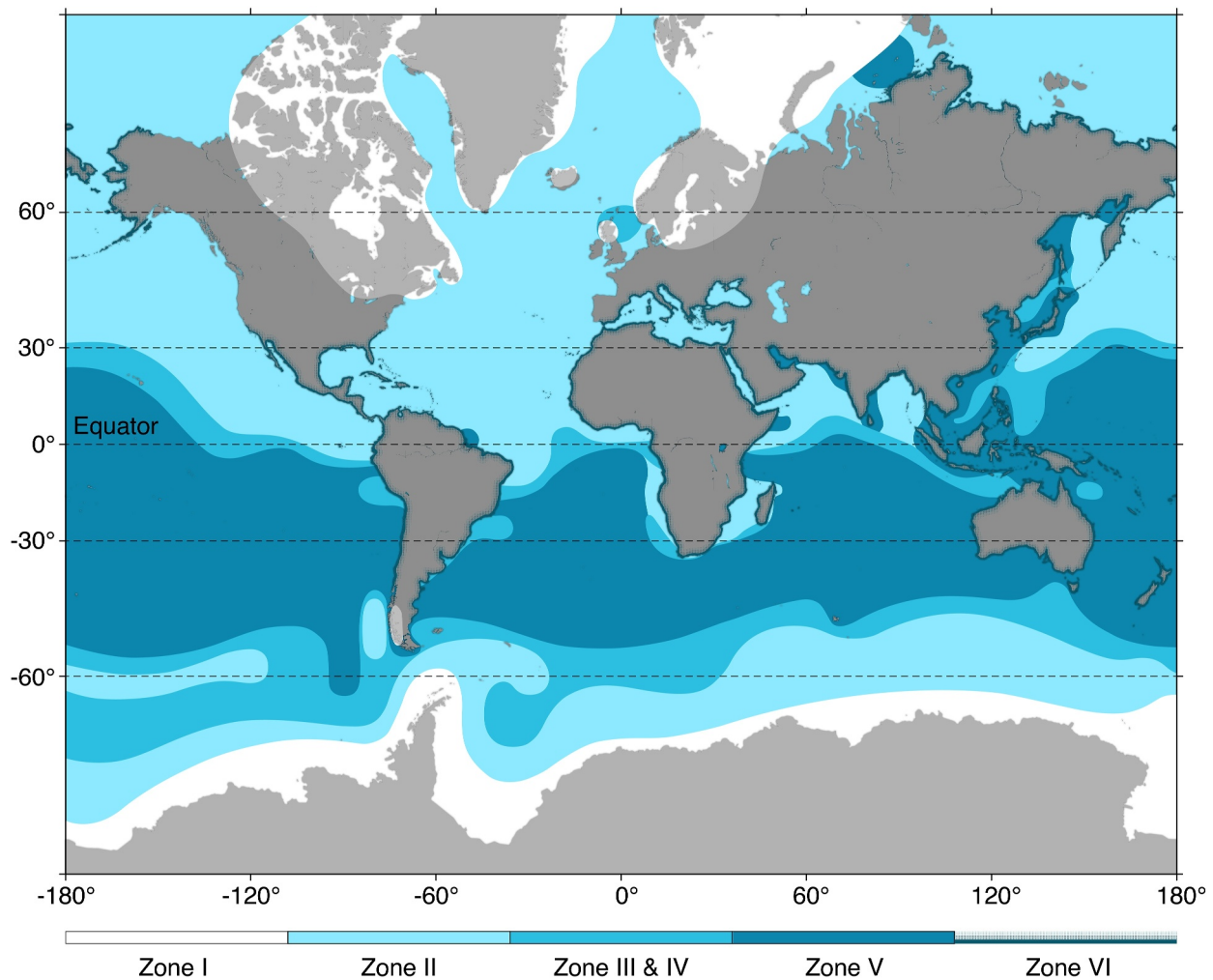


Figure 13. Map showing the locations of various relative sea level (RSL) zones predicted by a state-of-the-art glacial isostatic adjustment model consisting of 3D Earth model HetM140 with ICE-6G_C including growth cycle before last glacial maximum. The characteristics of the RSL zones are defined in Clark et al. (1978) and Peltier et al. (1978) and shown in Figure 12. See text for details.

variation). Adhikari et al. (2019) computed a GRACE (Gravity Recovery and Climate Experiment) based estimate of global sea-level fingerprints due to continental water mass changes. They suggested that future results from space altimetry mission when combined with GRACE based results would give the desired sea-level fingerprints. Coulson et al. (2022), who used 30 years of satellite altimetry data around the Greenland Ice Sheet and the ocean near Greenland, claimed to have the first detection of the sea-level fingerprint there. In short, sea-level fingerprints are determined by the motion of the forebulge produced by loading/unloading events in the last few hundred years, and are affected by the location, distribution, timing and rate of recent rapid ice melting events.

7. Stress Pattern of the Forebulge and the Termination of the Strain Rate-Stress Paradox

The deformation of the Earth due to glacial loads, as revealed from observed land uplift rate and RSL change, is also inducing an additional stress field, which we refer here as glacially induced stresses. These stresses are due to the bending of the lithosphere, the load itself and a process called stress migration (R. Steffen et al., 2021; Wu & Hasegawa, 1996a) which arises from relaxation in the viscoelastic mantle (see discussion in Section 3.2). Stresses due to the load only exist beneath the glacial load and vanish with it after the end of deglaciation. In contrast, stresses due to bending of the lithosphere and stress migration occur not only beneath the load but also prevail outside the glaciated area especially in the forebulge region. In addition, the bending stresses relax much more

slowly even after the ice sheet is gone. This is important as glacially induced stresses can lead to the reactivation of pre-existing faults and thus have a direct impact on the seismic hazard potential (Muir-Wood, 2000).

Such a reactivation of faults due to stress-field changes in response to the decay of the Weichselian ice sheet in Europe was already recognized in the 1970s (Lagerbäck, 1978; Möner, 1978). Most of these studies focused on areas below the former ice sheet in Europe (Arvidsson, 1996; Dehls et al., 2000; Gregersen, 2002; Kukkonen et al., 2010; Lagerbäck & Sundh, 2008; Mattila et al., 2019; Mikko et al., 2015; Ojala et al., 2017; Olesen et al., 2021; Palmu et al., 2015; Smith et al., 2014; Sutinen et al., 2014, 2021) and North America (Adams, 1989; Adams & Brooks, 2021; Brooks & Adams, 2020; Sauber et al., 2021). However, it has been recognized earlier that recent earthquakes in Denmark cluster in a belt parallel to the former ice margin (Daly, 1934), pointing to a relationship between glacially induced crustal movement even outside the ice sheet and seismicity (Gergersen, 2002; Gergersen et al., 1996; Sandersen et al., 2021). Over the last decade, geological evidence was found for a comparable fault reactivation in the forebulge region (Brandes et al., 2015; Craig et al., 2023; Houtgast et al., 2005; Müller et al., 2020, 2021; van Balen et al., 2019, 2021, 2024; Štěpančíková et al., 2022), which was previously assumed to be unaffected by glacially triggered earthquakes. Moreover, the forebulge has been a tectonically and seismically active area during glaciation and deglaciation (Brandes et al., 2011; Pisarska-Jamroży et al., 2018, 2019, 2021, 2022, 2024; Sandersen et al., 2021; Štěpančíková et al., 2022). The findings of fault reactivation due to glacially induced stresses were supported by numerical simulations (Grollimund & Zoback, 2001; Hampel & Hetzel, 2006; Hampel et al., 2009, 2010; Hetzel & Hampel, 2005; Ivins et al., 2003; P. Johnston et al., 1998; Klemann & Wolf, 1998; Lund, 2015; Lund & Näslund, 2009; R. Steffen & Steffen, 2021; R. Steffen et al., 2014a, 2014b, 2014c, 2019; Turpeinen et al., 2008; Wu, 1997, 1998; Wu & Hasegawa, 1996a, 1996b; Wu & Johnston, 2000; Wu et al., 1998) that analyze the interplay of glacial loading and fault activity. The glacial stresses are combined with tectonic stresses to understand the change in the fault stability margin (FSM, e.g., A. C. Johnston, 1989; Wu & Hasegawa, 1996a, 1996b) or the Coulomb failure stress (CFS; R. Steffen & Steffen, 2021; R. Steffen et al., 2020). For Europe, numerical simulations of changes in the FSM or Coulomb failure stresses were done in connection with paleoseismological studies (Brandes et al., 2012, 2018; Pisarska-Jamroży et al., 2019, 2022, 2024; Seidel et al., 2025) and the analysis of historic seismicity (Brandes et al., 2015) and recent seismicity (Brandes et al., 2019).

Further investigations show that deglaciation seismicity apparently wandered from the Netherlands over northern Germany to northern Denmark, thus partially concerning formerly ice-free areas. This is interpreted as a consequence of forebulge migration (Van Balen et al., 2021). Some parts of the forebulge might become active 10 to 20 ka after the end of the deglaciation making the forebulge an interesting area to understand the relationship between normal intraplate seismicity and glacially triggered seismicity.

The direction of the stresses differs depending on their location with respect to the ice sheet as well as with depth. As typical for bending stresses in an elastic plate, half of the plate is contracted, the other half is extended, and these two domains are separated by the neutral plane (Figure 14a; e.g., Beer et al., 2015; Turcotte & Schubert, 2014). The neutral plane between the two domains is free of stress and the stress increases away from the neutral axis (Turcotte & Schubert, 2014; Watts, 2001). Below the ice sheet compressional stresses prevail in the upper half of the lithospheric plate and extensional stresses in the lower half (Stewart et al., 2000) (Figure 14a). In the forebulge area, the bending induces extensional stresses in the upper half of the lithosphere and compressional stresses in the lower half (Grollimund & Zoback, 2003). The area with maximum tension typically lies outside the edge of the load but inside the forebulge front (R. Steffen et al., 2021).

In addition to the location dependency of the stresses, the stress distribution is also time dependent. During loading and forebulge growth, the upper half of the lithosphere (in the forebulge area) undergoes extension, whereas the lower half is characterized by contraction (Grollimund & Zoback, 2003; Stewart et al., 2000) (Figure 14a). During the decay of the ice sheet, the load is reduced and the forebulge decays (e.g., Barrell, 1915; Daly, 1934; Nansen, 1922; Van Bemmelen & Berlage, 1934) (Figure 14b). The above scenario assumes that the initial state of the lithosphere before the onset of glaciation was in isostatic equilibrium. On the other hand, if the equilibrium state was attained at LGM instead of before the onset of glaciation, the state of stress would be different (Figure 14c) and this will lead to the “postglacial strain rate-stress paradox.” Furthermore, this assumption of an equilibrium state at LGM has many problems and is not supported by observations. This issue will be discussed in detail below.

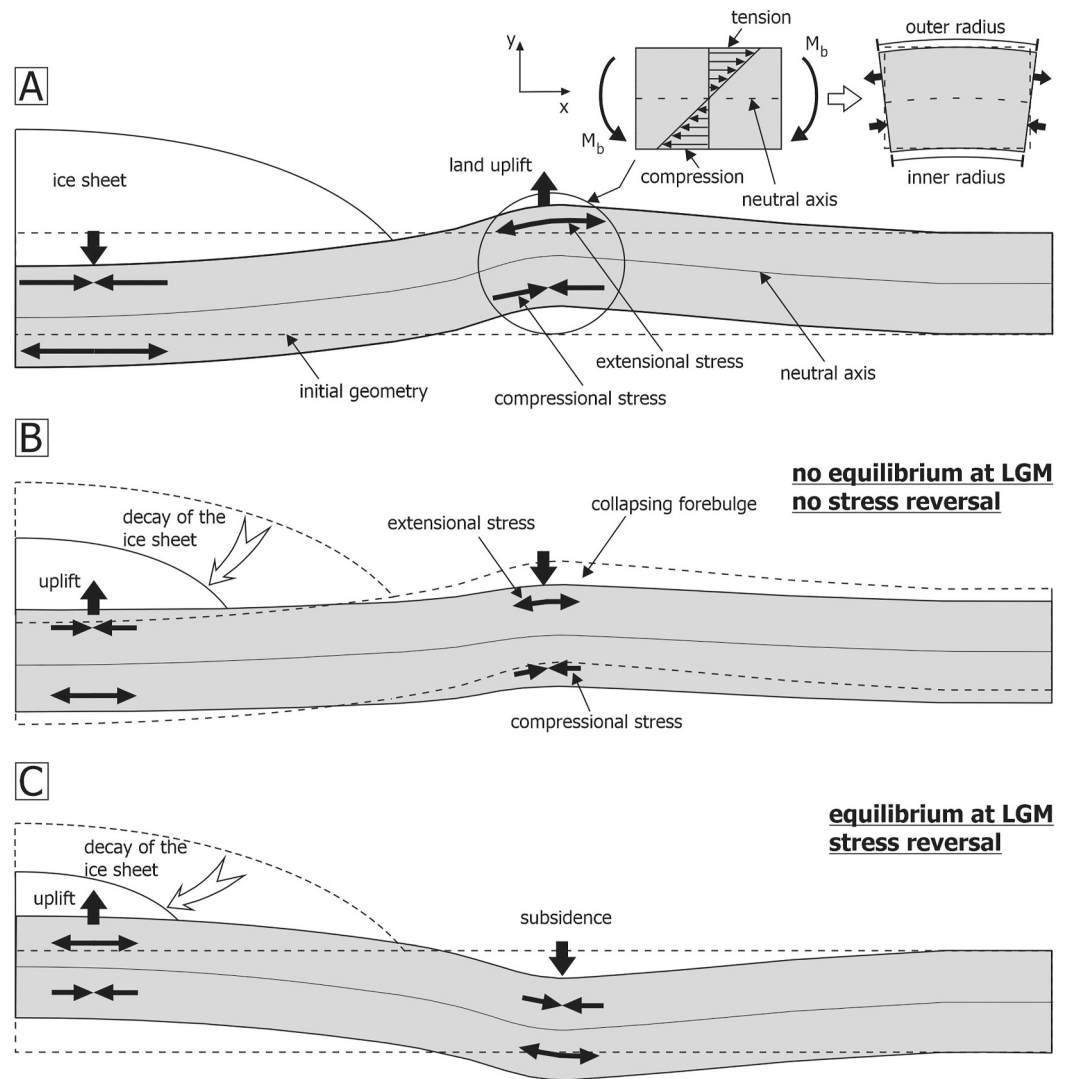


Figure 14. The stress pattern of the glacial forebulge. Major terms are presented for the forebulge development during glacialiation (a) and deglaciation (b) and (c). Two possible stress behaviors during deglaciation are shown for comparison: no stress reversal (b) and stress reversal (c). The black arrows indicate the stress directions induced by the load. Compressional stresses are marked by arrows pointing at each other and extensional stresses by divergent arrows. The initial geometry is shown as dashed line indicating the state before glacialiation (a) and at glacial maximum in (b) and (c). The figure is based on Stewart et al. (2000), Grollmund and Zoback (2003), and Keiding et al. (2015).

As pointed out in Section 2.2, in the early 1970s, our knowledge of ice history before the LGM was inadequate, thus many studies of GIA assumed that isostatic equilibrium was achieved at the LGM, and crustal deformation and stress or sea-level changes were computed relative to this equilibrium state at LGM. To attain isostatic equilibrium at the LGM, one usually argues that the period of glacial loading is long relative to the relaxation time of the mantle which is proportional to its viscosity. Since the time scale of glacial loading was not adequately known at the time but was suspected to be of the order of tens of thousands of years, the assumption of isostatic equilibrium at the LGM seemed to be reasonable. This is underpinned by the assumption that the relaxation of the mantle, inferred from RSL data, is on the order of a few thousand years, much shorter than the glacialiation period.

Based on this assumption, Stein et al. (1989) considered the Earth's surface and the base of the lithosphere to be flat at LGM—otherwise some forces are required to maintain the topography and thus violate the assumption of an equilibrium state. Now, ice removal after LGM is equivalent to applying a negative load on the deglaciated

region, so land uplift should occur in the deglaciated areas and slightly outside it, while subsidence should result in a depression area around the forebulge outside the ice margin (Haskell, 1935; McGinnis, 1968; Van Bemmelen & Berlage, 1934) (Figure 14c). The uplift motion underneath the deglaciated areas should cause the land to up-dome, resulting in tensional stresses induced near the top of the lithosphere (see Figure 14c). On the other hand, for areas outside the deglaciated areas, the depression over the forebulge area should result in compression near the top of the lithosphere.

Since GNSS measurements in Fennoscandia show divergent motion from the center of rebound, proponents of isostatic equilibrium at the LGM interpreted that the strain-rate is tensional in the deglaciated areas today. Furthermore, land uplift is also observed today by GNSS data in Fennoscandia—agreeing with the prediction of Stein et al. (1989) inside the deglaciated area. However, seismic activities in the centers of rebound within Fennoscandia and Laurentia point to a compressional state, which is contrary to the tensional state implied by GNSS data. This has led to the “strain rate-stress paradox in GIA” (Craig et al., 2016; Grosset et al., 2023). In the rest of this subsection, we will show that this assumption of isostatic equilibrium at the LGM is not supported by observational data outside the ice margin.

Walcott (1970) found that the RSL observations cannot be adequately described by a simple exponential decay curve to describe the relaxation time of the Earth (with a single relaxation time) but require the sum of two or more exponential decays. This is consistent with the theoretical description of the viscoelastic relaxation of a Maxwell Earth using normal modes (e.g., Wu & Peltier, 1982). There, the harmonic deformation of a laterally homogenous Earth can be written as the weighted sum of several exponential decay curves of different relaxation times, and each term represents the relaxation of a normal mode. The normal modes arise because of the elastic and viscoelastic structures of the Earth, for example, the M modes are due to the density contrast between mantle layers. The C modes, L modes and T modes are due to the core structure, the lithosphere and viscoelastic transition, respectively. The M0 mode is usually the dominant mode and has relaxation times of the order of thousands of years, but other modes (e.g., M1, M2) have much longer relaxation times—some exceeding the period of many glacial cycles. These modes with very long relaxation times prevent the mantle from reaching isostatic equilibrium during a glacial cycle. In addition, the very high viscosity near the top of the lithosphere prevents the lithosphere from doing the same. This is supported by the observation that the lithosphere is strong enough that mountains of short wavelengths (so supported by the elastic lithosphere) can reside on it for millions of years without sinking into the mantle. In view of that the loading period is relatively short compared to the long relaxation times in the mantle and the lithosphere, it is not likely that isostatic equilibrium can be reached at LGM.

As discussed above, under the assumption of isostatic equilibrium at LGM, Stein et al. (1989) showed that applying a negative load on the deglaciated region will result in a depression outside the ice margin. This means that instead of a forebulge, one should find a “trough” there. So, the existence of a forebulge outside the ice margin can be used to argue against the assumption of isostatic equilibrium at LGM. Also, from the discussion above, the uplift motion within the ice margin of Fennoscandia predicted by Stein et al. (1989) and observed by GNSS data never resulted in an uplifted dome that gives tensional strain-rate there. Instead, a trough filled with water which is called the Gulf of Bothnia exist. Actually, if one starts with today's surface topography of the Gulf of Bothnia and use the observed land uplift to work backwards and find the surface topography at LGM, then one will find that an even deeper trough existed at LGM. This is contrary to the assumption of a flat Earth surface at LGM and violates the assumption of isostatic equilibrium because non-equilibrium forces are required to maintain the deep trough.

The problem with the argument of tensional strain-rate from GNSS uplift rates is that the measurements are relative to the immediate past, and not measured relative to the LGM or before the onset of glaciation. In other words, the “uplift motion” and the “tension” is not the whole motion but is only a perturbed motion or perturbed strain-rate from some “background” state at LGM. If isostatic equilibrium and a flat surface was attained before the onset of glaciation, then ice loading will cause a surface point within the ice margin to move inwards towards the ice center and downwards, so that the upper part of the lithosphere below will be in a state of compression. Thus, the background state at LGM would be the deep trough and a state of compression. After deglaciation started at LGM, this surface point will move back towards its initial position (so upwards and outwards), while the upper part of the lithosphere below will be less compressive relative to the initial state. Relative to any time after deglaciation, the restoring motion can be viewed as a tensional perturbation to the much larger compressional state achieved at LGM.

In short, observations, especially those that support the presence of a forebulge, so far do not support the “strain rate-stress paradox in GIA” nor the assumption of isostatic equilibrium at the LGM. The forebulge has thus been key evidence for termination of the strain rate-stress paradox.

8. Conclusions and Outlook

Studies of the glacial forebulge, an area outside the former glaciated area, and its dynamics have been ongoing for more than a hundred years. This paper reviews the progress in understanding glacial forebulge and its dynamics and points out areas that need more consistent data gathering and more GIA modeling work.

Knowledge of the forebulge history is crucial for understanding the evolution of fluvial networks and sea-level signals derived from the geological record, as well as to estimate future sea-level rise. The location, height and dynamic behavior of the forebulge are controlled by the flexural rigidity of the lithosphere, by mantle viscosity structures, and by the ice sheet geometry and history. The glacial forebulge is thus a very important lithospheric feature driven by GIA.

Today, the channel-flow model with rigid lower boundary has been abandoned. However, the study of micro-physics of mantle rocks and temperature variations in the mantle implies that a viscosity contrast exist between the UM and LM. The magnitude of the viscosity contrast determines if mantle flow is purely deep-flow or a mixture between deep- and channel-like flow. Conversely, the time evolution of the height and width of the glacial forebulge and the direction of its migration can be used to constrain the viscosity structure in the mantle and better understand mantle dynamics and global sea-level change pattern.

The dynamics of the glacial forebulge also affect the uplift pattern around the ice margin and the migration of the hinge line with zero vertical velocity. Thus, by monitoring the movement of the hinge line, one can learn about forebulge dynamics, which can also affect the movement of water flow on land and ocean water movement through gravitational attraction with the migrating and decaying forebulge. In other words, glacial forebulge dynamics affects sea-level change, water resource management and coastal engineering. In addition, it can also affect the stress changes below the ice load and neighboring areas including the forebulge. These stress changes play an important role in the triggering of seismicity in these areas.

The forebulge in North America has its most prominent effects along both the western and eastern coasts where it causes a complex sea-level history since the LGM. It becomes visible in geological records and in geodetic measurements although it is difficult to identify at the west coast due to tectonic activity there. The regional differences in the uplift behavior especially along the east coast must be considered in the adaptation planning to climate change-induced sea-level rise.

The forebulge related to the last (Weichselian) glaciation in Europe is yet hard to determine, especially with geodetic techniques (e.g., Kierulf et al., 2021). Our modeling examples show that the present-day subsidence of (much) less than 2 mm/a is at the current detection level of geodetic techniques (0.2–0.3 mm/a uncertainty for stations with more than 10 years of observations and before applying further corrections, see Kierulf et al., 2021) or, in the worst case, is already close to zero. In northeastern Europe, the forebulge cannot be traced yet due to missing geodetic data but is evident in RSL data. In Norway, the forebulge is located offshore which hampers its identification in both geodetic and RSL data. Furthermore, the expected GIA-induced horizontal motion of GNSS stations in the forebulge is below 0.2 mm/a, which is around the current detection level (Kierulf et al., 2021). In addition, a highly accurate plate motion model would be then needed for removing the plate motion sufficiently to extract these small values that may help identify forebulge migration.

In view of the above, there are many opportunities for future research. This review mentioned some areas where the observational data of a forebulge are still lacking or appear to be conflicting. These are areas where more high-quality data and GIA modeling work are needed.

High-resolution airborne Lidar (Light Detection and Ranging) based digital elevation models are available for many areas and Interferometric synthetic-aperture radar (InSAR)-based Ground Motion Services are already or soon to be installed, for example, the European Ground Motion Service (EGMS, Crosetto et al., 2021). These data sets can be used among others to map the river network in more detail to derive subsidence processes. In addition, longitudinal river profiles can be used to identify areas where the river has not reached an equilibrium, which can point to vertical elevation changes. Precise terrestrial GNSS measurements and satellite data, if they provide

uncertainties in the vertical velocity of better than 0.3 mm/a, should be utilized to enhance the understanding of forebulge evolution and may help to delineate its subsidence signal from the subsidence caused by groundwater extraction or natural gas recovery. Accurate GNSS measurements of the forebulge decay and migration can help to develop better mantle flow models that in turn can be used to improve current GIA models. Investigations with GIA models, for example, should use 3D spherical models with self-gravitation, compressibility and high spatial resolution in the forebulge area, thereby applying the latest generation of ice models. For example, Reusen et al. (2023) showed that compressibility in GIA models is needed if one wants to investigate GIA-induced horizontal motion. Furthermore, it will be profitable to have an integrated study that interprets all the observations and modeling results related to the forebulge (including e.g., height and direction of forebulge movement, uplift pattern, RSL changes, stress changes and seismicity, etc.) to get a more coherent view of its dynamics. Research should also be carried out on the forebulge of previous glaciations in North America and Europe. This of course needs geological tools.

Conflict of Interest

The authors declare no conflicts of interest relevant to this study.

Data Availability Statement

No new data were used in this study. The GNSS data in Figure 9 are taken from Peltier et al. (2015) and Kierulf et al. (2021). The 3D GIA modeling results are available through Li and Wu (2019), Li et al. (2020), and Huang et al. (2019).

Glossary

Channel-flow:

When a low viscosity asthenospheric layer is sandwiched between the lithosphere and a high viscosity, more rigid mantle layer below, a channel is formed. If the flow in this low viscosity channel is mainly horizontal, then the flow is called channel-flow. This is illustrated in Figure 3b where the bottom of the channel/asthenosphere flows like the pressure induced laminar flow in a pipe (or Poiseuille flow).

Deep-flow:

Deep-flow occurs if mantle viscosity in a mantle layer underneath the ice load does not increase rapidly with depth so that there is nothing to impede the deep penetration of the vertical motion of the flow. Such mainly vertical flow (as illustrated in Figure 3b) can penetrate much deeper into the Earth than that in channel-flow.

DHHN92/DHHN2016:

Deutsches Haupthöhennetz with versions from 1992 to 2016; German height system that provides a precise reference for elevations across Germany. It is based on precise leveling and accounts for geoid undulations, ensuring consistent height measurements relative to sea level.

Effective thickness of the lithosphere:

This is the thickness of the mechanically strong outer shell of the Earth that does not relax to become a fluid within the duration of surface loading. For the study of glacial loading and unloading, the thickness of this layer is typically of the order of 100 km or more under old and cold cratons but can vary laterally over continental margins or under oceans due to lateral changes in mantle temperature.

Flexural rigidity:	The flexural rigidity is a material property that determines how an elastic beam or plate reacts to an applied force for example, represented by a load. The flexural rigidity is controlled by the Young's modulus, the Poisson's ratio, and the cube of the elastic thickness. The higher the flexural rigidity, the less an elastic beam is bend by a given load, but the wider is the zone that is deformed under the load.
Forebulge crest:	The forebulge crest is the area of the forebulge where its maximum height is reached (see Figure 1).
Forebulge front:	If a flat Earth is subjected with a load, the forebulge front line represents the closest line outside the load where there is no vertical deflection when compared to the state before loading occurs (see Figure 1). It separates the area that is pushed down under and near the load from the uplifted area of the forebulge. After the onset of deglaciation, the forebulge front may coincide with the hinge line and thus may be detectable with GNSS observations.
Forebulge migration:	Forebulge migration is the lateral motion of the forebulge especially during and after ice deglaciation—that is, whether the forebulge migrates inwards, outwards or remain stationary—as these may be diagnostic of mantle rheology.
Glacial isostatic adjustment/GIA:	Glacial isostatic adjustment (GIA) is the adjustment of the Earth that leads to a new re-equilibration state due to the redistribution of surface ice and ocean masses and the flow of mantle rocks driven by the growth and decay of large ice sheets on the Earth's surface. The uplift of former glaciated areas is part of GIA and is commonly named postglacial rebound. But GIA is more than just postglacial uplift and sea-level change in previously glaciation areas—the adjustment process actually involves the whole Earth during the past, present and future. Next to radial and tangential motion, changes in sea levels, the Earth's gravity field and rotational motion, GIA also involves changes in lithospheric bending and the state of stress inside the Earth. Hence, it envelopes Earth's response to past glaciations as well as recent melting processes, for example, in Greenland and Antarctica. In the past, GIA was also called “glacial isostasy,” but “isostasy” is usually used to describe the equilibrium state of the crust and mountains as they float on the mantle. On the other hand, the term “isostatic adjustment” emphasizes more on the dynamics of the adjustment process that occurs over many thousands of years.
GNSS:	The Global Navigation Satellite System (GNSS) is a satellite-based system that allows to derive the precise height and geographical position of a point on the Earth's surface. GNSS is the umbrella term for different navigations systems like the NAVSTAR GPS (USA) or the Galileo system (Europe).

Hinge line:	The hinge line is the line that separates the region, which rises after the decay of the ice sheet began, from the region that subsides since the onset of deglaciation. The hinge line is the zero-line, along which, no vertical movements at the Earth's surface occur. It may be detectable with GNSS observations. The location of the hinge line and of the forebulge front may not coincide. Hence, the hinge line can only serve as a rough estimate of location of the forebulge front.
IGb08:	Realization of the International Terrestrial Reference Frame (ITRF) based on data from the International GNSS Service (IGS). It provides precise coordinates and velocities for a global network of GNSS stations. Adopted in 2011.
IGS08:	Specific realization of the International GNSS Service (IGS) reference frame, derived from the IGS network data and released in 2008. It provides accurate coordinates and velocities for GNSS stations worldwide.
ITRF2000/ITRF2005/ITRF2008/ITRF2014:	International Terrestrial Reference Frame, a global reference frame used for precise positioning and navigation. The versions 2000, 2005, 2008, and 2014 represent different realizations of the ITRF, each based on data from various geodetic techniques, including GNSS measurements. Each iteration reflects advancements in geodetic measurements and techniques, contributing to better understanding of Earth's dynamics. The most recent version is ITRF2020-u2023.
Last glacial maximum/LGM:	The last glacial maximum (LGM) is the maximum extent of the last (Wisconsinan/Weichselian) glaciation that was reached between 26,000 and 18,000 years before present.
Maxwell Earth:	The concept of the Maxwell Earth describes the observation that the Earth consists of different materials, which have a time-dependent deformation behavior. Maxwell materials behave elastic, if a force is applied on a short term, but flows viscously, if a force is applied over a longer time (longer than the Maxwell time of the material). The duration of the Maxwell time depends on the material properties like shear modulus and viscosity.
NAD83v70VG:	A specific version of the North American Datum of 1983 (NAD83) that incorporates adjustments made in 2010, with "VG" indicating that it includes "Vertical Grid" adjustments for improved vertical accuracy.
Peripheral bulge:	Another term for forebulge.
Peripheral forebulge:	Another term for forebulge, but actually a pleonasm.
Postglacial rebound:	see glacial isostatic adjustment
Stream longitudinal profile/longitudinal river profile:	A stream longitudinal profile/longitudinal river profile is a diagram showing the profile of a river depicting the change in elevation of its channel bed over the entire length of the river from its origin to its mouth.

Acknowledgments

We would like to thank Jutta Winsemann and David Tanner for discussion, and Pingping Huang for providing the modeling results shown in Figure 11. We are grateful for the helpful reviews of Volker Klemann and two anonymous reviewers. Rebekka Steffen is supported by a project grant from Rymdstyrelsen (Swedish National Space Board; Grant 2018-00140). Tanghua Li is supported by the Ministry of Education, Singapore, under its MOE AcRF Tier 3 Award MOE2019-T3-1-004, and MOE AcRF Tier 2 Award MOE-T2EP50120-0007. This work is Earth Observatory of Singapore contribution 513. Open Access funding enabled and organized by Projekt DEAL.

References

- Abe-Ouchi, A., Saito, F., Kawamura, K., Raymo, M., Okuno, J., Takahashi, K., & Blatter, H. (2013). Insolation-driven 100,000-year glacial cycles and hysteresis of ice-sheet volume. *Nature*, 500(7461), 190–193. <https://doi.org/10.1038/nature12374>
- Adams, J. (1989). Postglacial faulting in eastern Canada: Nature, origin and seismic hazard implications. *Tectonophysics*, 163(3–4), 323–331. [https://doi.org/10.1016/0040-1951\(89\)90267-9](https://doi.org/10.1016/0040-1951(89)90267-9)
- Adams, J., & Brooks, G. (2021). The search for glacially induced faults in eastern Canada. In H. Steffen, O. Olesen, & R. Sutinen (Eds.), *Glacially-triggered faulting* (pp. 341–352). Cambridge University Press. <https://doi.org/10.1017/9781108779906.025>
- Adhikari, S., Ivins, E. R., Frederikse, T., Landerer, F. W., & Caron, L. (2019). Sea-level fingerprints emergent from GRACE mission data. *Earth Systems Science Data*, 11(2), 629–646. <https://doi.org/10.5194/essd-11-629-2019>
- Albrecht, T., Bagge, M., & Klemann, V. (2024). Feedback mechanisms controlling Antarctic glacial-cycle dynamics simulated with a coupled ice sheet–solid Earth model. *The Cryosphere*, 18(9), 4233–4255. <https://doi.org/10.5194/tc-18-4233-2024>
- Anderson, R. C. (1988). Reconstruction of preglacial drainage and its diversion by earliest glacial forebulge in the upper Mississippi valley region. *Geology*, 16(3), 254–257. [https://doi.org/10.1130/0091-7613\(1988\)016<0254:ROPDAI>2.3.CO;2](https://doi.org/10.1130/0091-7613(1988)016<0254:ROPDAI>2.3.CO;2)
- Argus, D. F. (2007). Defining the translational velocity of the reference frame of Earth. *Geophysical Journal International*, 169(3), 830–838. <https://doi.org/10.1111/j.1365-246X.2007.03344.x>
- Argus, D. F., & Peltier, W. R. (2010). Constraining models of postglacial rebound using space geodesy: A detailed assessment of model ICE-5G (VM2) and its relatives. *Geophysical Journal International*, 181, 697–723. <https://doi.org/10.1111/j.1365-246X.2010.04562.x>
- Argus, D. F., Peltier, W. R., Drummond, R., & Moore, A. W. (2014). The Antarctica component of postglacial rebound model ICE-6G_C (VM5a) based on GPS positioning, exposure age dating of ice thicknesses, and relative sea level histories. *Geophysical Journal International*, 198(1), 537–563. <https://doi.org/10.1093/gji/ggu140>
- Arvidsson, R. (1996). Fennoscandian earthquakes: Whole crustal rupturing related to postglacial rebound. *Science*, 274(5288), 744–746. <https://doi.org/10.1126/science.274.5288.744>
- Bagge, M., Klemann, V., Steinberger, B., Latinović, M., & Thomas, M. (2021). Glacial-isostatic adjustment models using geodynamically constrained 3D Earth structures. *Geochemistry, Geophysics, Geosystems*, 22(11), e2021GC009853. <https://doi.org/10.1029/2021GC009853>
- Baichtal, J. F., Lesnek, A. J., Carlson, R. J., Schmuck, N. S., Smith, J. L., Landwehr, D. J., & Briner, J. P. (2021). Late Pleistocene and early Holocene sea-level history and glacial retreat interpreted from shell-bearing marine deposits of southeastern Alaska, USA. *Geosphere*, 17(6), 1590–1615. <https://doi.org/10.1130/GES02359.1>
- Baranskaya, A. V., Khan, N. S., Romanenko, F. A., Roy, K., Peltier, W. R., & Horton, B. P. (2018). A postglacial relative sea-level database for the Russian Arctic coast. *Quaternary Science Reviews*, 199, 188–205. <https://doi.org/10.1016/j.quascirev.2018.07.033>
- Barnhardt, W. A., Gehrels, W. R., Belknap, D. F., & Kelley, J. T. (1995). Late Quaternary relative sea-level change in the western Gulf of Maine: Evidence for a migrating glacial forebulge. *Geology*, 23(4), 317–320. [https://doi.org/10.1130/0091-7613\(1995\)023<0317:LQSLC>2.3.CO;2](https://doi.org/10.1130/0091-7613(1995)023<0317:LQSLC>2.3.CO;2)
- Barrell, J. (1915). Factors in movements of the strand line. *Journal of the Washington Academy of Sciences*, 5, 413–420.
- Beer, F. P., Johnston, E. R., DeWolf, J. T., & Mazurek, D. F. (2015). *Mechanics of materials* (7th ed., p. 831). McGraw-Hill Education.
- Bell, T., Daly, J., Batterson, M. J., Liverman, D. G. E., Shaw, J., & Smith, I. R. (2005). Late Quaternary relative sea-level change on the west coast of Newfoundland. *Géographie Physique et Quaternaire*, 59(2–3), 129–140. <https://doi.org/10.7202/014751ar>
- Bills, B. G., & James, T. S. (1996). Late Quaternary variations in relative sea level due to glacial cycle polar wander. *Geophysical Research Letters*, 23(21), 3023–3026. <https://doi.org/10.1029/96GL02886>
- Bird, P. (1991). Lateral extrusion of lower crust from under high topography, in the isostatic limit. *Journal of Geophysical Research*, 96(B6), 10275–10286. <https://doi.org/10.1029/91JB00370>
- Bogusz, J., Klos, A., & Pokonieczny, K. (2019). Optimal strategy of a GPS position time series analysis for post-glacial rebound investigation in Europe. *Remote Sensing*, 11(10), 1209. <https://doi.org/10.3390/rs11101209>
- Brandes, C., Plenefisch, T., Tanner, D. C., Gestermaun, N., & Steffen, H. (2019). Evaluation of deep crustal earthquakes in northern Germany—Possible tectonic causes. *Terra Nova*, 31(2), 83–93. <https://doi.org/10.1111/ter.12372>
- Brandes, C., Polom, U., & Winsemann, J. (2011). Reactivation of basement faults: Interplay of ice-sheet advance, glacial lake formation and sediment loading. *Basin Research*, 23, 53–64. <https://doi.org/10.1111/j.1365-2117.2010.00468.x>
- Brandes, C., Steffen, H., Sandersen, P. B. E., Wu, P., & Winsemann, J. (2018). Glacially induced faulting along the NW segment of the Sorgenfrei-Tornquist Zone, northern Denmark: Implications for neotectonics and Lateglacial fault-bound basin formation. *Quaternary Science Reviews*, 189, 149–168. <https://doi.org/10.1016/j.quascirev.2018.03.036>
- Brandes, C., Steffen, H., Steffen, R., & Wu, P. (2015). Intraplate seismicity in northern Central Europe is induced by the last glaciation. *Geology*, 43(7), 611–614. <https://doi.org/10.1130/G36710.1>
- Brandes, C., Winsemann, J., Roskosch, J., Meinsen, J., Tanner, D. C., Frechen, M., et al. (2012). Activity along the Osning thrust in Central Europe during the Lateglacial: Ice-sheet and lithosphere interactions. *Quaternary Science Reviews*, 38, 49–62. <https://doi.org/10.1016/j.quascirev.2012.01.021>
- Brevik, I., & Jensen, O. (1992). Fennoscandian glacial depression: On the lithospheric forebulge problem. *Theoretical Physics Seminar in Trondheim*, 5, 1–36.
- Briggs, R. D., Pollard, D., & Tarasov, L. (2014). A data-constrained large ensemble analysis of Antarctic evolution since the Eemian. *Quaternary Science Reviews*, 103, 91–115. <https://doi.org/10.1016/j.quascirev.2014.09.003>
- Brooks, G. R., & Adams, J. (2020). A review of evidence of glacially-induced faulting and seismic shaking in eastern Canada. *Quaternary Science Reviews*, 228, 106070. <https://doi.org/10.1016/j.quascirev.2019.106070>
- Brotchie, J. F., & Silvester, R. (1969). On crustal flexure. *Journal of Geophysical Research*, 22, 5240–5252. <https://doi.org/10.1029/JB074i022p05240>
- Bürgmann, R., & Dresen, G. (2008). Rheology of the lower crust and upper mantle: Evidence from rock mechanics, geodesy and field observations. *Annual Review of Earth and Planetary Sciences*, 36, 531–567. <https://doi.org/10.1146/annurev.earth.36.031207.124326>
- Burov, E. B. (2011). Rheology and strength of the lithosphere. *Marine and Petroleum Geology*, 28(8), 1402–1443. <https://doi.org/10.1016/j.marpetgeo.2011.05.008>
- Burov, E. B., & Diamant, M. (1995). The effective elastic thickness (T_e) of continental lithosphere: What does it really mean? *Journal of Geophysical Research*, 100, 3905–3927.
- Busschers, F. S., Kasse, C., van Balen, R. T., Vandenberghe, J., Cohen, K. M., Weerts, H. J. T., et al. (2007). Late Pleistocene evolution of the Rhine-Meuse system in the southern North Sea Basin: Imprints of climate change, sea-level oscillation and glacio-isostasy. *Quaternary Science Reviews*, 26(25–28), 3216–3248. <https://doi.org/10.1016/j.quascirev.2007.07.013>

- Cambiotti, G., Klemann, V., & Sabadini, R. (2013). Compressible viscoelastodynamics of a spherical body at long timescales and its isostatic equilibrium. *Geophysical Journal International*, 193(3), 1071–1082. <https://doi.org/10.1093/gji/ggt026>
- Castellanos, J. C., Perry-Houts, J., Clayton, R. W., Kim, Y. H., Stanciu, A. C., Niday, B., & Humphreys, E. (2020). Seismic anisotropy reveals crustal flow driven by mantle vertical loading in the Pacific NW. *Science Advances*, 6(28), eabb0476. <https://doi.org/10.1126/sciadv.abb0476>
- Cathles, L. M. (1975). *The viscosity of the earth's mantle* (p. 386). Princeton University Press.
- Cathles, L. M. (1980). Interpretation of postglacial isostatic adjustment Phenomena in terms of mantle rheology. In N.-A. Möller (Ed.), *Earth rheology, isostasy and eustasy* (Vol. 599, pp. 11–43). John Wiley & Sons.
- Chester, S. J., Austermann, J., D'Andrea, W. J., Lloyd, A. J., & Creel, R. C. (2024). On the origin of Holocene sea-level transgressions in formerly glaciated regions. *Quaternary Science Reviews*, 345, 108986. <https://doi.org/10.1016/j.quascirev.2024.108986>
- Clague, J., Harper, J. R., Hebda, R. J., & Howes, D. E. (1982). Late Quaternary sea levels and crustal movements, coastal British Columbia. *Canadian Journal of Earth Sciences*, 19(3), 597–618. <https://doi.org/10.1139/e82-048>
- Clark, J. A., & Lingle, C. S. (1977). Future sea-level changes due to West Antarctic ice sheet fluctuations. *Nature*, 269(5625), 206–209. <https://doi.org/10.1038/269206a0>
- Clark, J. A., Farrell, W. E., & Peltier, W. R. (1978). Global changes in postglacial sea level: A numerical calculation. *Quaternary Research*, 9(3), 265–287. [https://doi.org/10.1016/0033-5894\(78\)90033-9](https://doi.org/10.1016/0033-5894(78)90033-9)
- Conrad, C. P., & Hager, B. H. (1997). Spatial variations in the rate of sea level rise caused by present-day melting of glaciers and ice sheets. *Geophysical Research Letters*, 24(12), 1503–1506. <https://doi.org/10.1029/97GL01338>
- Coulson, S., Dangendorf, S., Mitrovica, J. X., Tamisiea, M. E., Pan, L., & Sandwell, D. T. (2022). A detection of the sea level fingerprint of Greenland Ice Sheet melt. *Science*, 377, 1550–1554. <https://doi.org/10.1126/science.abo0926>
- Craig, T. J., Calais, E., Fleitout, L., Bollinger, L., & Scotti, O. (2016). Evidence for the release of long-term tectonic strain stored in continental interiors through intraplate earthquakes. *Geophysical Research Letters*, 43(13), 6826–6836. <https://doi.org/10.1002/2016GL069359>
- Craig, T. J., Calais, E., Fleitout, L., Bollinger, L., & Scotti, O. (2023). Time-variable strain and stress rates induced by Holocene glacial isostatic adjustment in continental interiors. *Tectonophysics*, 854, 229815. <https://doi.org/10.1016/j.tecto.2023.229815>
- Creel, R. C., Austermann, J., Khan, N. S., D'Andrea, W. J., Balascio, N., Dyer, B., et al. (2022). Postglacial relative sea level change in Norway. *Quaternary Science Reviews*, 282, 107422. <https://doi.org/10.1016/j.quascirev.2022.107422>
- Crosetto, M., Solari, L., Balasis-Levinson, J., Bateson, L., Casagli, N., Frei, M., et al. (2021). Deformation monitoring at European scale: The COPERNICUS Ground motion Service. In *The International Archives of the Photogrammetry, Remote Sensing and Spatial Information Sciences, XLIII-B3-2021* (pp. 141–146). <https://doi.org/10.5194/isprs-archives-XLIII-B3-2021-141-2021>
- Daly, R. A. (1934). *The changing world of the ice age* (p. 271). Yale University Press.
- Davis, J. L., & Mitrovica, J. X. (1996). Glacial isostatic adjustment and the anomalous tide gauge record of eastern North America. *Nature*, 379(6563), 331–333. <https://doi.org/10.1038/379331a0>
- de Wit, K., van de Wal, R. S. W., & Cohen, K. M. (2022). Reconstructing large scale differential subsidence in the Netherlands using a spatio-temporal 3D paleo-groundwater level interpolation, 2022. *EGU General Assembly*, 2022, 8350. <https://doi.org/10.5194/egusphere-egu22-8350>
- Dehls, J. F., Olesen, O., Olsen, L., & Blikra, L. H. (2000). Neotectonic faulting in northern Norway; the Storaagurra and Nordmannvikdalen postglacial faults. *Quaternary Science Reviews*, 19(14–15), 1447–1460. [https://doi.org/10.1016/S0277-3791\(00\)00073-1](https://doi.org/10.1016/S0277-3791(00)00073-1)
- Dewey, J. F. (2005). Orogeny can be very short. *Proceedings of the National Academy of Sciences*, 102(43), 15286–15293. <https://doi.org/10.1073/pnas.0505516102>
- Dostal, J. (2018). Geodetic activities in Germany. In *National Report of Germany at the PosKEN Communication workshop 2018*. Retrieved from https://eurogeographics.org/wp-content/uploads/2018/04/13_National_report_Germany.pdf
- Dyke, A. S., & Peltier, W. R. (2000). Forms, response times and variability of relative sea-level curves, glaciated North America. *Geomorphology*, 32(3–4), 315–333. [https://doi.org/10.1016/S0169-555X\(99\)00102-6](https://doi.org/10.1016/S0169-555X(99)00102-6)
- Engelhart, S. E., & Horton, B. P. (2012). Holocene sea-level database for the Atlantic coast of the United States. *Quaternary Science Reviews*, 54, 12–25. <https://doi.org/10.1016/j.quascirev.2011.09.013>
- Engelhart, S. E., Horton, B. P., Douglas, B. C., Peltier, W. R., & Törnqvist, T. E. (2009). Spatial variability of late Holocene and 20th century sea-level rise along the Atlantic coast of the United States. *Geology*, 37(12), 1115–1118. <https://doi.org/10.1130/G30360A.1>
- Farrell, W. E., & Clark, J. A. (1976). On postglacial sea level. *Geophysical Journal International*, 46(3), 647–667. <https://doi.org/10.1111/j.1365-246X.1976.tb01252.x>
- Fjeldskaar, W. (1994). The amplitude and decay of the glacial forebulge in Fennoscandia. *Norwegian Journal of Geology*, 74, 2–8.
- Fjeldskaar, W., & Bondevik, S. (2020). The Early-Mid Holocene transgression (Tapes) at the Norwegian coast—Comparing observations with numerical modelling. *Quaternary Science Reviews*, 242, 106435. <https://doi.org/10.1016/j.quascirev.2020.106435>
- Fjeldskaar, W., & Cathles, L. M. (1991). The present rate of uplift of Fennoscandia implies a low-viscosity asthenosphere. *Terra Nova*, 3(4), 393–400. <https://doi.org/10.1111/j.1365-3121.1991.tb00168.x>
- García-Artola, A., Stephan, P., Cearreta, A., Kopp, R. E., Khan, N. S., & Horton, B. P. (2018). Holocene sea-level database from the Atlantic coast of Europe. *Quaternary Science Reviews*, 196, 177–192. <https://doi.org/10.1016/j.quascirev.2018.07.031>
- Gornitz, V., & Seeber, L. (1990). Vertical crustal movements along the East Coast, North America, from historic and late Holocene sea level data. *Tectonophysics*, 178(2–4), 127–150. [https://doi.org/10.1016/0040-1951\(90\)90143-V](https://doi.org/10.1016/0040-1951(90)90143-V)
- Goslin, J., Van Vliet Lanoë, B., Spada, G., Bradley, S., Tarasov, L., Neill, S., & Suanez, S. (2015). A new Holocene relative sea-level curve for western Brittany (France): Insights on isostatic dynamics along the Atlantic coasts of North-western Europe. *Quaternary Science Reviews*, 129, 341–365. <https://doi.org/10.1016/j.quascirev.2015.10.029>
- Goudarzi, M. A., Coccard, M., & Santerre, R. (2016). Present-day 3D velocity field of eastern north America based on continuous GPS observations. *Pure and Applied Geophysics*, 173(7), 2387–2412. <https://doi.org/10.1007/s00024-016-1270-7>
- Gowan, E. J., Zhang, X., Khosravi, S., Rovere, A., Stocchi, P., Hughes, A. L., et al. (2021). A new global ice sheet reconstruction for the past 80 000 years. *Nature Communications*, 12(1), 1199. <https://doi.org/10.1038/s41467-021-21469-w>
- Gregersen, S. (2002). Earthquakes and change of stress since the ice age in Scandinavia. *Bulletin of the Geological Society of Denmark*, 49, 73–78.
- Gregersen, S., Leth, J., Lind, G., & Lykke-Andersen, H. (1996). Earthquake activity and its relationship with geologically recent motion in Denmark. *Tectonophysics*, 257(2–4), 265–273. [https://doi.org/10.1016/0040-1951\(95\)00193-X](https://doi.org/10.1016/0040-1951(95)00193-X)
- Grollimund, B., & Zoback, M. D. (2001). Did deglaciation trigger intraplate seismicity in the New Madrid seismic zone? *Geology*, 29(2), 175–178. [https://doi.org/10.1130/0091-7613\(2001\)029<0175:BDTISI>2.0.CO;2](https://doi.org/10.1130/0091-7613(2001)029<0175:BDTISI>2.0.CO;2)
- Grollimund, B., & Zoback, M. D. (2003). Impact of glacially induced stress changes on fault-seal integrity offshore Norway. *AAPG Bulletin*, 87, 493–506. <https://doi.org/10.1306/08010401134>
- Grosset, J., Mazzotti, S., & Vernant, P. (2023). Glacial-isostatic-adjustment strain rate–stress paradox in the Western Alps and impact on active faults and seismicity. *Solid Earth*, 14(10), 1067–1081. <https://doi.org/10.5194/se-14-1067-2023>

- Hampel, A., & Hetzel, R. (2006). Response of normal faults to glacial-interglacial fluctuations of ice and water masses on Earth's surface. *Journal of Geophysical Research*, 111(B6), B06406. <https://doi.org/10.1029/2005JB004124>
- Hampel, A., Hetzel, R., Maniatis, G., & Karow, T. (2009). Three-dimensional numerical modeling of slip rate variations on normal and thrust fault arrays during ice cap growth and melting. *Journal of Geophysical Research*, 114(B8), B08406. <https://doi.org/10.1029/2008JB006113>
- Hampel, A., Karow, T., Maniatis, G., & Hetzel, R. (2010). Slip rate variations on faults during glacial loading and post-glacial unloading: Implications for the viscosity structure of the lithosphere. In C. Pascal, I. S. Stewart, & B. L. A. Vermeersen (Eds.), *Neotectonics, Seismicity and Stress in Glaciated Regions*, *Journal of the Geological Society, London* (Vol. 167, pp. 385–399). <https://doi.org/10.1144/0016-76492008-137>
- Han, D., & Wahr, J. (1989). Post-glacial rebound analysis for a rotating earth, in slow deformations and Transmission of stress in the earth. In S. Cohen & P. Vanicek (Eds.), *Slow deformation and transmission of stress in the earth, geophysical monograph series* (Vol. 49, pp. 1–6). <https://doi.org/10.1029/GM049p0001>
- Harvey, T. C., Hamlington, B. D., Frederikse, T., Nerem, R. S., Piecuch, C. G., Hammond, W. C., et al. (2021). Ocean mass, sterodynamic effects, and vertical land motion largely explain US coast relative sea level rise. *Communications Earth & Environment*, 2(1), 233. <https://doi.org/10.1038/s43247-021-00300-w>
- Haskell, N. A. (1935). The motion of a viscous fluid under a surface load. *Physics*, 6(8), 265–269. <https://doi.org/10.1063/1.1745329>
- Hays, J. D., Imbrie, J., & Shackleton, N. J. (1976). Variations in the earth's orbit: Pacemaker of the ice ages. *Science*, 194(4270), 1121–1132. <https://doi.org/10.1126/science.194.4270.1121>
- Hertz, H. (1884). Ueber das Gleichgewicht schwimmender elastischer Platten. *Annalen der Physik*, 258(7), 449–455. <https://doi.org/10.1002/andp.18842580711>
- Hetényi, M. (1950). A general solution for the bending of beams on an elastic foundation of arbitrary continuity. *Journal of Applied Physics*, 21(1), 55–58. <https://doi.org/10.1063/1.1699420>
- Hetzel, R., & Hampel, A. (2005). Slip rate variations on normal faults during glacial-interglacial changes in surface loads. *Nature*, 435, 81–84. <https://doi.org/10.1038/nature03562>
- Hijma, M. P., Bradley, S. L., Cohen, K. M., van der Wal, W., Barlow, N. L. M., Blank, B., et al. (2025). Global sea-level rise in the early Holocene revealed from North Sea peats. *Nature*, 639(8055), 652–657. <https://doi.org/10.1038/s41586-025-08769-7>
- Horton, B. P., Peltier, W. R., Culver, S. J., Drummond, R., Engelhart, S. E., Kemp, A. C., et al. (2009). Holocene sea-level changes along the North Carolina coastline and their implications for glacial isostatic adjustment models. *Quaternary Science Reviews*, 28(17–18), 1725–1736. <https://doi.org/10.1016/j.quascirev.2009.02.002>
- Houtgast, R. F., Van Balen, R. T., & Kasse, C. (2005). Late Quaternary evolution of the Feldbiss fault (Roer valley Rift system, the Netherlands) based on trenching, and its potential relation to glacial unloading. *Quaternary Science Reviews*, 24(3–4), 491–510. <https://doi.org/10.1016/j.quascirev.2004.01.012>
- Huang, P., Wu, P., & Steffen, H. (2019). In search of an ice history that is consistent with composite rheology in Glacial Isostatic Adjustment modeling. *Earth and Planetary Science Letters*, 517, 26–37. <https://doi.org/10.1016/j.epsl.2019.04.011>
- Ivins, E. R., Caron, L., Adhikari, S., Larour, E., & Scheinert, M. (2020). A linear viscoelasticity for decadal to centennial time scale mantle deformation. *Reports on Progress in Physics*, 83(10), 106801. <https://doi.org/10.1088/1361-6633/aba346>
- Ivins, E. R., James, T. S., & Klemann, V. (2003). Glacial isostatic stress shadowing by the Antarctic ice sheet. *Journal of Geophysical Research*, 108(B12), 2560. <https://doi.org/10.1029/2002JB002182>
- Jamieson, T. F. (1882). On the cause of the depression and re-elevation of the land during the glacial period. *Geological Magazine*, 9, 400–407. <https://doi.org/10.1017/s0016756800172061>
- Johnston, A. C. (1989). The effect of large ice sheets on earthquake genesis. In S. Gregersen, & P. W. Basham (Eds.), *Earthquakes at North-Atlantic Passive Margins: Neotectonics and postglacial rebound*. NATO ASI series (Vol. 266, 581–599). Springer. https://doi.org/10.1007/978-94-009-2311-9_34
- Johnston, P. (1993). The effect of spatially non-uniform water loads on predictions of sea level change. *Geophysical Journal International*, 114(3), 615–634. <https://doi.org/10.1111/j.1365-246X.1993.tb06992.x>
- Johnston, P., Wu, P., & Lambeck, K. (1998). Dependence of horizontal stress magnitude on load dimension in glacial rebound models. *Geophysical Journal International*, 132(1), 41–60. <https://doi.org/10.1046/j.1365-246x.1998.00387.x>
- Karato, S., & Wu, P. (1993). Rheology of the upper mantle: A synthesis. *Science*, 260(5109), 771–778. <https://doi.org/10.1126/science.260.5109.771>
- Karegar, M. A., Dixon, T. H., & Engelhart, S. E. (2016). Subsidence along the Atlantic coast of North America: Insights from GPS and late Holocene relative sea level data. *Geophysical Research Letters*, 43(7), 3126–3133. <https://doi.org/10.1002/2016GL068015>
- Karegar, M. A., Dixon, T. H., Malservisi, R., Kusche, J., & Engelhart, S. E. (2017). Nuisance flooding and relative sea-level rise: The importance of present-day land motion. *Scientific Reports*, 7(1), 11197. <https://doi.org/10.1038/s41598-017-11544-y>
- Kaufmann, G., Wu, P., & Ivins, E. R. (2005). Lateral viscosity variations beneath Antarctica and their implications on regional rebound motions and seismotectonics. *Journal of Geodynamics*, 39(2), 165–181. <https://doi.org/10.1016/j.jog.2004.08.009>
- Kaufmann, G., Wu, P., & Li, G. (2000). Glacial isostatic adjustment in Fennoscandia for a laterally heterogeneous earth. *Geophysical Journal International*, 143(1), 262–273. <https://doi.org/10.1046/j.1365-246x.2000.00247.x>
- Kaufmann, G., Wu, P., & Wolf, D. (1997). Some effects of lateral heterogeneities in the upper mantle on postglacial land uplift close to continental margins. *Geophysical Journal International*, 128(1), 175–187. <https://doi.org/10.1111/j.1365-246X.1997.tb04078.x>
- Keiding, M., Kreemer, C., Lindholm, C. D., Gradmann, S., Olesen, O., & Kierulf, H. P. (2015). A comparison of strain rates and seismicity for Fennoscandia: Depth dependency of deformation from glacial isostatic adjustment. *Geophysical Journal International*, 202(2), 1021–1028. <https://doi.org/10.1093/gji/ggv207>
- Kennett, B. L. N., & Tkalcic, H. (2008). Dynamic earth: Crustal and mantle heterogeneity. *Australian Journal of Earth Sciences*, 55(3), 265–279. <https://doi.org/10.1080/08120090701883042>
- Ketelaar, V. B. H. (2009). Subsidence due to hydrocarbon production in the Netherlands. In V. B. H. Ketelaar (Ed.), *Satellite radar interferometry. Remote sensing and digital image processing* (Vol. 14, pp. 7–26). Springer Netherlands. https://doi.org/10.1007/978-1-4020-9428-6_2
- Khan, N. S., Ashe, E., Shaw, T. A., Vacchi, M., Walker, J., Peltier, W. R., et al. (2015). Holocene relative sea-level changes from near-intermediate- and far-field locations. *Current Climate Change Reports*, 1(4), 247–262. <https://doi.org/10.1007/s40641-015-0029-z>
- Khan, N. S., Horton, B. P., Engelhart, S., Rovere, A., Vacchi, M., Ashe, E. L., et al. (2019). Inception of a global atlas of sea levels since the Last Glacial Maximum. *Quaternary Science Reviews*, 220, 359–371. <https://doi.org/10.1016/j.quascirev.2019.07.016>
- Kiden, P., Denys, L., & Johnston, P. (2002). Late Quaternary sea-level change and isostatic and tectonic land movements along the Belgian-Dutch North Sea coast: Geological data and model results. *Journal of Quaternary Science*, 17(5–6), 535–546. <https://doi.org/10.1002/jqs.709>
- Kierulf, H. P., Steffen, H., Barletta, V. R., Lidberg, M., Johansson, J., Kristiansen, O., & Tarasov, L. (2021). A GNSS velocity field for geophysical applications in Fennoscandia. *Journal of Geodynamics*, 146, 101845. <https://doi.org/10.1016/j.jog.2021.101845>

- Kierulf, H. P., Steffen, H., Simpson, M. J. R., Lidberg, M., Wu, P., & Wang, H. (2014). A GPS velocity field for Fennoscandia and a consistent comparison to glacial isostatic adjustment models. *Journal of Geophysical Research: Solid Earth*, 119(8), 6613–6629. <https://doi.org/10.1002/2013JB010889>
- Klemann, V., & Wolf, D. (1998). Modelling of stresses in the Fennoscandian lithosphere induced by Pleistocene glaciations. *Tectonophysics*, 294(3–4), 291–303. [https://doi.org/10.1016/S0040-1951\(98\)00107-3](https://doi.org/10.1016/S0040-1951(98)00107-3)
- Klemann, V., & Wolf, D. (1999). Implications of a ductile crustal layer for the deformation caused by the Fennoscandian ice sheet. *Geophysical Journal International*, 139(1), 216–226. <https://doi.org/10.1046/j.1365-246X.1999.00936.x>
- Klemann, V., Wu, P., & Wolf, D. (2003). Compressible viscoelasticity: Stability of solutions for homogeneous plane-earth models. *Geophysical Journal International*, 153(3), 569–585. <https://doi.org/10.1046/j.1365-246X.2003.01920.x>
- Kowalczyk, K. (2006). New model of the vertical crustal movements in the area of Poland. *Geodezija i Kartografija*, 32(4), 83–87. <https://doi.org/10.1080/13921541.2006.9636702>
- Kremer, C., Hammond, W. C., & Blewitt, G. (2018). A robust estimation of the 3-D intraplate deformation of the North American plate from GPS. *Journal of Geophysical Research: Solid Earth*, 123(5), 4388–4412. <https://doi.org/10.1029/2017JB015257>
- Kuchar, J., & Milne, G. A. (2015). The influence of viscosity structure in the lithosphere on predictions from models of glacial isostatic adjustment. *Journal of Geodynamics*, 86, 1–9. <https://doi.org/10.1016/j.jog.2015.01.002>
- Kukkonen, I. T., Olesen, O., Ask, M. V. S., & PFDP Working Group. (2010). Postglacial faults in Fennoscandia: Targets for scientific drilling (Vol. 132, pp. 71–81). <https://doi.org/10.1080/11035891003692934>
- Lagerbäck, R. (1978). Neotectonic structures in northern Sweden. *Geologiska Föreningens i Stockholm Förhandlingar*, 100(3), 263–269. <https://doi.org/10.1080/11035897809452533>
- Lagerbäck, R., & Sundh, M. (2008). Early Holocene faulting and Paleoseismicity in northern Sweden. In *SGU research paper*, C386 (pp. 1–80).
- Lahtinen, S., Jivall, L., Häkli, P., Kall, T., Kollo, K., Kosenko, K., et al. (2019). Densification of the ITRF2014 position and velocity solution in the Nordic and Baltic countries. *GPS Solutions*, 23(4), 95. <https://doi.org/10.1007/s10291-019-0886-3>
- Lambeck, K. (1997). Sea-level change along the French Atlantic and Channel coasts since the time of the last glacial maximum. *Palaeogeography, Palaeoclimatology, Palaeoecology*, 129(1–2), 1–22. [https://doi.org/10.1016/S0031-0182\(96\)00061-2](https://doi.org/10.1016/S0031-0182(96)00061-2)
- Lambeck, K., & Nakiboglu, S. M. (1980). Seamount loading and stress in the ocean lithosphere. *Journal of Geophysical Research*, 85, 6403–6418. <https://doi.org/10.1029/JB086iB08p06961>
- Lambeck, K., Rouby, H., Purcell, A., Sun, Y., & Sambridge, M. (2014). Sea level and global ice volumes from the last glacial maximum to the Holocene. *Proceedings of the National Academy of Sciences of the United States of America*, 111(43), 15296–15303. <https://doi.org/10.1073/pnas.1411762111>
- Lau, H. C. P., Austermann, J., Holtzman, B. K., Havlin, C., Lloyd, A. J., Book, C., & Hopper, E. (2021). Frequency dependent mantle viscoelasticity via the complex viscosity: Cases from Antarctica. *Journal of Geophysical Research: Solid Earth*, 126(11), e2021JB022622. <https://doi.org/10.1029/2021JB022622>
- Lau, N., Borsa, A. A., & Becker, T. W. (2020). Present-day crustal vertical velocity field for the contiguous United States. *Journal of Geophysical Research: Solid Earth*, 125(10), e2020JB020066. <https://doi.org/10.1029/2020JB020066>
- Leorri, E., Cearreta, A., & Milne, G. (2012). Field observations and modeling of Holocene sea-level changes in the southern Bay of Biscay: Implications for understanding current rates of relative sea-level change and vertical land motion along the Atlantic coast of SW Europe. *Quaternary Science Reviews*, 42, 59–73. <https://doi.org/10.1016/j.quascirev.2012.03.014>
- Letham, B., Fedje, D., Hebda, C. F. G., Dyck, A., Stafford, J., Hutchinson, I., et al. (2024). Postglacial relative sea level histories of northern Vancouver Island, Canada. *Quaternary Science Reviews*, 326, 108415. <https://doi.org/10.1016/j.quascirev.2023.108415>
- Li, T., & Wu, P. (2019). Laterally heterogeneous lithosphere, asthenosphere and sub-lithospheric properties under Laurentia and Fennoscandia from glacial isostatic adjustment. *Geophysical Journal International*, 216(3), 1633–1647. <https://doi.org/10.1093/gji/ggy475>
- Li, T., Chua, S., Tan, F., Khan, N. S., Shaw, T. A., Majewski, J., et al. (2023). Glacial isostatic adjustment modelling of the mid-Holocene sea-level highstand of Singapore and Southeast Asia. *Quaternary Science Reviews*, 319, 108332. <https://doi.org/10.1016/j.quascirev.2023.108332>
- Li, T., García-Artola, A., Shaw, T. A., Peng, D., Walker, J. S., Cearreta, A., & Horton, B. P. (2024). Vertical land motion is underestimated in sea-level projections from the Oka estuary, northern Spain. *Scientific Reports*, 14(1), 31302. <https://doi.org/10.1038/s41598-024-82692-1>
- Li, T., Wu, P., Steffen, H., & Wang, H. (2018). In search of laterally heterogeneous viscosity models of glacial isostatic adjustment with the ICE-6G_C global ice history model. *Geophysical Journal International*, 214(2), 1191–1205. <https://doi.org/10.1093/gji/ggy181>
- Li, T., Wu, P., Wang, H. S., Steffen, H., Khan, N. S., Engelhart, S. E., et al. (2020). Uncertainties of glacial isostatic adjustment model predictions in North America associated with 3D structure. *Geophysical Research Letters*, 47(10), e2020GL087944. <https://doi.org/10.1029/2020GL087944>
- Lidberg, M., Johansson, J. M., Scherneck, H. G., & Davis, J. L. (2007). An improved and extended GPS derived 3D velocity field for the glacial isostatic adjustment (GIA) in Fennoscandia. *Journal of Geodesy*, 81(3), 213–230. <https://doi.org/10.1007/s00190-006-0102-4>
- Lidberg, M., Johansson, J. M., Scherneck, H. G., & Milne, G. A. (2010). Recent results based on continuous GPS observations of the GIA process in Fennoscandia from BIFROST. *Journal of Geodynamics*, 50(1), 8–18. <https://doi.org/10.1016/j.jog.2009.11.010>
- Liverman, D. G. E. (1994). Relative sea-level history and isostatic rebound in Newfoundland, Canada. *Boreas*, 23(3), 217–230. <https://doi.org/10.1111/j.1502-3885.1994.tb00944.x>
- Lliboutry, L. A. (1971). Rheological properties of the Asthenosphere from Fennoscandian data. *Journal of Geophysical Research*, 76, 1433–1446. <https://doi.org/10.1029/JB076i005p01433>
- Love, R., Milne, G. A., Tarasov, L., Engelhart, S. E., Hijma, M. P., Latychev, K., et al. (2016). The contribution of glacial isostatic adjustment to projections of sea-level change along the Atlantic and Gulf coasts of North America. *Earth's Future*, 4(10), 440–464. <https://doi.org/10.1002/2016EF000363>
- Lund, B. (2015). Palaeoseismology of glaciated terrain. In M. Beer, I. Kougioumtzoglou, E. Patelli, & I. K. Au (Eds.), *Encyclopedia of earthquake engineering* (pp. 1765–1779). Springer-Verlag. https://doi.org/10.1007/978-3-642-36197-5_25-1
- Lund, B., & Näslund, J. O. (2009). Glacial isostatic adjustment: Implications for glacially induced faulting and nuclear waste repositories. In C. B. Connor, N. A. Chapman, & L. J. Connor (Eds.), *Volcanic and tectonic hazard assessment for nuclear facilities* (pp. 142–155). <https://doi.org/10.1017/CBO9780511635380.006>
- Mattila, J., Ojala, A. E. K., Ruskeenieni, T., Palmu, J.-P., Aaltonen, I., Käpyaho, A., et al. (2019). Evidence of multiple slip events on postglacial faults in northern Fennoscandia. *Quaternary Science Reviews*, 215, 242–252. <https://doi.org/10.1016/j.quascirev.2019.05.022>
- McGinnis, L. D. (1968). Glacial crustal bending. *GSA Bulletin*, 79(6), 769–776. [https://doi.org/10.1130/0016-7606\(1968\)79\[769:GCB\]2.0.CO;2](https://doi.org/10.1130/0016-7606(1968)79[769:GCB]2.0.CO;2)

- McLaren, D., Fedje, D., Hay, M. B., Mackie, Q., Walker, I. J., Shugar, D. H., et al. (2014). A post-glacial sea level hinge on the central Pacific coast of Canada. *Quaternary Science Reviews*, 97, 148–169. <https://doi.org/10.1016/j.quascirev.2014.05.023>
- McLaren, D., Martindale, A., Fedje, D., & Mackie, Q. (2011). Relict shorelines and shell middens of the Dundas Archipelago. *Canadian Journal of Archaeology*, 35, 86–116.
- Meade, C., & Jeanloz, R. (1990). The strength of mantle silicates at high pressures and room temperature: Implications for the viscosity of the mantle. *Nature*, 348(6301), 533–535. <https://doi.org/10.1038/348533a0>
- Meyer, M., & Harff, J. (2005). Modelling Palaeo coastline changes of the Baltic Sea. *Journal of Coastal Research*, 21, 598–609. <https://doi.org/10.2112/04-703A.1>
- Mikko, H., Smith, C. A., Lund, B., Ask, M. V. S., & Munier, R. (2015). LiDAR-derived inventory of post-glacial fault scarps in Sweden. *GFF*, 137(4), 334–338. <https://doi.org/10.1080/11035897.2015.1036360>
- Miller, L., & Douglas, B. C. (2006). On the rate and causes of twentieth century sea-level rise. *Philosophical Transactions of the Royal Society A*, 364(1841), 805–820. <https://doi.org/10.1098/rsta.2006.1738>
- Milne, G. A., & Mitrova, J. X. (1996). Postglacial sea-level change on a rotating earth: First results from a gravitationally self-consistent sea-level equation. *Geophysical Journal International*, 126(3), F13–F20. <https://doi.org/10.1111/j.1365-246X.1996.tb04691.x>
- Minster, J. B., & Anderson, D. L. (1980). Dislocations and nonelastic processes in the mantle. *Journal of Geophysical Research*, 85(B11), 6347–6352. <https://doi.org/10.1029/JB085iB11p06347>
- Mitrova, J. X., & Milne, G. A. (2002). On the origin of late Holocene sea-level highstands within equatorial ocean basins. *Quaternary Science Reviews*, 21(20–22), 2179–2190. [https://doi.org/10.1016/S0277-3791\(02\)00080-X](https://doi.org/10.1016/S0277-3791(02)00080-X)
- Mitrova, J. X., & Peltier, W. R. (1991). A complete formalism for the inversion of post glacial rebound data: Resolving power analysis. *Geophysical Journal International*, 104(2), 267–288. <https://doi.org/10.1111/j.1365-246X.1991.tb02511.x>
- Mitrova, J. X., Davis, J. L., & Shapiro, I. I. (1994). A spectral formalism for computing three-dimensional deformations due to surface loads 1. Theory. *Journal of Geophysical Research*, 99, 7057–7073. <https://doi.org/10.1029/93JB03128>
- Mitrova, J. X., Gomez, N., Morrow, E., Hay, C., Latychev, K., & Tamisiea, M. E. (2011). On the robustness of predictions of sea level fingerprints. *Geophysical Journal International*, 187(2), 729–742. <https://doi.org/10.1111/j.1365-246X.2011.05090.x>
- Mitrova, J. X., Tamisiea, M. E., Davis, J. L., & Milne, G. A. (2001). Recent mass balance of polar ice sheets inferred from patterns of global sea-level change. *Nature*, 409(6823), 1026–1029. <https://doi.org/10.1038/35059054>
- Mörner, N. A. (1979). The Fennoscandian uplift and late Cenozoic geodynamics: Geological evidence. *Geojournal*, 3, 287–318. <https://doi.org/10.1007/BF00177634>
- Mörner, N.-A. (1978). Faulting, fracturing, and seismicity as functions of glacio-isostasy in Fennoscandia. *Geology*, 6(1), 41–45. [https://doi.org/10.1130/0091-7613\(1978\)6<41:FFASAF>2.0.CO;2](https://doi.org/10.1130/0091-7613(1978)6<41:FFASAF>2.0.CO;2)
- Muir-Wood, R. (2000). Deglaciation seismotectonics: A principal influence on intraplate seismogenesis at high latitudes. *Quaternary Science Reviews*, 19(14–15), 1399–1411. [https://doi.org/10.1016/S0277-3791\(00\)00069-X](https://doi.org/10.1016/S0277-3791(00)00069-X)
- Müller, K., Polom, U., Winsemann, J., Steffen, H., Tsukamoto, S., Günther, T., et al. (2020). Structural style and neotectonic activity along the Harz boundary fault, northern Germany: A multimethod approach integrating geophysics, outcrop data and numerical simulations. *International Journal of Earth Sciences*, 109(5), 1811–1835. <https://doi.org/10.1007/s00531-020-01874-0>
- Müller, K., Winsemann, J., Tanner, D., Lege, T., Spies, T., & Brandes, C. (2021). Glacially induced faults in Germany. In H. Steffen, O. Olesen, & R. Sutinen (Eds.), *Glacially-triggered faulting* (pp. 283–303). Cambridge University Press. <https://doi.org/10.1017/9781108779906.021>
- Nansen, F. (1922). The strandflat and isostasy. *Videnskapsselskapets Skrifter, 1. Math-Naturv. Klasse Kristiania*, 11, 1–313.
- Newman, W. S., & March, S. (1968). Littoral of the northeastern United States: Late Quaternary warping. *Science*, 160(3832), 1110–1112. <https://doi.org/10.1126/science.160.3832.1110>
- Nocquet, J.-M., Calais, E., & Parsons, B. (2005). Geodetic constraints on glacial isostatic adjustment in Europe. *Geophysical Research Letters*, 32(6), L06308. <https://doi.org/10.1029/2004GL022174>
- O’Keefe, K., & Wu, P. (1998). Viscoelastic Channel flow. In P. Wu (Ed.), *Dynamics of the ice age earth, a modern perspective* (pp. 203–216). Trans Tech Publications. <https://doi.org/10.4028/www.scientific.net/RC.38>
- O’Keefe, K., & Wu, P. (2002). Effect of mantle structure on postglacial induced horizontal displacement. In J. X. Mitrova & B. L. A. Vermeersen (Eds.), *Ice sheets, sea level and the dynamic earth. AGU geodynamics series* (Vol. 29, pp. 109–118). American Geophysical Union. <https://doi.org/10.1002/9781118670101.ch7>
- Oakley, B. A., & Boothroyd, J. C. (2012). Reconstructed topography of Southern New England prior to isostatic rebound with implications of total isostatic depression and relative sea level. *Quaternary Research*, 78(1), 110–118. <https://doi.org/10.1016/j.yqres.2012.03.002>
- Ojala, A. E. K., Mattila, J., Ruskeeniemi, T., Palmu, J.-P., Lindberg, A., Hänninen, P., & Sutinen, R. (2017). Postglacial seismic activity along the Isovaara-Riikonkumpu fault complex. *Global and Planetary Change*, 157, 59–72. <https://doi.org/10.1016/j.gloplacha.2017.08.015>
- Olesen, O., Olsen, L., Gibbons, S. J., Ruud, B. O., Høgaas, F., Johansen, T. A., & Kværna, T. (2021). Postglacial faulting in Norway—Large magnitude earthquakes of the Late Holocene Age. In H. Steffen, O. Olesen, & R. Sutinen (Eds.), *Glacially-triggered faulting* (pp. 198–217). Cambridge University Press. <https://doi.org/10.1017/9781108779906.015>
- Palmu, J.-P., Ojala, A. E. K., Ruskeeniemi, T., Sutinen, R., & Mattila, J. (2015). LiDAR DEM detection and classification of postglacial faults and seismically-induced landforms in Finland: A paleoseismic database. *GFF*, 137(4), 344–352. <https://doi.org/10.1080/11035897.2015.1068370>
- Panin, A., Adamiec, G., & Filippov, V. (2015). Fluvial response to proglacial effects and climate in the upper Dnieper valley (Western Russia) during the Late Weichselian and the Holocene. *Quaternaire*, 26(vol. 26/1), 27–48. <https://doi.org/10.4000/quaternaire.7141>
- Peltier, W. R. (1974). The impulse response of a Maxwell Earth. *Reviews of Geophysics*, 12(4), 649–669. <https://doi.org/10.1029/RG012i004p00649>
- Peltier, W. R. (1998). Postglacial variations in the level of the sea: Implications for climate dynamics and solid earth geophysics. *Reviews of Geophysics*, 36(4), 603–689. <https://doi.org/10.1029/98RG02638>
- Peltier, W. R. (2002). Global glacial isostatic adjustment: Palaeogeodetic and space-geodetic tests of the ICE-4G (VM2) model. *Journal of Quaternary Science*, 17(5–6), 491–510. <https://doi.org/10.1002/jqs.713>
- Peltier, W. R. (2004). Global glacial isostasy and the surface of the ice age earth: The ICE-5G (VM2) model and GRACE. *Annual Review of Earth and Planetary Sciences*, 32(1), 111–149. <https://doi.org/10.1146/annurev.earth.32.082503.144359>
- Peltier, W. R., & Tushingham, A. M. (1991). Influence of glacial isostatic adjustment on tide gauge measurements of secular sea level change. *Journal of Geophysical Research*, 96(B4), 6779–6796. <https://doi.org/10.1029/90JB02067>
- Peltier, W. R., Argus, D. F., & Drummond, R. (2015). Space geodesy constrains ice age terminal deglaciation: The global ICE-6G_C (VM5a) model. *Journal of Geophysical Research*, 120(1), 450–487. <https://doi.org/10.1002/2014JB011176>
- Peltier, W. R., Drummond, R. A., & Tushingham, A. M. (1986). Post-glacial rebound and transient lower mantle rheology. *Geophysical Journal International*, 87(1), 79–116. <https://doi.org/10.1111/j.1365-246X.1986.tb04548.x>

- Peltier, W. R., Farrell, W. E., & Clark, J. A. (1978). Glacial isostasy and relative sea level: A global finite element model. *Tectonophysics*, 50(2–3), 81–110. [https://doi.org/10.1016/0040-1951\(78\)90129-4](https://doi.org/10.1016/0040-1951(78)90129-4)
- Peltier, W. R., Wu, P., Argus, D. F., Li, T., & Velay-Vitow, J. (2022). Glacial isostatic adjustment: Physical models and observational constraints. *Reports on Progress in Physics*, 85(9), 096801. <https://doi.org/10.1088/1361-6633/ac805b>
- Peltier, W. R., Yuen, D. A., & Wu, P. (1980). Postglacial rebound and transient rheology. *Geophysical Research Letters*, 7(10), 733–736. <https://doi.org/10.1029/GL007i010p00733>
- Pico, T., Mitrovica, J. X., Braun, J., & Ferrier, K. L. (2018). Glacial isostatic adjustment deflects the path of the ancestral Hudson River. *Geology*, 46(7), 591–594. <https://doi.org/10.1130/G40221.1>
- Piecuch, C. G., Huybers, P., Hay, C. C., Kemp, A. C., Little, C. M., Mitrovica, J. X., et al. (2018). Origin of spatial variation in US East Coast sea-level trends during 1900–2017. *Nature*, 564(7736), 400–404. <https://doi.org/10.1038/s41586-018-0787-6>
- Pisarska-Jamroży, M., Belzyt, S., Börner, A., Hoffmann, G., Hüneke, H., Kenzler, M., et al. (2018). Evidence from seismites for glacio-isostatically induced crustal faulting in front of an advancing land-ice mass (Rügen Island, SW Baltic Sea). *Tectonophysics*, 745, 338–348. <https://doi.org/10.1016/j.tecto.2018.08.004>
- Pisarska-Jamroży, M., Belzyt, S., Börner, A., Hoffmann, G., Hüneke, H., Kenzler, M., et al. (2019). The sea cliff at Dwasieden: Soft-sediment deformation structures triggered by glacial isostatic adjustment in front of the advancing Scandinavian Ice Sheet. *DEUQUA Special Publication*, 2, 61–67. <https://doi.org/10.5194/deuquasp-2-61-2019>
- Pisarska-Jamroży, M., Belzyt, S., Börner, A., Hoffmann, G., Kenzler, M., Rother, H., et al. (2022). Late Pleistocene earthquakes imprinted on glaciolacustrine sediments on Gnitza Peninsula (Usedom Island, NE Germany). *Quaternary Science Reviews*, 296, 107807. <https://doi.org/10.1016/j.quascirev.2022.107807>
- Pisarska-Jamroży, M., Woronko, B., Woźniak, P. P., Rosentau, A., Hang, T., Steffen, H., & Steffen, R. (2024). Deformation structures as key hints for interpretation of ice sheet dynamics—A case study from northeastern Estonia. *Quaternary Science Reviews*, 336, 108788. <https://doi.org/10.1016/j.quascirev.2024.108788>
- Pisarska-Jamroży, M., Woźniak, P., & Van Loon, A. (2021). Glacially induced faulting in Poland. In H. Steffen, O. Olesen, & R. Sutinen (Eds.), *Glacially-triggered faulting* (pp. 304–319). Cambridge University Press. <https://doi.org/10.1017/9781108779906.022>
- Plag, H.-P. (2006). Recent relative sea-level trends: An attempt to quantify the forcing factors. *Philosophical Transactions of the Royal Society A*, 364(1841), 821–844. <https://doi.org/10.1098/rsta.2006.1739>
- Plag, H.-P., & Jüttner, H. U. (2001). Inversion of global tide gauge data for present-day ice load changes. *Memoirs of National Institute of Polar Research - Special Issue*, 54, 301–318.
- Puziene, R., Anikieniene, A., & Karsokiene, G. (2014). Inquiry into vertical movements of the earth's crust based on samples from eastern Lithuania. *Geodesy and Cartography*, 40(2), 58–67. <https://doi.org/10.3846/20296991.2014.890308>
- Ranalli, G. (1995). *Rheology of the earth* (2nd ed., p. 414). Chapman & Hall.
- Reusen, J. M., Steffen, R., Steffen, H., Root, B. C., & van der Wal, W. (2023). Simulating horizontal crustal motions of glacial isostatic adjustment using compressible cartesian models. *Geophysical Journal International*, 235(1), 542–553. <https://doi.org/10.1093/gji/ggad232>
- Reusser, L. J., Bierman, P. R., Pavich, M. J., Zen, E., Larsen, J., & Finkel, R. (2004). Rapid Late Pleistocene incision of Atlantic passive margin river gorges. *Science*, 305(5683), 499–502. <https://doi.org/10.1126/science.1097780>
- Robin, C. M. I., Craymer, M. R., Ferland, R., James, T. S., Lapelle, E., Piraszewski, M., & Zhao, Y. A. (2020). NAD83v70VG: A new national crustal velocity model for Canada. *Geomatics Canada*, 62, 70. <https://doi.org/10.4095/327592>
- Rosentau, A., Klemann, V., Bennike, O., Steffen, H., Wehr, J., Latinović, M., et al. (2021). A Holocene relative sea-level database for the Baltic Sea. *Quaternary Science Reviews*, 266, 107071. <https://doi.org/10.1016/j.quascirev.2021.107071>
- Rosentau, A., Vassiljev, J., Saarse, L., & Miidel, A. (2007). Palaeogeographic reconstruction of proglacial lakes in Estonia. *Boreas*, 36(2), 211–221. <https://doi.org/10.1111/j.1502-3885.2007.tb01193.x>
- Rosentau, A., Vassiljev, J., Saarse, L., & Miidel, A. (2008). Proglacial lake shorelines of Estonia and adjoining areas. *Polish Geological Institute Special Papers*, 23, 81–86.
- Roy, K., & Peltier, W. R. (2018). Relative sea level in the western Mediterranean basin: A regional test of the ICE-7G_NA (VM7) model and a constraint on late Holocene Antarctic deglaciation. *Quaternary Science Reviews*, 183, 76–87. <https://doi.org/10.1016/j.quascirev.2017.12.021>
- Rudzik, M. P. (1899). Deformation der Erde unter der Last des Inlandeises. *Anzeiger der Akademie der Wissenschaften in Krakau*, 4, 169–215.
- Saarse, L., Vassiljev, J., Rosentau, A., & Miidel, A. (2007). Reconstructed late glacial shore displacement in Estonia. *Baltica*, 20, 35–45.
- Sandersen, P., Gregersen, S., & Voss, P. (2021). Lateglacial and postglacial faulting in Denmark. In H. Steffen, O. Olesen, & R. Sutinen (Eds.), *Glacially-triggered faulting* (pp. 263–282). Cambridge University Press. <https://doi.org/10.1017/9781108779906.020>
- Sauber, J., Rollins, C., Freymueller, J., & Ruppert, N. (2021). Glacially induced faulting in Alaska. In H. Steffen, O. Olesen, & R. Sutinen (Eds.), *Glacially-triggered faulting* (pp. 353–365). Cambridge University Press. <https://doi.org/10.1017/9781108779906.026>
- Sbarra, C. M., Briner, J. P., Graham, B. L., Poinar, K., Thomas, E. K., & Young, N. E. (2022). Evidence for a more extensive Greenland ice sheet in southwestern Greenland during the last glacial maximum. *Geosphere*, 18(4), 1316–1329. <https://doi.org/10.1130/GES02432.1>
- Scott, D. B., Boyd, R., & Medioli, F. S. (1987). Relative sea-level changes in Atlantic Canada: Observed level and sedimentological changes vs. theoretical models. In D. Nummedal, O. H. Pilkey, & J. D. Howard (Eds.), *Sea-level fluctuation and coastal evolution* (Vol. 41, pp. 87–96). SEPM Society for Sedimentary Geology Special Publication. <https://doi.org/10.2110/pec.87.41.0087>
- Seidel, E., Steffen, H., Steffen, R., Ahlrichs, N., & Hübscher, C. (2025). Drivers of glacially induced fault reactivation in the Baltic Sea sector of the Tornquist Fan. *Boreas*, 54(2), 220–245. <https://doi.org/10.1111/bor.12689>
- Sella, G. F., Stein, S., Dixon, T. H., Craymer, M., James, T. S., Mazzotti, S., & Dokka, R. K. (2007). Observation of glacial isostatic adjustment in “stable” North America with GPS. *Geophysical Research Letters*, 34(2), L02306. <https://doi.org/10.1029/2006GL027081>
- Shaler, N. S. (1874). Recent changes of level on the coast of Maine: With reference to their origin and relation to other similar changes. In *Memoirs of the Boston society of natural history, volume II. Part III. Number III* (pp. 320–340).
- Shugar, D. H., Walker, I. J., Lian, O. B., Eamer, J. B. R., Neudorf, C., McLaren, D., & Fedje, D. (2014). Post-glacial sea level change along the Pacific coast of North America. *Quaternary Science Reviews*, 97, 170–192. <https://doi.org/10.1016/j.quascirev.2014.05.022>
- Smith, C. A., Sundh, M., & Mikko, H. (2014). Surficial geology indicates early Holocene faulting and seismicity, central Sweden. *International Journal of Earth Sciences*, 103(6), 1711–1724. <https://doi.org/10.1007/s00531-014-1025-6>
- Stanford, S. D. (2010). Onshore record of Hudson River drainage to the continental shelf from the late Miocene through the late Wisconsinian deglaciation, USA: Synthesis and revision. *Boreas*, 39, 1–17. <https://doi.org/10.1111/j.1502-3885.2009.00106.x>
- Stea, R. R., Fader, G. B. J., Scott, D. B., & Wu, P. (2001). Glaciation and relative sea-level change in Maritime Canada. In T. K. Weddle & M. J. Retelle (Eds.), *Deglacial history and relative sea-level changes, northern New England and adjacent Canada. GSA Special Papers* (Vol. 351, pp. 35–49). <https://doi.org/10.1130/0-8137-2351-5.35>

- Steffen, H., Kaufmann, G., & Wu, P. (2006). Three dimensional finite-element modeling of the glacial isostatic adjustment in Fennoscandia. *Earth and Planetary Science Letters*, 250(1–2), 358–375. <https://doi.org/10.1016/j.epsl.2006.08.003>
- Steffen, H., Steffen, R., & Tarasov, L. (2019). Modelling of glacially-induced stress changes in Latvia, Lithuania and the Kaliningrad District of Russia. *Baltica*, 32(1), 78–90. <https://doi.org/10.5200/baltica.2019.1.7>
- Steffen, H., & Wu, P. (2011). Glacial isostatic adjustment in Fennoscandia—A review of data and modeling. *Journal of Geodynamics*, 52(3–4), 169–204. <https://doi.org/10.1016/j.jog.2011.03.002>
- Steffen, R., & Steffen, H. (2021). Reactivation of non-optimally orientated faults due to glacially induced stresses. *Tectonics*, 40(11), e2021TC006853. <https://doi.org/10.1029/2021TC006853>
- Steffen, R., Steffen, H., Weiss, R., Lecavalier, B. S., Milne, G. A., Woodroffe, S. A., & Bennike, O. (2020). Early Holocene Greenland-ice mass loss likely triggered earthquakes and tsunamis. *Earth and Planetary Science Letters*, 546, 116443. <https://doi.org/10.1016/j.epsl.2020.116443>
- Steffen, R., Steffen, H., Wu, P., & Eaton, D. W. (2014c). Stress and fault parameters affecting fault slip magnitude and activation time during a glacial cycle. *Tectonics*, 33(7), 1461–1476. <https://doi.org/10.1002/2013TC003450>
- Steffen, R., Wu, P., & Lund, B. (2021). Geomechanics of glacially triggered faulting. In H. Steffen, O. Olesen, & R. Sutinen (Eds.), *Glacially-triggered faulting* (pp. 20–40). Cambridge University Press. <https://doi.org/10.1017/9781108779906.004>
- Steffen, R., Wu, P., Steffen, H., & Eaton, D. W. (2014a). On the implementation of faults in finite-element glacial isostatic adjustment models. *Computers and Geoscience*, 62, 150–159. <https://doi.org/10.1016/j.cageo.2013.06.012>
- Steffen, R., Wu, P., Steffen, H., & Eaton, D. W. (2014b). The effect of earth rheology and ice-sheet size on fault-slip and magnitude of postglacial earthquakes. *Earth and Planetary Science Letters*, 388, 71–80. <https://doi.org/10.1016/j.epsl.2013.11.058>
- Stein, S., Cloetingh, S., Sleep, N. H., & Wortel, R. (1989). Passive margin earthquakes, stresses and rheology. In S. Gregersen, & P. W. Basham (Eds.), *Earthquakes at North-Atlantic Passive Margins: Neotectonics and postglacial rebound*. NATO ASI series (Vol. 266, pp. 231–259). Springer. https://doi.org/10.1007/978-94-009-2311-9_14
- Štěpánčíková, P., Rockwell, T. K., Stemberk, J., Rhodes, E. J., Hartvich, F., Luttrell, K., et al. (2022). Acceleration of Late Pleistocene activity of a Central European fault driven by ice loading. *Earth and Planetary Science Letters*, 591, 117596. <https://doi.org/10.1016/j.epsl.2022.117596>
- Stewart, I. S., Sauber, J., & Rose, J. (2000). Glacio-seismotectonics: Ice sheets, crustal deformation and seismicity. *Quaternary Science Reviews*, 19(14–15), 1367–1389. [https://doi.org/10.1016/S0277-3791\(00\)00094-9](https://doi.org/10.1016/S0277-3791(00)00094-9)
- Sutinen, R., Hyvönen, E., Markovaara-Koivisto, M., Middleton, M., Ojala, A. E. K., Palmu, J.-P., et al. (2021). Glacially induced faults in Finland. In H. Steffen, O. Olesen, & R. Sutinen (Eds.), *Glacially-triggered faulting* (pp. 231–245). Cambridge University Press. <https://doi.org/10.1017/9781108779906.017>
- Sutinen, R., Hyvönen, E., Middleton, M., & Ruskeeniemi, T. (2014). Airborne LiDAR detection of postglacial faults and Pulju moraine in Palojärvi, Finnish Lapland. *Global and Planetary Change*, 115, 24–32. <https://doi.org/10.1016/j.gloplacha.2014.01.007>
- Tamisiea, M. E., Mitrovica, J. X., Milne, G. A., & Davis, J. L. (2001). Global geoid and sea level changes due to present-day ice mass fluctuations. *Journal of Geophysical Research*, 106(B12), 30849–30863. <https://doi.org/10.1029/2000JB000011>
- Tan, F., Khan, N. S., Li, T., Meltzner, A. J., Majewski, J., Chan, N., et al. (2023). Holocene relative sea-level histories of far-field islands in the mid-Pacific. *Quaternary Science Reviews*, 310, 107995. <https://doi.org/10.1016/j.quascirev.2023.107995>
- Tarasov, L., & Peltier, W. R. (2002). Greenland glacial history and local geodynamic consequences. *Geophysical Journal International*, 150(1), 198–229. <https://doi.org/10.1046/j.1365-246X.2002.01702.x>
- Tarasov, L., Dyke, A. S., Neal, R. M., & Peltier, W. R. (2012). A data-calibrated distribution of deglacial chronologies for the North American ice complex from glaciological modeling. *Earth and Planetary Science Letters*, 315–316, 30–40. <https://doi.org/10.1016/j.epsl.2011.09.010>
- Tarasov, L., Hughes, A., Gyllencreutz, R., Lohne, O. S., Mangerud, J., & Svendsen, J. I. (2014). The global GLAC-1c deglaciation chronology, meltwater pulse 1-a, and a question of missing ice. In *IGS Symposium on contribution of glaciers and ice sheets to sea-level change*.
- Toucanne, S., Zaragosi, S., Bourillet, J. F., Gibbard, P. L., Eynaud, F., Giraudeau, J., et al. (2009). A 1.2 Ma record of glaciation and fluvial discharge from the West European Atlantic margin. *Quaternary Science Reviews*, 28(25–26), 2974–2981. <https://doi.org/10.1016/j.quascirev.2009.08.003>
- Turcotte, D. L., & Schubert, G. (2014). *Geodynamics* (p. 636). Cambridge University Press.
- Turpeinen, H., Hampel, A., Karow, T., & Maniatis, G. (2008). Effect of ice sheet growth and melting on the slip evolution of thrust faults. *Earth and Planetary Science Letters*, 269(1–2), 230–241. <https://doi.org/10.1016/j.epsl.2008.02.017>
- Tushingham, A. M., & Peltier, W. R. (1991). ICE-3G: A new global model of late Pleistocene deglaciation based upon geophysical predictions of post-glacial relative sea level change. *Journal of Geophysical Research*, 96(B3), 4497–4523. <https://doi.org/10.1029/90JB01583>
- Uścińowicz, S. (2003). Relative sea level changes, glacio-isostatic rebound and shoreline displacement in the Southern Baltic. *Polish Geological Institute Special Papers*, 10, 1–79.
- Vacchi, M., Engelhart, S. E., Nikitina, D., Ashe, E. L., Peltier, W. R., Roy, K., et al. (2018). Postglacial relative sea-level histories along the eastern Canadian coastline. *Quaternary Science Reviews*, 201, 124–146. <https://doi.org/10.1016/j.quascirev.2018.09.043>
- Van Balen, R. T., Bakker, M. A. J., Kasse, C., Wallinger, J., & Woolderink, H. A. G. (2019). A late glacial surface rupturing earthquake at the Peel boundary fault zone, Roer Valley Rift system, the Netherlands. *Quaternary Science Reviews*, 218, 254–266. <https://doi.org/10.1016/j.quascirev.2019.06.033>
- Van Balen, R. T., Busschers, F. S., & Tucker, G. T. (2010). Modeling the response of the Rhine-Meuse fluvial system to Late Pleistocene climate change. *Geomorphology*, 114(3), 440–452. <https://doi.org/10.1016/j.geomorph.2009.08.007>
- Van Balen, R. T., Kasse, C., Wallinger, J., & Woolderink, H. A. G. (2021). Middle to late Pleistocene faulting history of the Heerlerheide fault, Roer Valley Rift system, influenced by glacio-isostasy and mining-induced displacement. *Quaternary Science Reviews*, 268, 107111. <https://doi.org/10.1016/j.quascirev.2021.107111>
- Van Balen, R. T., Lapperre, R. E., Woolderink, H. A. G., Wallinga, J., & Kasse, C. (2024). Magnitudes and surface rupture lengths of paleo-earthquakes at the NW-part of the Peel boundary fault zone, Roer Valley Rift system. *Tectonophysics*, 879, 230322. <https://doi.org/10.1016/j.tecto.2024.230322>
- Van Bemmelen, R. W., & Berlage, H. P. (1934). Versuch einer mathematischen Behandlung geotektonischer Bewegungen unter besonderer Berücksichtigung der Undationstheorie. *Gerlands Beiträge zur Geophysik*, 34, 2–55.
- Van der Wal, W., Wu, P., Wang, H., & Sideris, M. G. (2010). Sea levels and uplift rate from composite rheology in glacial isostatic adjustment modeling. *Journal of Geodynamics*, 50(1), 38–48. <https://doi.org/10.1016/j.jog.2010.01.006>
- Vink, A., Steffen, H., Reinhardt, L., & Kaufmann, G. (2007). Holocene relative sea-level change, isostatic subsidence and the radial viscosity structure of the mantle of northwest Europe (Belgium, the Netherlands, Germany, southern North Sea). *Quaternary Science Reviews*, 26(25–28), 3249–3275. <https://doi.org/10.1016/j.quascirev.2007.07.014>
- von Drygalski, E. (1887). Die Geoiddeformationen der Eiszeit. In *Zeitschrift der Gesellschaft für Erdkunde* (pp. 169–280). Verlag Dietrich Reimer.

- Walcott, R. I. (1970). Isostatic response to loading of the crust in Canada. *Canadian Journal of Earth Sciences*, 7(2), 716–727. <https://doi.org/10.1139/e70-070>
- Walcott, R. I. (1972). Past sea levels, eustasy and deformation of the earth. *Quaternary Research*, 2, 1–14. [https://doi.org/10.1016/0033-5894\(72\)90001-4](https://doi.org/10.1016/0033-5894(72)90001-4)
- Walker, J. S., Kopp, R. E., Shaw, T. A., Cahill, N., Khan, N. S., Barber, D. C., et al. (2021). Common Era sea-level budgets along the U.S. Atlantic coast. *Nature Communications*, 12(1), 1841. <https://doi.org/10.1038/s41467-021-22079-2>
- Walker, J. S., Li, T., Shaw, T. A., Cahill, N., Barber, D. C., Brain, M. J., et al. (2023). A 5000-year record of relative sea-level change in New Jersey, USA. *The Holocene*, 33(2), 167–180. <https://doi.org/10.1177/09596836221131696>
- Wang, F., Zong, Y., Mauz, B., Li, J., Fang, J., Tian, L., et al. (2020). Holocene sea-level change on the central coast of Bohai Bay, China. *Earth Surface Dynamics*, 8(3), 679–693. <https://doi.org/10.5194/esurf-8-679-2020>
- Wang, H., & Wu, P. (2006). Effects of lateral variations in lithospheric thickness and mantle viscosity on glacially induced surface motion on a spherical, self-gravitating Maxwell Earth. *Earth and Planetary Science Letters*, 244(3–4), 576–589. <https://doi.org/10.1016/j.epsl.2006.02.026>
- Watts, A. B. (2001). *Isostasy and flexure of the lithosphere* (p. 458). Cambridge University Press.
- Watts, A. B., & Burov, E. (2003). Lithospheric strength and its relationship to the elastic and seismogenic layer thickness. *Earth and Planetary Science Letters*, 213(1–2), 113–131. [https://doi.org/10.1016/s0012-821x\(03\)00289-9](https://doi.org/10.1016/s0012-821x(03)00289-9)
- Watts, A. B., Zhong, S. J., & Hunter, J. (2013). The behavior of the lithosphere on seismic to geologic timescales. *Annual Review of Earth and Planetary Sciences*, 41(1), 443–468. <https://doi.org/10.1146/annurev-earth-042711-105457>
- Whitehouse, P. L. (2018). Glacial isostatic adjustment modelling: Historical perspectives, recent advances, and future directions. *Earth Surface Dynamics*, 6(2), 401–429. <https://doi.org/10.5194/esurf-6-401-2018>
- Whitehouse, P., Latychev, K., Milne, G. A., Mitrovica, J. X., & Kendall, R. (2006). Impact of 3-D Earth structure on Fennoscandian glacial isostatic adjustment: Implications for space-geodetic estimates of present-day crustal deformations. *Geophysical Research Letters*, 33, L13502. <https://doi.org/10.1029/2006GL026568>
- Wickert, A. D., Anderson, R. S., Mitrovica, J. X., Naylor, S., & Carson, E. C. (2019). The Mississippi River records glacial-isostatic deformation of North America. *Science Advances*, 5(1), eaav2366. <https://doi.org/10.1126/sciadv.aav2366>
- Winsemann, J., Lang, J., Roskosch, J., Polom, U., Böhner, U., Brandes, C., et al. (2015). Terrace styles and timing of terrace formation in the Weser and Leine valleys, northern Germany: Response of a fluvial system to climate change and glaciation. *Quaternary Science Reviews*, 123, 31–57. <https://doi.org/10.1016/j.quascirev.2015.06.005>
- Wolf, D. (1986). Glacio-isostatic adjustment in Fennoscandia revisited. *Journal of Geophysics*, 59(1), 42–48. <https://doi.org/10.18419/opus-7130>
- Wolf, D. (1993). The changing role of the lithosphere in models of glacial isostasy: A historical review. *Global and Planetary Change*, 8(3), 95–106. [https://doi.org/10.1016/0921-8181\(93\)90017-1](https://doi.org/10.1016/0921-8181(93)90017-1)
- Wong, M. C., & Wu, P. (2019). Using commercial finite-element packages for the study of glacial isostatic adjustment on a compressible self-gravitating spherical Earth—I: Harmonic loads. *Geophysical Journal International*, 217(3), 1798–1820. <https://doi.org/10.1093/gji/ggz108>
- Wu, P. (1978). *Response of a Maxwell earth to applied surface mass loads: Glacial isostatic adjustment*. M.Sc., Thesis. Department of Physics, University of Toronto.
- Wu, P. (1993). Postglacial rebound in a power-law medium with axial symmetry and the existence of the transition zone in relative sea-level data. *Geophysical Journal International*, 114(3), 417–432. <https://doi.org/10.1111/j.1365-246X.1993.tb06976.x>
- Wu, P. (1995). Can observations of postglacial rebound tell whether the rheology of the mantle is linear or nonlinear? *Geophysical Research Letters*, 22(13), 1645–1648. <https://doi.org/10.1029/95gl01594>
- Wu, P. (1997). Effect of viscosity structure of fault potential and stress orientations in eastern Canada. *Geophysical Journal International*, 130(2), 365–382. <https://doi.org/10.1111/j.1365-246X.1997.tb05653.x>
- Wu, P. (1998). Will earthquake activity in Eastern Canada increase in the next few thousand years? *Canadian Journal of Earth Sciences*, 35(5), 562–568. <https://doi.org/10.1139/e97-125>
- Wu, P. (1999). Modeling postglacial sea-levels with power-law rheology and a realistic ice model in the absence of ambient tectonic stress. *Geophysical Journal International*, 139(3), 691–702. <https://doi.org/10.1046/j.1365-246x.1999.00965.x>
- Wu, P. (2005). Effects of lateral variations in lithospheric thickness and mantle viscosity on glacially induced surface motion in Laurentia. *Earth and Planetary Science Letters*, 235(3–4), 549–563. <https://doi.org/10.1016/j.epsl.2005.04.038>
- Wu, P., & Hasegawa, H. S. (1996a). Induced stresses and fault potential in eastern Canada due to a disc load: A preliminary analysis. *Geophysical Journal International*, 125(2), 415–430. <https://doi.org/10.1111/j.1365-246X.1996.tb00008.x>
- Wu, P., & Hasegawa, H. S. (1996b). Induced stresses and fault potential in eastern Canada due to a realistic load: A preliminary analysis. *Geophysical Journal International*, 127(1), 215–229. <https://doi.org/10.1111/j.1365-246X.1996.tb01546.x>
- Wu, P., & Johnston, P. (2000). Can deglaciation trigger earthquakes in N. America? *Geophysical Research Letters*, 27(9), 1323–1326. <https://doi.org/10.1029/1999GL011070>
- Wu, P., & Mazzotti, S. (2007). Effects of a lithospheric weak zone on postglacial seismotectonics in Eastern Canada and the Northeastern United States. In S. Stein & S. Mazzotti (Eds.), *Continental intraplate earthquakes: Science, hazard and policy issues*. GSA special paper (Vol. 425, pp. 113–128). [https://doi.org/10.1130/2007.2425\(09\)](https://doi.org/10.1130/2007.2425(09))
- Wu, P., & Peltier, W. R. (1982). Viscous gravitational relaxation. *Geophysical Journal International*, 70(2), 435–485. <https://doi.org/10.1111/j.1365-246X.1982.tb04976.x>
- Wu, P., & Peltier, W. R. (1983). Glacial isostatic adjustment and the free air gravity anomaly as a constraint on deep mantle viscosity. *Geophysical Journal International*, 74, 377–449. <https://doi.org/10.1111/j.1365-246X.1983.tb01884.x>
- Wu, P., & van der Wal, W. (2003). Postglacial sea levels on a spherical, self-gravitating viscoelastic earth: Effects of lateral viscosity variations in the upper mantle on the inference of viscosity contrasts in the lower mantle. *Earth and Planetary Science Letters*, 211, 57–68. [https://doi.org/10.1016/S0012-821X\(03\)00199-7](https://doi.org/10.1016/S0012-821X(03)00199-7)
- Wu, P., Ni, Z., & Kaufmann, G. (1998). Postglacial rebound with lateral heterogeneities: From 2D to 3D modeling. In P. Wu (Ed.), *Dynamics of the ice age Earth, a modern perspective* (pp. 557–582). Trans Tech Publications. <https://doi.org/10.4028/www.scientific.net/RC.38>
- Wu, P., Wang, H., & Steffen, H. (2013). The role of thermal effect on mantle seismic anomalies under Laurentia and Fennoscandia from observations of Glacial Isostatic Adjustment. *Geophysical Journal International*, 192(1), 7–17. <https://doi.org/10.1093/gji/ggs009>
- Yousefi, M., Milne, G. A., & Latychev, K. (2021). Glacial isostatic adjustment of the Pacific coast of North America: The influence of lateral earth structure. *Geophysical Journal International*, 226(1), 91–113. <https://doi.org/10.1093/gji/ggab053>
- Yuen, D. A., Sabadini, R., & Boschi, E. (1982). Mantle rheology from a geodynamical standpoint. *Revista del Nuovo Cimento*, 5(8), 1–35. <https://doi.org/10.1007/bf02740829>

- Zhong, S., Kang, K., A, G., & Qin, C. (2022). CitcomSVE: A three-dimensional finite element software package for modeling planetary mantle's viscoelastic deformation in response to surface and tidal loads. *Geochemistry, Geophysics, Geosystems*, 23(10), e2022GC010359. <https://doi.org/10.1029/2022GC010359>
- Zhong, S., Paulson, A., & Wahr, J. (2003). Three-dimensional finite element modeling of Earth's viscoelastic deformation: Effects of lateral variations in lithospheric thickness. *Geophysical Journal International*, 155(2), 679–695. <https://doi.org/10.1046/j.1365-246X.2003.02084.x>
- Zong, Y. (2004). Mid-Holocene sea-level highstand along the southeast coast of China. *Quaternary International*, 117(1), 55–67. [https://doi.org/10.1016/S1040-6182\(03\)00116-2](https://doi.org/10.1016/S1040-6182(03)00116-2)